

The role of *Talpid3* in skeletal muscle satellite cells and skeletal muscle regeneration

Danielle Louise Blackwell

Thesis submitted for the degree of Doctor of
Philosophy

University of East Anglia
School of Biological Sciences
Norwich
United Kingdom
November 2017

© This copy of the thesis has been supplied on condition that anyone who consults it is understood to recognise that its copyright rests with the author and that use of any information derived there from must be in accordance with current UK Copyright Law. In addition, any quotation or extract must include full attribution.

Abstract

The primary cilium has recently been recognised as an essential regulator of the Sonic hedgehog (Shh) signalling pathway. Mutations that disrupt cilia function in humans can cause conditions known as ciliopathies. A wide range of phenotypes is observed in chick and mouse ciliopathy models, including polydactyly, craniofacial defects and polycystic kidneys. The Shh pathway and therefore primary cilia are vital for many developmental processes, including embryonic muscle development, with recent evidence suggesting they may also play a role in adult muscle regeneration. Our studies focus on the *Talpid3* gene, which encodes a centrosomal protein required for primary cilia formation and Shh signalling. The *Talpid3* loss-of-function mutant has perturbed ciliogenesis and displays many of the phenotypes that are typically associated with developmental Shh mutants and with ciliopathies. *Talpid3* mutants have defects in Shh signalling, and processing of Gli transcription factors is affected in structures such as the developing limb buds and the neural tube. However, the role of *Talpid3* in muscle development and regeneration remains unknown.

The role of *Talpid3* in adult muscle regeneration was investigated using a tamoxifen inducible, satellite cell specific knock-out of *Talpid3* in mice. This mouse model was generated by crossing *Talpid3* floxed mice to a mouse carrying an inducible *Pax7-CreERT2* allele. To determine whether loss of *Talpid3* affects muscle regeneration a cardiotoxin injury model was used. This showed that loss of *Talpid3* in satellite cells results in a regeneration defect as fibres were smaller after 5, 10, 15 and 25 days of regeneration compared to control mice. This defect may be due to a reduced ability of *Talpid3* mutant satellite cells to differentiate. We also show that *Talpid3* plays a role in satellite cell self-renewal as we observe a complete loss of regeneration in some areas of the muscle following repeat injuries.

We provide the first evidence that *Talpid3* is critical for the regeneration of skeletal muscle following injury.

Table of Contents

| | |
|--|------------|
| Abstract | i |
| Table of Contents | ii |
| List of Figures | vii |
| List of Tables | ix |
| Abbreviations | x |
| Acknowledgements | xii |
| Chapter 1 Introduction | 1 |
| 1.1 Skeletal Muscle | 1 |
| 1.1.1 <i>Structure of skeletal muscle</i> | 1 |
| 1.1.2 <i>Embryonic development of skeletal muscle</i> | 4 |
| 1.1.2.1 <i>Inductive signals controlling somitogenesis</i> | 4 |
| 1.1.2.2 <i>Paired box (PAX) transcription factor family</i> | 6 |
| 1.1.2.3 <i>Myogenic regulatory factors (MRFs)</i> | 7 |
| 1.1.3 <i>Satellite cell structure and origin</i> | 11 |
| 1.1.4 <i>Skeletal muscle regeneration</i> | 15 |
| 1.1.4.1 <i>Muscle degeneration and inflammatory response</i> | 15 |
| 1.1.4.2 <i>Satellite cell activation and differentiation</i> | 16 |
| 1.1.4.3 <i>Satellite cell self-renewal</i> | 19 |
| 1.1.4.4 <i>Contribution of other cell types to muscle regeneration</i> | 20 |
| 1.2 Primary Cilia | 21 |
| 1.2.1 <i>Structure and Function</i> | 21 |
| 1.2.2 <i>Ciliogenesis</i> | 23 |
| 1.2.3 <i>Ciliopathies</i> | 26 |
| 1.2.4 <i>Primary cilia and hedgehog signalling</i> | 28 |
| 1.2.5 <i>Primary cilia function in skeletal muscle</i> | 28 |
| 1.3 Sonic Hedgehog signalling | 30 |
| 1.3.1 <i>Overview of the pathway</i> | 30 |
| 1.3.2 <i>GLI proteins</i> | 32 |

| | | |
|------------------|---|-----------|
| 1.3.3 | <i>Shh</i> role in muscle development | 35 |
| 1.3.4 | <i>Shh</i> role in muscle regeneration | 36 |
| 1.4 | Talpid 3 (Ta3)..... | 38 |
| 1.4.1 | <i>Discovery of the Talpid3 mutant</i> | 38 |
| 1.4.2 | <i>The Talpid3 gene (KIAA0586)</i> | 38 |
| 1.4.3 | <i>The Talpid3 protein</i> | 39 |
| 1.4.4 | <i>Talpid3 functions elucidated by studying Talpid3 mutants</i> | 39 |
| 1.4.5 | <i>Creation of the Talpid3 mutant mouse</i> | 42 |
| 1.4.6 | <i>Sonic hedgehog signalling in Talpid3 mutants</i> | 43 |
| 1.5 | Project Aims and Hypotheses | 45 |
| | | |
| Chapter 2 | Materials and Methods | 46 |
| 2.1 | Mouse lines | 46 |
| 2.1.1 | <i>Conditional Talpid3 mutant mice</i> | 46 |
| 2.1.2 | <i>Reporter mouse lines</i> | 47 |
| 2.1.3 | <i>Animal maintenance</i> | 47 |
| 2.2 | Molecular biology techniques | 47 |
| 2.2.1 | <i>Genotyping PCR</i> | 47 |
| 2.2.2 | <i>Agarose gel electrophoresis</i> | 49 |
| 2.3 | Cardiotoxin (CTX) injection..... | 50 |
| 2.4 | Dissection of mice | 50 |
| 2.4.1 | <i>Tibialis anterior (TA) isolation</i> | 50 |
| 2.4.2 | <i>Single myofibre isolation</i> | 50 |
| 2.5 | Histology..... | 51 |
| 2.5.1 | <i>Cryosectioning</i> | 51 |
| 2.5.2 | <i>Immunolabelling on muscle sections</i> | 51 |
| 2.5.3 | <i>Immunolabelling on single myofibres</i> | 52 |
| 2.5.4 | <i>Immunolabelling on satellite cells in culture</i> | 52 |
| 2.5.5 | <i>Immunolabelling on C2C12 cells</i> | 53 |
| 2.5.6 | <i>Haematoxylin and Eosin (H&E) staining</i> | 55 |
| 2.5.7 | <i>X-gal staining for the detection of LacZ</i> | 56 |
| 2.6 | Tissue culture..... | 57 |

| | | |
|------------|---|-----------|
| 2.6.1 | <i>Culture of single myofibres in Collagen I gels</i> | 57 |
| 2.6.2 | <i>Outgrowth and culture of satellite cells</i> | 57 |
| 2.6.3 | <i>Culture of C2C12 myoblasts</i> | 58 |
| 2.6.4 | <i>Transfection of C2C12 cells</i> | 58 |
| 2.7 | Microscopy | 59 |
| 2.7.1 | <i>Imaging of muscle sections, single myofibres and C2C12 cells</i> | 59 |
| 2.7.2 | <i>Time lapse imaging</i> | 59 |
| 2.7.3 | <i>Imaging of satellite cells in culture</i> | 59 |
| 2.8 | Image analysis – Image J | 59 |
| 2.8.1 | <i>Muscle fibre diameter</i> | 59 |
| 2.8.2 | <i>Analysis of time lapse movies</i> | 60 |
| 2.9 | Statistics and Graphs | 60 |
| 2.9.1 | <i>Statistical analysis</i> | 60 |
| 2.9.2 | <i>Graphs</i> | 61 |

| | | |
|------------------|--|-----------|
| Chapter 3 | The loss of <i>Talpid3</i> in muscle satellite cells impairs muscle regeneration following injury | 62 |
| 3.1 | Introduction | 62 |
| 3.2 | Generation of <i>Talpid3</i> conditional knockout in skeletal muscle satellite cells | 63 |
| 3.2.1 | <i>Breeding strategies to generate tamoxifen inducible conditional <i>Talpid3</i> mutants</i> | 63 |
| 3.2.2 | <i>Genotyping of <i>Talpid3</i> cKO mice</i> | 63 |
| 3.2.3 | <i>Confirming the efficient recombination of the <i>Talpid3</i> locus</i> | 65 |
| 3.2.4 | <i>The effect of a <i>Talpid3</i> mutation on the presence of primary cilia in satellite cells</i> | 68 |
| 3.3 | Analysis of muscle regeneration following short-term removal of <i>Talpid3</i> in skeletal muscle satellite cells | 70 |
| 3.3.1 | <i>Tamoxifen induction and injury experiment protocol</i> | 70 |
| 3.3.2 | <i>Histological analysis of regenerating skeletal muscle following CTX injury</i> | 71 |

| | | |
|-------|---|----|
| 3.3.3 | <i>Quantitative analysis of regenerating skeletal muscle following CTX injury</i> | 73 |
| 3.3.4 | <i>α-Smooth Muscle Actin expression is prolonged in Pax7-Ta3^{ff} mutants</i> | 77 |
| 3.4 | Analysis of muscle regeneration following long-term removal of <i>Talpid3</i> in skeletal muscle satellite cells | 79 |
| 3.4.1 | <i>Tamoxifen induction and injury experiment protocol</i> | 79 |
| 3.4.2 | <i>Histological analysis of regenerating skeletal muscle following CTX injury</i> | 80 |
| 3.4.3 | <i>Quantitative analysis of regenerating skeletal muscle following CTX injury</i> | 82 |
| 3.5 | Analysis of <i>Talpid3</i> mutant satellite cells ability to self-renew . | 84 |
| 3.5.1 | <i>Tamoxifen induction and injury experiment protocol</i> | 84 |
| 3.5.2 | <i>Analysis of myofibres after double CTX injury</i> | 85 |
| 3.6 | Discussion | 88 |

Chapter 4 The loss of *Talpid3* in muscle satellite cells on their ability to migrate, proliferate and differentiate92

| | | |
|-------|---|-----|
| 4.1 | Introduction | 92 |
| 4.2 | Analysis of migration of <i>Talpid3</i> mutant satellite cells | 93 |
| 4.2.1 | <i>Migration speed</i> | 93 |
| 4.3 | Analysis of proliferation of <i>Talpid3</i> mutant satellite cells | 96 |
| 4.3.1 | <i>Timing of proliferation</i> | 96 |
| 4.3.2 | <i>Number of divisions</i> | 97 |
| 4.4 | Analysis of differentiation of <i>Talpid3</i> mutant satellite cells | 99 |
| 4.5 | Discussion | 102 |

Chapter 5 The effect of *Talpid3* loss in satellite cells on their expression of myogenic regulatory genes 106

| | | |
|-----|--|-----|
| 5.1 | Introduction | 106 |
| 5.2 | Analysis of SC number | 109 |
| 5.3 | The expression of Pax7 and Myf5 at SC isolation | 110 |

| | | |
|----------------------------------|--|------------|
| 5.4 | The expression of Pax7, Myf5 and MyoD at T24 | 112 |
| 5.5 | The expression of Pax7 and MyoD at T48 | 114 |
| 5.6 | The expression of Pax7, MyoD and Mgn at T72..... | 116 |
| 5.6.1 | <i>Terminal differentiation</i> | 116 |
| 5.6.2 | <i>Satellite cell self-renewal</i> | 118 |
| 5.7 | Expression of Pax7 and MRFs over time during SC activation and differentiation..... | 120 |
| 5.8 | Discussion..... | 121 |
| Chapter 6 Discussion..... | | 125 |
| 6.1 | Satellite cell proliferation | 126 |
| 6.2 | Satellite cell differentiation | 128 |
| 6.3 | Satellite cell self-renewal | 129 |
| 6.4 | <i>Ta3</i> mutations and primary cilia | 129 |
| 6.5 | <i>Ta3</i> mutations and Shh signalling..... | 130 |
| 6.6 | Other signalling pathways | 132 |
| 6.7 | Impact of research | 133 |
| 6.8 | Future research..... | 134 |
| Appendix 1 | | 136 |
| References | | 138 |

List of Figures

| | |
|--|----|
| Figure 1.1 Skeletal muscle structure..... | 3 |
| Figure 1.2 The inductive signals required for the differentiation of somites. | 5 |
| Figure 1.3 Regulation of myogenesis by specific temporal expression of MRFs..... | 10 |
| Figure 1.4 The structure and location of SCs on myofibres. | 12 |
| Figure 1.5 The basic structure of the primary cilium..... | 22 |
| Figure 1.6 Ciliogenesis and the cell cycle. | 25 |
| Figure 1.7 The Sonic Hedgehog pathway. | 32 |
| Figure 1.8 Structure of the Ci/GLI proteins..... | 34 |
| Figure 1.9 Ciliogenesis fails in <i>Ta3</i> mutants. | 41 |
| Figure 1.10 Cloning strategy for the generation of a <i>Ta3^{ff}</i> allele..... | 43 |
| | |
| Figure 3.1 Generation of a tamoxifen inducible, satellite cell specific Talp3 KO mouse line..... | 64 |
| Figure 3.2 The <i>Talp3</i> locus is efficiently recombined in satellite cells upon induction with tamoxifen in <i>Ta3^{ff}Pax7^{Cre-ERT2}</i> mice..... | 67 |
| Figure 3.3 Primary cilia on C2C12 cells | 69 |
| Figure 3.4 Satellite cell specific deletion of <i>Ta3</i> impairs muscle regeneration after CTX injury. | 72 |
| Figure 3.5 Method of quantitative analysis of minimum feret diameter using ImageJ software. | 74 |
| Figure 3.6 Myofibre size is significantly smaller after injury with CTX in satellite cell specific <i>Ta3</i> mutants..... | 76 |
| Figure 3.7 Satellite cell specific KO of <i>Ta3</i> leads to prolonged expression of α -SMA..... | 78 |
| Figure 3.8 Satellite Cell specific deletion of <i>Ta3</i> for an extended period impairs muscle regeneration following injury with CTX but does not affect muscle homeostasis..... | 81 |
| Figure 3.9 Muscle regeneration is not further impaired by the removal of <i>Ta3</i> for an extended period before injury. | 83 |
| Figure 3.10 Whole muscle sections following double cardiotoxin injury.. | 85 |

| | |
|---|-----|
| Figure 3.11 Satellite cell specific loss of <i>Ta3</i> results in limited SC self-renewal and loss of muscle regeneration after repeated CTX injuries. | 87 |
| Figure 4.1 Satellite cell specific loss of <i>Ta3</i> does not affect satellite cell migration speed. | 95 |
| Figure 4.2 Satellite cells specific loss of <i>Ta3</i> does not affect the time taken for SCs to divide after activation..... | 97 |
| Figure 4.3 Satellite specific loss of <i>Ta3</i> does not affect the number of divisions activated SCs go through..... | 98 |
| Figure 4.4 Satellite specific loss of <i>Ta3</i> disrupts differentiation ability of SCs in culture..... | 101 |
| Figure 5.1 Expression of MRFs during SC activation and differentiation | 107 |
| Figure 5.2 Tamoxifen and isolation protocol. | 108 |
| Figure 5.3 The average number of SCs per myofibre increases less over time in mice with SC specific loss of <i>Ta3</i> | 109 |
| Figure 5.4 The SC specific loss of <i>Ta3</i> leads to a reduction in MyoD expression at T0. | 111 |
| Figure 5.5 A SC specific loss of <i>Ta3</i> does not significantly affect the expression of Myf5 or MyoD at T24. | 113 |
| Figure 5.6 A SC specific loss of <i>Ta3</i> does not significantly affect the expression of Pax7 or MyoD at T48. | 115 |
| Figure 5.7 A SC specific loss of <i>Ta3</i> does not affect the expression of Mgn at T72. | 117 |
| Figure 5.8 The effect of a SC specific loss of <i>Ta3</i> on Pax7 expression at T72..... | 119 |
| Figure 5.9 Trend in expression of Pax7 and MRFs over 72hrs following SC activation and in vitro culture..... | 120 |

List of Tables

| | |
|---|-----|
| Table 1.1 Summary of MRF temporal expression during embryonic development..... | 8 |
| Table 1.2 Examples of single gene ciliopathies. | 27 |
| Table 2.1 Expected PCR product size for genotyping PCR..... | 48 |
| Table 2.2 Genotyping primer sequences | 48 |
| Table 2.3 Master mix for genotyping PCR..... | 49 |
| Table 2.4 Conditions for genotyping PCR..... | 49 |
| Table 2.5 Culture conditions of single myofibres | 51 |
| Table 2.6 Gelvatol recipe | 52 |
| Table 2.7 Primary antibodies used for immunolabelling | 54 |
| Table 2.8 Secondary antibodies used for immunolabelling..... | 55 |
| Table 2.9 Reagents for X-Gal Staining | 56 |
| Table 2.10 Reagents used for 4x Media to make collagen gels | 57 |
| Table 2.11 Reagents used to make collagen gels | 57 |
| Table 2.12 Reagents used for C2C12 myoblast media | 58 |
| Table 2.13 Interpretation of p value to assess statistical significance | 60 |
| Table 3.1 Mice used for short term regeneration experiments | 70 |
| Table 5.1 Number of SCs and myofibres analysed at each time point. ... | 106 |
| Table 5.2 Comparison of Pax7 and MRF expression in <i>Ta3</i> mutant and control SCs to published data..... | 123 |

Abbreviations

| | |
|---------------|-------------------------------------|
| α -SMA | Alpha smooth muscle actin |
| bp | Base pairs |
| BM | Basement membrane |
| BMP | Bone Morphogenic Protein |
| BSA | Bovine serum albumin |
| CTX | Cardiotoxin |
| C | Celsius |
| CKO | Conditional knock out |
| Cre | Cre-recombinase |
| CDK | Cyclin-dependant kinase |
| dpi | Days post isolation |
| Dhh | Desert Hedgehog |
| DMD | Duchenne Muscular Dystrophy |
| DMEM | Dulbecco's Modified Eagle Medium |
| EDL | Extensor digitorum longus |
| FAPs | Fibro/adipogenic progenitors |
| FGF | Fibroblast growth factor |
| Fig | Figure |
| FACS | Fluorescence activated cell sorting |
| GliA | Gli activator |
| Gli R | Gli repressor |
| g | grams |
| H&E | Haematoxylin and Eosin |
| Hh | Hedgehog |
| Hrs | Hours |
| Ihh | Indian Hedgehog |
| IFT | Intraflagella transport |
| IM | Intramuscular |
| IP | Intraperitoneal |
| KO | Knock out |
| LT | Long term |
| miRNA | micro-RNA |

| | |
|-----------|---|
| μg | micrograms |
| μl | microlitres |
| MTOC | Microtubule organising centre |
| mg | miligrams |
| ml | mililitres |
| Mgn | Myogenin |
| MHC | Myosin heavy chain |
| NGS | Normal goats serum |
| Pax | Paired box |
| PFA | Paraformaldehyde |
| Ptc | Patched |
| Pen/Strep | Penicillin and streptomycin antibiotic |
| PBS | Phosphate Buffer Solution |
| PM | Plasma membrane |
| PCR | Polymerase chain reaction |
| PDD | Processing determining domain |
| PKA | Protein Kinase A |
| RT-PCR | Reverse transcription polymerase chain reaction |
| SCs | Satellite Cells |
| S1P | Shingosine-1-phosphate |
| ST | Short term |
| SP | Side population |
| Smo | Smoothend |
| Shh | Sonic Hedgehog |
| SEM | Standard error of mean |
| Ta3 | Talpid3 |
| TA | Tibialis Anterior |
| TAD | Transcription activator domain |
| WT | Wild type |
| Wnt | Wingless |

Acknowledgements

Andrea Münsterberg. Thank you for all the guidance and support you have provided throughout this project. Although at times it has been tough, I am very grateful for the supportive and encouraging environment you have provided whilst completing my PhD.

Ulrike Mayer. Thank you for all the knowledge and technical wisdom you have brought to this project, it wouldn't have gone anywhere without your input.

Grant Wheeler and Ernst Pöschl. Thank you for all your input and advice.

Geoffrey Mok. As much as I want to say something derogatory, horrible or sarcastic... all I can really say is... I wouldn't be here without you! You know that dude!

Ines Desanlis. My best French friend! You made these 4 years worth it. Thank you for always being you, no matter how much it annoyed me at times... I know I have found a friend for life!

Nicole Ward. The first person I met in this crazy PhD journey and I'm so glad that you are still here at the end! You never failed to pull me out of a bad mood and always listened to my rants! Thanks for always being there!

Katy Saide. Thanks for being the most hilarious person I know, without even trying! You brightened up every situation... no really!

Adam Hendry, James McColl, Vicky Hatch, Angels Ruyra. Thank you all for making the lab somewhere I looked forward to going. You guys are the best!

Devina Divekar. Thank you for being a great source of advice and support! Your patience whilst I was learning techniques made everything so much easier.

Jamie Taylor. Thank you for being the smiling face to greet me in the BMRC and my partner in crime in lab meetings. You made each day a little more enjoyable.

Members of Münsterberg/ Wheeler lab. Thank you for all the support and knowledge you have provided over the years. I couldn't have asked for a better lab to work in.

Paul Thomas. Thank you for your expertise and patience. You were always on hand to answer any microscope or imaging problem I encountered.

DMU Staff. Without all your work behind the scenes research would not be possible. Thank you for all the knowledge, training and advice, it really did make working with the mice so much easier.

Craig Jacobs. I don't know how I would have done this without you. Even though you have been half way round the world for most of it, you have been my constant in this rollercoaster journey. I hope I can be as supportive for you when your turn comes.

Mum, Dad, Rhys, Aiden and the rest of my family. For your unconditional love and support I will be forever grateful, you have made me the person I am today. Some extra thanks are needed for you all putting up with me during the last few weeks of writing this... I know I was a nightmare to live with at times!

Chapter 1 Introduction

1.1 Skeletal Muscle

Skeletal muscle is by weight the largest organ in the human body, making up approximately 40% of total body weight and containing 50-75% of the body's proteins (Frontera and Ochala, 2015). Skeletal muscle is vitally important to health and wellbeing, contributing to many bodily functions, both mechanical and metabolic. Mechanically it can convert chemical energy to mechanical energy to produce force for movement and posture. Chemically it contributes to basal energy metabolism to produce heat and serves as a store of carbohydrates and amino acids that can be used by the body in times of starvation, stress and chronic illness. It is therefore of great importance that proper muscle structure and function is maintained.

1.1.1 *Structure of skeletal muscle*

The structure of skeletal muscle is characterised by its very ordered arrangement of muscle cells and their associated extracellular matrix (**Fig. 1.1**). An individual muscle is surrounded by a connective tissue layer called the epimysium, within which are bundles of muscle cells surrounded by their own connective tissue layer called the perimysium. Individual muscle cells (from here on referred to as myofibres) are multinucleated, post-mitotic cylindrical cells with a cell membrane known as the sarcolemma. Myofibres are large, 10-50µm in diameter (Lodish et al., 2000) and can range from 1-500mm in length depending on the muscle and species (Paul and Rosenthal, 2002). Myofibres can run the full length of the muscle from tendon to tendon (as in most muscles in humans and rodents) or will terminate intrafascicularly (rabbits, cats, cattle and chick) (Paul and Rosenthal, 2002).

As mentioned myofibres are multinucleated, with the nuclei, for the most part, being evenly spaced throughout the cell and located at the periphery. Exceptions are seen in the end plate and at some myotendinous junctions in which nuclei are observed at a higher density (Bruusgaard et al., 2003). Each nucleus has its own domain, known as the myonuclear domain, and is responsible for the synthesis of proteins required within that domain. After

synthesis organelles and structural proteins will remain in the vicinity of their creating nucleus (Pavlath et al., 1989).

The cytoplasm of myofibres, referred to as sarcoplasm, is filled mainly with myofibrils. Myofibrils are made up of myofilaments, the two most abundant being actin and myosin, arranged in a very ordered manner into structures known as sarcomeres that make up the basic contractile elements of skeletal muscle. It is the sliding of the actin and myosin filaments over each other that allows for force generation and contraction of skeletal muscle (Frontera and Ochala, 2015).

Other non-cellular components of skeletal muscle that are vital for function include a complex of proteins that are associated with the sarcolemma and connect to the internal myofilaments. Perhaps the most well studied of these is the dystrophin glycoprotein complex, which links the actin filaments with the sarcolemma and the extracellular matrix which stabilises the myofibres. Mutations in the dystrophin gene that lead to total or partial loss of dystrophin leave the sarcolemma destabilised making myofibres susceptible to injury during contraction. These mutations are responsible for the Duchenne and Becker muscular dystrophy disorders (Thomas, 2013).

Finally, residing between the sarcolemma of myofibres and the basement membrane, a specialised extracellular matrix, are the resident stem cells of skeletal muscle named satellite cells (SCs). SCs contribute to growth and homeostasis of skeletal muscle and are also the primary cell population responsible for repair and regeneration of myofibres following trauma or injury. More detail on SC structure and function is given in section 1.1.6.

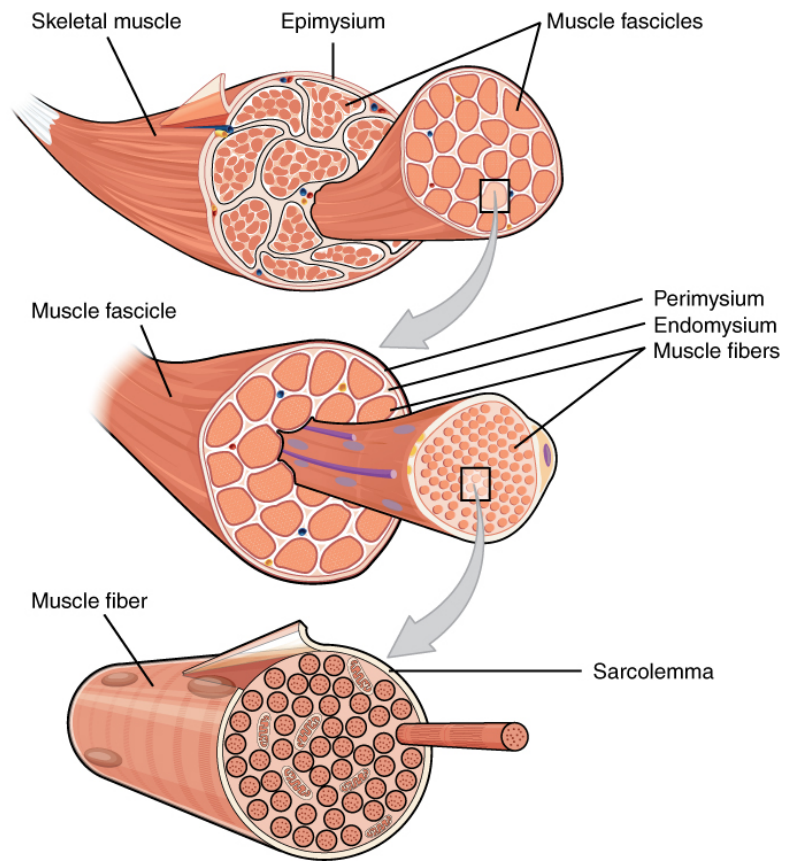


Figure 1.1 Skeletal muscle structure.

Skeletal muscle is composed of multinucleated myofibres, each of which is surrounded by a connective tissue layer known as the endomysium, bundled together into muscle fascicles and surrounded by the perimysium. Multiple muscle fascicles are surrounded by the epimysium and form the individual muscle. Image from (OpenStax, 2016)

1.1.2 ***Embryonic development of skeletal muscle***

All skeletal muscle found in vertebrates, except some muscles of the head and neck, develops from mesodermal structures that form either side of the neural tube and notochord known as somites. These transient structures start off as epithelial spheres; the ventral portion undergoes an epithelial to mesenchymal transition to form the sclerotome, a cartilage precursor cell layer, whilst the dorsal portion of the somite remains epithelial, forming the dermomyotome, a layer of skeletal muscle and dermis precursors. The dermomyotome can be further segregated into the medial and lateral portions; cells in the medial dermomyotome are precursors for the epaxial muscles of the back and intercostal muscles; cells in the lateral dermomyotome are precursors for the hypaxial muscle of the limbs and the remaining skeletal muscle (Ordahl and Le Douarin, 1992).

Following the initial segmentation of the somite, muscle precursor cells begin to migrate from the dermomyotome, either into other locations within the embryo such as the limbs or towards the anterior, or migrate below the dermomyotome to create a structure within the somite known as the myotome. From these locations precursor cells begin to differentiate into myoblasts (committed muscle progenitors), multiple myoblast will then fuse together to form multinucleated myotubes. The final maturation of skeletal muscle is the formation of myofibres from multiple myotubes. The molecular signals involved in this process have been well characterised over many years of research and are detailed in the following sections.

1.1.2.1 *Inductive signals controlling somitogenesis*

The development and specification of the somites is controlled by signals from surrounding structures; the neural tube, the notochord and the overlying ectoderm (Munsterberg and Lassar, 1995). Somite explant experiments and *in vitro* manipulation of chick embryos have been used to reveal the combinatorial signals required to induce myogenesis within the somite. These types of experiments allow for co-culture of somites with other tissues or the addition of growth factors to investigate the inductive signals and have revealed that it is a combination of Shh, Wnt and BMP signals that determine the differentiation of

the different layers of the somite (Munsterberg et al., 1995; Zammit et al., 2006) (Fig 1.2).

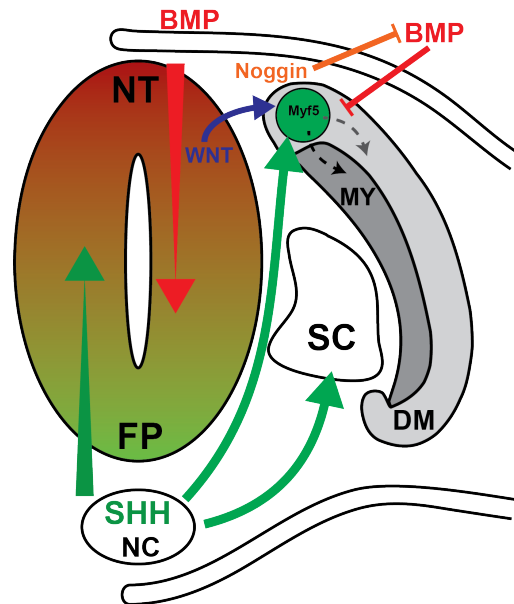


Figure 1.2 The inductive signals required for the differentiation of somites.

A combination of Shh, Wnt and BMP are required to pattern the somite. In the dorsal dermomyotome Wnt and SHH signals induce myogenesis through upregulation of Myf5. A combination of Shh and Wnt signals are required for the development of the dermomyotome, whilst Shh alone causes the differentiation of sclerotome. Repressive activity of BMP in the dorsal dermomyotome is inhibited by Noggin to allow cells migrating to the myotome to continue with a myogenic programme (black arrow), whilst other cells are exposed to high BMP and adopt a dermatome fate (grey arrow). NT= Neural tube, FP= Floor plate, NC= Notochord, SC= Sclerotome, DM= Dermomyotome, MY= Myotome. Adapted from (Gustafsson et al., 2002)

The early differentiation of somites and the specification towards the myogenic lineage occurs in a multistep process that requires specific spatial and temporal expression of *Sonic Hedgehog* (*Shh*) and members of the *Wingless* (*Wnt*) and *Bone Morphogenic Protein* (*BMP*) families. It was somite culture experiments with bacterially produced N-Shh and cells that expressed *Wnt-1*, *Wnt-3* or *Wnt-4* that showed a transient *Shh* signal with prolonged *Wnt* signals can stably induce myogenesis in the *ex vivo* tissue (Munsterberg et al., 1995).

1.1.2.2 Paired box (PAX) transcription factor family

The initial inductive signals of *Shh*, *Wnt* and the inhibitory signals of *BMP* (Reshef et al., 1998) together control the expression of a family of paired box (PAX) transcription factors. *Pax1* is expressed in the cells of the sclerotome and is maintained by continuous *Shh* signals, which alters the way in which these cells respond to BMP signalling, priming them for chondrogenesis (Munsterberg et al., 1995; Murtaugh et al., 1999) whilst *Pax3* is expressed initially in the pre-somitic mesoderm and throughout the whole early somite. *Pax3* expression is repressed by high levels of *Shh* and therefore becomes confined to the dermomyotome containing cells fated for the myogenic lineage (Cairns et al., 2008).

Following the initial acquisition of cell fate within the somite some cells fated for the myogenic lineage must delaminate and migrate away from the somite to produce distal muscles, such as in the limb. *Pax3* is required for this migration to occur. The spontaneous *Pax3* mouse mutant, *plotch*, shows a severe myogenic phenotype; this mutant has been used extensively to study the role of *Pax3* in skeletal muscle development. *In situ* hybridisation of wild type embryos at E9.5 showed *Pax3* expression in cells in the limb bud, this expression is not present in the homozygous *plotch* mutant (Bober et al., 1994), Dil labelling of somitic cells in wild type and homozygous *plotch* mutants revealed that it is not a failure of the *plotch* mutant cells within the limb bud to express *Pax3* but instead a failure of these cells to migrate from the somite. In wild type embryos Dil labelled cells were seen up to 300µm from the injection site however labelled cells failed to migrate further than 30µm in *plotch* mutants (Daston et al., 1996). The requirement for *Pax3* for myoblast migration is due to its ability to modulate the expression of *c-MET*. The upregulation of *c-MET* promotes the migration of myoblasts towards the c-MET ligand, hepatocyte growth factor/ scatter factor which is expressed in the limb bud (Epstein et al., 1996).

Pax3 also plays a role in the migration of myoblasts into other regions of the embryo such as into the neck where myoblasts would contribute to the musculature of the throat and the tongue, this role was established following the

loss of *Myf5* positive cells in these areas in *Pax3* mutant mice (Tajbakhsh et al., 1997).

Once commitment to the myogenic lineage has been established there must be some regulation that allows the maintenance of the precursor pool whilst also allowing the differentiation and maturation into skeletal muscle. This is controlled in part by *Pax3* and members of the Fibroblast Growth Factor (FGF) family. FGF is a potent stimulator of proliferation in myoblast cells and must be downregulated in order for myoblasts to differentiate (Clegg et al., 1987). Interference of the FGF pathway by upregulating a mediator of the pathway, *Sprouty1*, prevents *Pax3/Pax7* positive myogenic cells from progressing through the muscle differentiation programme (Lagha et al., 2008). *Fgf4* is a direct target of PAX3, established through the presence of a PAX3 binding site located in the 3' flanking region of the gene. Together with the evidence that PAX3 also directly targets the *Myf5* gene, this shows the importance of PAX3 in maintaining a balance between stem cell maintenance and tissue differentiation.

Another member of the PAX family, *Pax7*, is also expressed during muscle development. *Pax3* and *Pax7* appear to have both similar and divergent roles during muscle development. Replacement of *Pax3* with *Pax7* allowed for normal somite development and formation of the dermomyotome however development of limb muscles was completely abolished. This further supports the role *Pax3* plays in the migration of myogenic cells to distant muscle locations (Relaix et al., 2004).

1.1.2.3 *Myogenic regulatory factors (MRFs)*

Whilst some myogenic precursors will migrate to other areas of the embryo, the first differentiated muscle appears within the somite, forming a structure called the myotome, located just below the dermomyotome. Subsequently myogenic cells from the dermomyotome will delaminate and migrate into the myotome, at this point *Pax3* is downregulated and these cells rapidly differentiate activating a collection of myogenic determination genes. These genes are a group of basic helix-loop-helix transcription factors known as myogenic regulatory factors (MRFs) which are exclusively expressed in skeletal muscle progenitors and are very potent in inducing the formation of skeletal

muscle. Artificial expression of the MRFs in other cells types can force the expression of myogenic specific proteins and induce the formation of muscle fibres demonstrating their potency as myogenic determining factors. The ability of the four main family members, MyoD (Davis et al., 1987), Myogenin (Wright et al., 1989), Myf5 (Braun et al., 1989) and MRF4 (Rhodes and Konieczny, 1989), to convert fibroblast cell lines to a myogenic fate aided in their discovery as master regulators of myogenesis.

The temporal and spatial expression of the MRFs has been well characterised using *in situ* hybridisation and is summarised in **Table 1.1**. The function of each MRF has also been well characterised by examining the muscular phenotypes of mouse mutants with different combinations of MRF genes inactivated.

Table 1.1 Summary of MRF temporal expression during embryonic

| Somites | E8 | E8.5 | E9 | E9.5 | E10 | E10.5 | E11 | E11.5 | E12 | E12.5 | E13 | E13.5 | E14 | E14.5 | E15 | E15.5 | E16 | Birth |
|-------------|----|------|----|------|-----|-------|-----|-------|-----|-------|-----|-------|-----|-------|-----|-------|-----|-------|
| Myf5 | | | | | | | | | | | | | | | | | | |
| MyoD | | | | | | | | | | | | | | | | | | |
| Myogenin | | | | | | | | | | | | | | | | | | |
| MRF4 | | | | | | | | | | | | | | | | | | |
| Limb | | | | | | | | | | | | | | | | | | |
| Myf5 | | | | | | | | | | | | | | | | | | |
| MyoD | | | | | | | | | | | | | | | | | | |
| Myogenin | | | | | | | | | | | | | | | | | | |
| MRF4 | | | | | | | | | | | | | | | | | | |

The first of the MRFs to be expressed in the developing somite is *Myf5* and its expression is regulated by *Pax3*. The loss of *Pax3* results in a loss of *Myf5* expression in the hypaxial domain, conversely over expression of *Pax3 in vitro* can induce the expression of *Myf5* in mesodermal tissue in the absence of other inductive signals such as *Shh* and *Wnt* (Maroto et al., 1997). *Pax3* has been shown to act directly upstream of *Myf5* in the hypaxial dermomyotome and its derivatives by binding to a regulatory region that is located 5' to the *Myf5* locus (Bajard et al., 2006).

Following the formation of the dermomyotome and the myotome, there begins to be a distinction between the medial and lateral portions, distinguishing the epaxial and hypaxial muscle. This is particularly evident with the expression of *Myf5* which is first activated in medial, epaxial muscle precursors at E8.0 and

at E9.75 in hypaxial muscle precursors in mouse embryos. *Myf5* expression disappears from somites by E14 (Ott et al., 1991).

The expression of the 3 remaining MRFs; *MyoD*, *Myogenin* and *Mrf4* differ in their timing of expression in different regions within the embryo. In mice *MyoD* expression is almost simultaneous to that of *Myf5* in the head and limb muscle precursors (Buckingham, 1992) but is the last MRF to be expressed in the epaxial and hypaxial somites at around E10.5. In the somite *Myogenin* is expressed at E8.5 and *Mrf4* at E9.5 (Sassoon et al., 1989). Although *Myf5* appears to activate the expression of *MyoD* in the hypaxial domain of the somites, the function of these two MRFs seems to be somewhat compensatory. Mutant mice with a homozygous inactivation of *Myf5* do not show any defects in skeletal muscle formation at birth, however they do show a delay in the expression of muscle proteins such as actin and myosin heavy chain (MHC), which are absent in the somites of E9.5 *Myf5* mutants but present in wild types (Braun et al., 1992). Similar results were also obtained when mutating *MyoD* in mice; formation, morphology and protein expression were indistinguishable from wild types, however mutant mice did show a significant increase in *Myf5* expression in neonatal skeletal muscle, which in wild types is almost absent (Rudnicki et al., 1992). These findings suggest that *Myf5* and *MyoD* may be able to compensate for each other. To further investigate the roles of *Myf5* and *MyoD*, mouse mutants were generated that lacked expression of both factors. These mice were completely void of skeletal muscle, showing that presence of either *Myf5* or *MyoD* is essential for muscle formation, but they are in part functionally redundant. The double mutants do not form myoblasts, suggesting that *Myf5* and *MyoD* play a role in the determination and differentiation of initial myoblasts (Rudnicki et al., 1993).

Analysis of *Myogenin* (*Mgn*) and MRF4 (also known as *Myf6*) mutants details sequential roles for these MRFs as myogenesis progresses. Mice with mutations in *Mgn* fail to form functional skeletal muscle while still generating a few isolated differentiated fibres surrounded by unfused cells in muscle developing regions. The levels of *MyoD* expression in E15.5 embryos suggests that these cells are committed myoblasts, but the lack of multi nucleated myofibres indicates *Mgn* plays a role in differentiation and fusion of myoblasts into myofibres. (Hasty et al., 1993).

The role of MRF4 has been somewhat harder to distinguish due to its biphasic expression throughout development. The initial phase is a short, transient phase of expression from E10-E11.5, which is followed by a second phase after E16. Expression in the second phase is prolonged, with MRF4 being the most abundantly expressed MRF postnatally (Bober et al., 1991). This biphasic expression suggests a potential early role for MRF4 in initial myoblast determination, supported by experiments in various *Myf5/MyoD* double mutants in which *Mrf4* expression is downregulated in some allelic variants but not others. In *Myf5/MyoD* double mutants in which *Mrf4* expression is maintained myogenesis is still able to occur (Kassar-Duchossoy et al., 2004). In *Mrf4* mutants there is a reduction in *Myf5*, *MyoD* and *Mgn* expression at E10. Suggesting a role for MRF4 in myoblast specification. The period of expression seen later in development during the foetal and postnatal stages suggests that MRF4 also plays a role in later myofibre formation, supported by the fact that *Mrf4* homozygous mutants show a reduction in some intercostal muscles between the ribs (Patapoutian et al., 1995; Vivian et al., 2000).

Using the spatiotemporal expression of MRFs along with the phenotypes of the mutants it is possible to construct a model of muscle development that details the factors involved in regulating and driving each stage of myogenesis, summarised in **Fig. 1.3**.

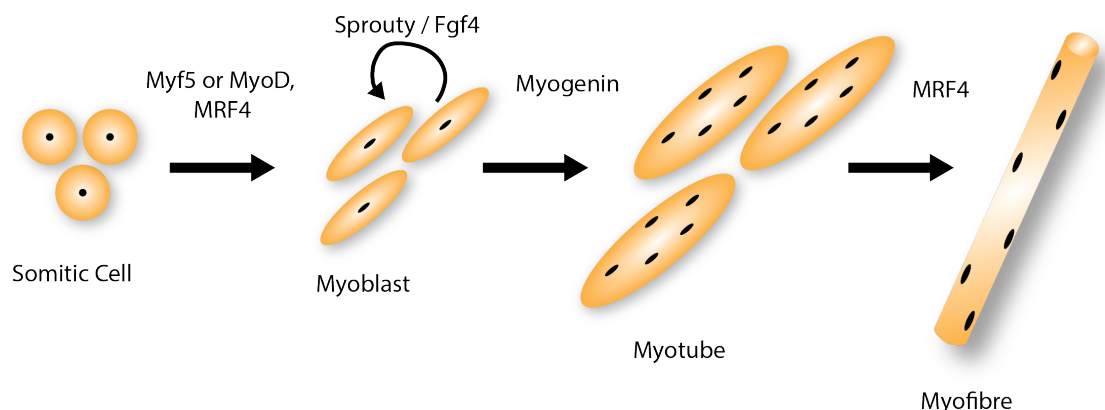


Figure 1.3 Regulation of myogenesis by specific temporal expression of MRFs.

Myf5 and *MyoD* are involved in the initial differentiation of somitic cells to primary myoblasts, however their functions are somewhat overlapping and can compensate for each other. There is also evidence that MRF4 may play a role at this stage, as a determining factor for the myogenic lineage. Myogenin is involved in the maturation and further differentiation of myoblasts to myotubes with MRF4 expression reappearing to induce maturation into myofibres. Adapted from (Rudnicki et al., 1993)

1.1.3 *Satellite cell structure and origin*

Satellite cells (SCs) are mononucleated, undifferentiated cells that were first observed independently by Alexander Mauro and Bernard Katz in 1961. They are resident stem cells in vertebrate skeletal muscle. Mauro described their location on the periphery of adult skeletal muscle fibres, between the plasma membrane (PM) and the basement membrane (BM) (**Fig. 1.4**). The SC has a distinct morphological appearance with the majority of the cell being taken up by the nucleus, leaving room for few organelles (Katz, 1961; Mauro, 1961). The nucleus is also significantly smaller than the myonuclei found within the myofibre (Watkins and Cullen, 1988).

Early labelling experiments with [³H]thymidine showed SCs in adult skeletal muscle are mitotically quiescent but can quickly enter the cell cycle and become mitotically active following muscle injury ((Snow, 1977) cited by (Yin et al., 2013)). These studies also demonstrated the ability of SCs to proliferate and give rise to myoblasts, contributing to myofibre nuclei during muscle growth and regeneration (Moss and Leblond, 1970; Reznik, 1969).

SCs were originally identified by their morphology and location within skeletal muscle. Nowadays many genetic and molecular markers are used to confirm the identity of a SC. The transcription factor Pax7 is expressed in all SCs and has become the canonical marker due to its specific expression in quiescent and early proliferating SCs across many species. Other transcription factors (Pax3, Myf5 and MyoD) and many membrane proteins such as, CD34, cMet, M-cadherin, integrin α 7 have also been used to identify SCs, however these are not unique to SCs in the adult organism and are not expressed in all SCs at a given time point, therefore Pax7 remains the most important marker (reviewed in (Yin et al., 2013)).

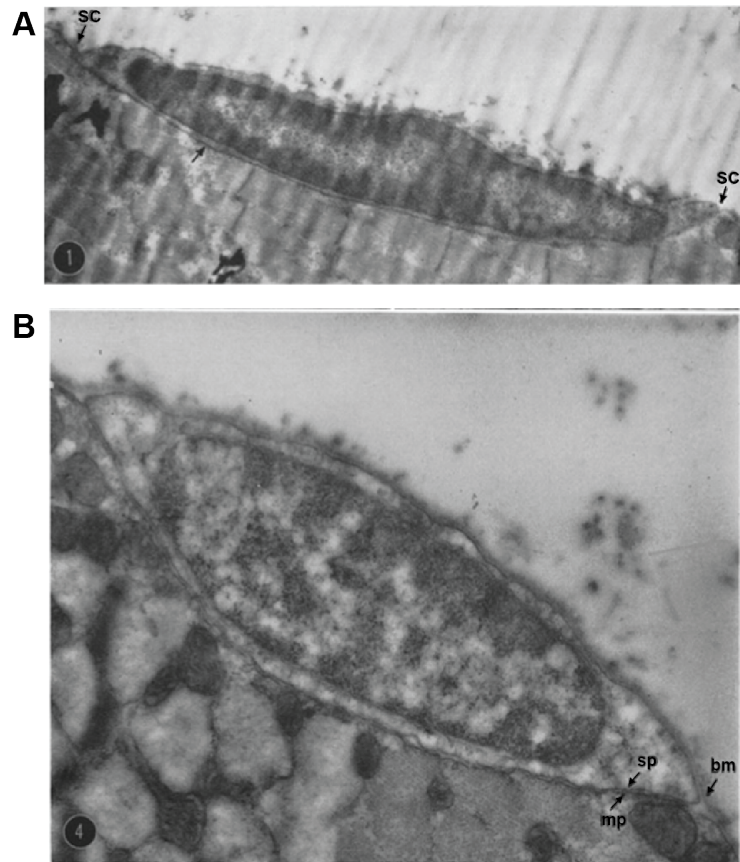


Figure 1.4 The structure and location of SCs on myofibres.

(A) A longitudinal view of satellite cells shows its presence on the periphery of the myofibre of the tibialis anticus of the frog. (B) A transverse section through the satellite cell on a rat sartorius myofibre reveals the close contact between the muscle cells plasma membrane (mp) and that of the satellite cell (sp) with the basement membrane overlaying the two (bm). Adapted from (Mauro, 1961)

The embryonic origin of SCs in adult skeletal muscle was first discovered using quail-chick chimera experiments in which quail somites were transplanted into developing chicken embryos. Using staining techniques to distinguish quail DNA from that of the chick, it could be seen that both myonuclei and SC nuclei contained quail DNA and were therefore of somitic origin ((Armand et al., 1983) cited in (Seale and Rudnicki, 2000)). The specific origin within the somite of SCs was not identified until many years later. GFP-labelling techniques and various *Pax3* reporter mouse lines have provided evidence that SCs, like myoblasts, originate from specific regions within the dermomyotome. Muscle

cells and SCs of the limbs develop from Pax3⁺ cells within the hypaxial dermomyotome (Schienda et al., 2006) whilst SCs located on muscles of the trunk originate from Pax3⁺ cells in the epaxial domain (Gros et al., 2005).

Having determined the somitic origin of the majority of SCs it is also important to note the timing of expression of Pax7 is different depending on the location of the developing SCs. Those cells originating in the central region of the dermomyotome and expressing both Pax3 and Pax7 migrate into the forming myotome. A proportion of these cells will then continue to proliferate and in late foetal stages become incorporated under the basal lamina of the developing muscle fibres within the trunk, these cells become the SCs of the postnatal trunk skeletal muscles (Relaix et al., 2005). In contrast, cells that migrate from the dermomyotome into the limb bud will express Pax3 but not Pax7 whilst migrating. Whilst only expressing Pax3 these progenitors remain multipotent and have the potential to give rise also to limb vasculature and muscle cells (Kardon et al., 2002). In the mouse, it is not until E11.5 that a population of these cells will begin to express Pax7 restricting them to the myogenic lineage (Hutcheson et al., 2009). Again, a proportion of these cells will withdraw from the cell cycle to become the SCs of the postnatal limb muscles.

As established, the majority of SCs have a somitic origin, however there is also an argument for a small portion of the SC pool to be of non-somitic origin. An unexpected finding from embryonic dorsal aorta explants showed they are able to give rise to myogenic precursor cells that have satellite cell like properties (morphology and expression of myosin). These cells expressed endothelial markers that true SCs also express and could contribute to foetal muscle growth and adult muscle regeneration (De Angelis et al., 1999) suggesting some SCs may be of a non-somitic origin. However, it has now been demonstrated that some cells of the somite are able to form both endothelial and myogenic lineages (Kardon et al., 2002), with later confirmation that some cells of the dorsal aorta are derived from the same Pax3⁺ population as myogenic cells, it is therefore possible that this relationship is due to having a common embryonic origin within the somite (Esner et al., 2006).

In foetal development for the determination of a cell to become a quiescent satellite cell (QSC) there must be the expression of Pax7, as shown

by the almost non-existence of satellite cell-like populations in surviving adult *Pax7* null mice (Seale et al., 2000). However, research by Lepper et al. (2009) suggested that the requirement of *Pax7* is restricted to the perinatal period. *Pax7*^{Cre/fl} mice in which *Pax7* expression is removed in adulthood by the administration of tamoxifen, appear to still undergo muscle regeneration. The distinction between the requirement of *Pax7*⁺ satellite cells and *Pax7* expression in already determined SCs was achieved by the use of *Pax7*^{+/CE;R26R}^{eGFP-DTA/lacZ} mouse to selectively ablate SCs upon induction with tamoxifen. In these mice muscle regeneration does not occur. This led to the conclusion that muscle regeneration is dependent on the presence of *Pax7*⁺ satellite cells but not necessarily on the active expression of *Pax7* (Lepper et al., 2011). However, it was later shown by von Maltzahn et al. (2013) and Gunther et al. (2013) that the level of recombination using the inducible *Pax7*-Cre lox system was highly dependent on the tamoxifen scheme used. Due to SCs amazing ability to proliferate and contribute to muscle repair any 'escaper' SCs that have not undergone recombination would be able to regenerate injured muscle, therefore producing results that appear to show *Pax7* null SCs repairing muscle. Using a tamoxifen scheme that minimised the possibility of 'escaper' cells later revealed a drastic loss of muscle regeneration following the removal of *Pax7*, concluding that *Pax7* is absolutely required for the normal function of SCs.

The satellite cells in uninjured muscle reside quiescently in their niche as indicated by their low metabolic rate, cytoplasmic volume and number of mitochondria (Montarras et al., 2013). Quiescence in stem cells is actively maintained through the production of intracellular inhibitors of signalling pathways such as *Sprouty1* (*Spry1*). QSCs express tyrosine kinase receptors that transduce IGF, FGF, HGF and PDGF signals, all of which can activate SCs. However, through the expression of *Spry1*, SCs can mitigate these signals and remain quiescent (Shea et al., 2010). Notch, BMP and Wnt signalling have also all been implicated in maintaining SC quiescence (reviewed in (Montarras et al., 2013)).

1.1.4 **Skeletal muscle regeneration**

As suggested in section 1.1.6 the primary function of SCs in the adult organism is to repair and regenerate skeletal muscle following injury. It has been shown by labelling Pax7⁺ satellite cells that all regenerated muscle fibres after injury develop from satellite cells (Murphy et al., 2011). Muscle regeneration occurs in a multistep process, starting with a period of muscle degeneration and an inflammatory response which leads to the activation, proliferation and differentiation of SCs, finally there is a period of myofibre maturation to restore muscle to its functional capacity.

1.1.4.1 *Muscle degeneration and inflammatory response*

Following an injury that causes damage to the muscle sarcolemma, there is a period of muscle degeneration. This involves cellular necrosis, promoting the breakdown of the plasma membrane, an influx of calcium and the activation of calcium dependent proteases which degrade myofibrils and other cellular proteins ((Armstrong, 1990) cited by (Yin et al., 2013)). This necrosis activates the inflammatory response prompting an influx of immune cells to the site of injury. The first immune cells to appear are neutrophils that can be detected within the first hour and can remain elevated for up to 5 days post injury (Tidball, 2005). The secondary influx of inflammatory cells is by macrophages which happens in two waves, the first being inflammatory macrophages (M1) that secrete pro-inflammatory cytokines and phagocytose necrotic debris, these reach their peak concentration within about 24hrs of injury. Following are the anti-inflammatory macrophages (M2) that secrete anti-inflammatory cytokines, reaching their peak 2-4 days after injury (reviewed in (Ciciliot and Schiaffino, 2010)). It is these M2 macrophages that are thought to be responsible in part for the activation and proliferation of myogenic precursors and SCs. Administration of macrophage enhanced medium has been shown to markedly increase the regenerative capacity of damaged muscle (Cantini et al., 2002). Conversely, suppression of M2 macrophages impairs muscle regeneration. More specifically, when M2 macrophages are impaired there is significantly less proliferation of SCs (Segawa et al., 2008).

1.1.4.2 *Satellite cell activation and differentiation*

The second stage of muscle regeneration is characterised by the activation, proliferation and differentiation of SCs. As mentioned earlier, SCs become activated in response to the influx of inflammatory cells, namely M2 macrophages, following injury. This prompts the SCs to re-enter the cell cycle and begin to proliferate. Multiple other signals have also been shown to trigger activation of SCs. Hepatocyte growth factor (HGF) was the first potent activator of SC proliferation to be discovered (Tatsumi et al., 1998). It can activate SCs both *in vivo* and *in vitro* however, its levels during muscle regeneration must be tightly regulated as it also inhibits differentiation. Injecting HGF into damaged limb muscles for three days after injury results in increased myoblast number but a reduction in muscle regeneration (Miller et al., 2000). Nitrous Oxide (NO) has been shown to play a regulatory role in this process. NO released following muscle injury stimulates the release of active HGF which then activates SCs by binding to c-Met on the SC surface promoting entry to the cell cycle (Tatsumi et al., 2006).

Sphingomyelin is a component of plasma membranes in many cell types across many species and acts as a reservoir of lipid metabolites. Sphingomyelin is expressed on quiescent but not activated SCs (Nagata et al., 2006a), one of its metabolites, sphingosine-1-phosphate (S1P) is a mitogenic factor and has been shown to play a role in SCs entering the cell cycle. As would be expected, if S1P is blocked SC proliferation is reduced and muscle regeneration is perturbed (Nagata et al., 2006b) demonstrating a requirement in SCs for sphingolipid signalling to enter the cell cycle.

The activation of SCs is not restricted to the immediate site of injury. It was established fairly early in SC research that SCs are able to migrate from a distant point on the myofibre to the site of injury ((Schultz et al., 1985) cited by (Yin et al., 2013)) and can even move from one myofibre to another crossing the basement membrane (Hughes and Blau, 1990). GFP-labelled muscle grafts have even shown the ability of muscle precursor cells to migrate between whole muscles (Jockusch and Voigt, 2003).

More recent research has also revealed the partial activation of SCs in muscles distant from the site of injury. In 2014, a new cell cycle state of QSCs was discovered and termed G_{Alert} . This state occurs in SCs via systemic signals

following an injury and is proposed as an adaptive state. SCs in G_{Alert} are able to enter the cell cycle more rapidly than those in G_0 leading to enhanced proliferation and differentiation (Rodgers et al., 2014).

After activation and a period of proliferation some SCs must begin to differentiate. The switch between proliferation and differentiation is controlled by a balance of Wnt and Notch signalling. Notch-1 is present on QSCs with activated Notch-1 levels increasing upon SC activation, this coincides with the expression of its ligand Delta. Expression of constitutively active Notch-1 in SCs in *ex vivo* culture increased myoblast proliferation and reduced differentiation and formation of myotubes, whilst over expression of a Notch inhibitor, Numb, results in a reduction in proliferation but an increase in myotube formation even in growth media (Conboy and Rando, 2002). These results suggest Notch is a potent mitogen that helps maintain SCs in a proliferative state following activation.

Using a TOPGAL reporter mouse, which expresses β -galactosidase in the presence of active β -catenin and therefore is a reporter of the canonical Wnt pathway, it has been shown that Wnt signalling is upregulated in SCs within 2-5 days of injury *in vitro* and increases progressively with time in cultured SCs isolated from myofibres. Artificial upregulation of the Wnt pathway by over-expression of Wnt-3A led to an accelerated myogenic lineage progression of activate progenitors in *ex vivo* culture. This was also mimicked *in vivo* with injections of Wnt-3A during the proliferative phase following injury, muscles were larger with a greater number of myotubes compared to controls suggesting a premature entry into a differentiation programme (Brack et al., 2008). This demonstrates the precise timing required for correct muscle regeneration as although there is an increase in myotubes, early differentiation can result in there not being enough myoblast to fully heal an injury. Having identified Notch signalling as an important regulator of SC proliferation and Wnt as a regulator of specification and differentiation (Polesskaya et al., 2003) it was shown that there is cross talk between the pathways via GSK3 β which allows for the switch from proliferation to differentiation by the reduction in Notch and increase in Wnt signalling (Brack et al., 2008).

As in embryonic muscle development, proper commitment, differentiation and maturation of skeletal muscle relies on sequential expression of the MRFs.

QSCs, in general, do not express MyoD, Mgn or MRF4. Approximately 90% of QSCs do express Myf5 as determined by the examination of SCs in *Myf5-LacZ* mice, suggesting the majority of SCs are already committed to the myogenic lineage (Beauchamp et al., 2000). These Myf5 positive SCs are also positive for CD34 and M-cadherin.

One of the first studies trying to characterise the temporal expression of the MRFs during SC activation used multiplex single cell RT-PCR and showed that at time 0 following myofibre and SC isolation all cells were Mgn and MRF4 negative with only very few expressing Myf5 or MyoD (it is likely that the technique was not sensitive enough to detect levels of Myf5). By 24hrs the majority of cells had begun to express Myf5 or MyoD alone (32%) or Myf5 and MyoD together (35%). Mgn positive cells started to appear after 48hrs and always coincided with expression of Myf5 and MyoD. MRF4 was also first detectable at 48hrs but was only ever seen in cells that were positive for all 4 MRFs (Cornelison and Wold, 1997). Mgn and MRF4 expression usually only occurs following one or more rounds of proliferation. However, it has been reported that MyoD, Desmin and Mgn can be detected in SCs 12hrs after injury without signs of proliferation, it has been suggested that these cells may be poised to differentiate without proliferation ((Rantanen et al., 1995) cited by (Yin et al., 2013)).

With the production of anti-MRF antibodies it was possible to begin to understand the expression pattern in SCs on a protein level which mimicked closely the findings from RT-PCR. During quiescence, very few SCs were MyoD⁺, by 24hrs MyoD protein expression could be detected in almost all SCs (Zammit et al., 2002). It should be noted that the SC population is heterogeneous and a very small number of SCs that are Myf5/CD34/M-cadherin negative do not express MyoD within the first 24hrs. The number of Myf5/CD34/M-cadherin negative cells does not change within the first 24hrs, suggesting this distinct population of SCs do not immediately activate upon isolation (Zammit et al., 2002).

The importance of MyoD in muscle regeneration has been demonstrated using *MyoD*^{-/-} mice that show a greatly decreased ability to undergo muscle regeneration but increase in the number of SCs following injury. This suggest

that in *MyoD*^{-/-} mice SCs are proliferating and undergoing self-renewal, but are not able to differentiate into myoblasts (Megenev et al., 1996).

The differing expression of Myf5 and MyoD in populations of SCs suggests that these transcription factors have different functions during adult muscle regeneration. While SCs from *MyoD*^{-/-} mice fail to differentiate but are able to proliferate (Megenev et al., 1996), SCs from *Myf5*^{-/-} mice show a defect in proliferation (Gayraud-Morel et al., 2007). It is suggested that Myf5⁺/MyoD⁻ SCs function to have increased proliferation with delayed differentiation, whilst Myf5⁻/MyoD⁺ SCs function to differentiate early. SCs that are Myf5⁺/MyoD⁺ are therefore somewhere intermediate in their proliferation and differentiation propensities (Yin et al., 2013).

The majority of SCs will enter the myogenic differentiation programme after a few rounds of proliferation with the expression of Mgn and MRF4 marking the initiation of terminal differentiation (Cornelison and Wold, 1997; Smith et al., 1994; Yablonka-Reuveni and Rivera, 1994) and exit from the cell cycle. This process is regulated by MyoD expression (reviewed in (Yin et al., 2013)). At this stage myoblasts begin to fuse to damaged fibres or to each other to begin repairing the damaged muscle.

1.1.4.3 *Satellite cell self-renewal*

The ability of SCs to self-renew is one of the hallmarks of them being stem cells. One of the key markers of SC self-renewal is the expression of Pax7. During regeneration, as SCs begin to differentiate Pax7 is downregulated. However, there is a small population of SCs that either maintain their Pax7 expression or re-express it after approximately 72hrs (Zammit et al., 2006). Stem cells can self-renew via two types of divisions; asymmetric division gives rise to one daughter cell that is destined for differentiation and one that retains its stem-ness to maintain the stem cell pool, whilst symmetric division gives rise to two daughter stem cells. Some stem cells will have a propensity to divide either symmetrically or asymmetrically, SC however have been shown to do both (Kuang et al., 2007; Le Grand et al., 2009).

Research has shown that Pax7⁺/Myf5⁻ or Pax7⁺/MyoD⁻ SCs often divide asymmetrically in an apical basal orientation on host myofibres producing one daughter cells that goes on to differentiate (Pax7⁺/Myf5⁺ or Pax7⁺/MyoD⁺) and

one daughter cell that exits the cell cycle to replenish the stem cell pool (Pax7⁺/Myf5⁻ or Pax7⁺/MyoD⁻) (Kuang et al., 2007; Zammit et al., 2006).

1.1.4.4 *Contribution of other cell types to muscle regeneration*

SCs have been shown to be the primary cell type required for skeletal muscle regeneration, however there is mounting evidence that other cell types also contribute. Through transplant experiments and lineage tracing it has been shown that bone marrow stem cells and pericytes can also contribute to regeneration of myofibres (reviewed in (Yin et al., 2013)).

Fibro/adipogenic progenitors (FAPs) play a unique role in the muscle regeneration process, they do not contribute to regenerating myofibres but instead proliferate in response to damage and become a pool of transient cells that provide pro-differentiation signals that enhance the rate of differentiation of myogenic progenitors (Joe et al., 2010).

Another cell type of particular interest is a population of multipotential progenitors known as side population (SP) cells. SP cells have been identified in several tissue types including muscle and are characterized by exclusion of Hoechst dye. Muscle derived SP cells initially express no myogenic markers but can differentiate into SCs and fuse to myofibres in injured or dystrophic muscle whilst also reconstituting the hematopoietic system in lethally irradiated mice (Asakura et al., 2002; Gussoni et al., 1999). These SP cells have been shown to still be present in Pax7^{-/-} mice and are therefore considered to have a distinct origin from SCs (Seale et al., 2000).

1.2 Primary Cilia

1.2.1 Structure and Function

Primary cilia are microtubular organelles that appear early in eukaryotic evolution. Whilst in non-vertebrates, such as *C. elegans* and *D. melanogaster*, cilia are only present on certain cell types, almost all vertebrate cell types are ciliated (Gerdes et al., 2009). Unlike motile cilia, the primary cilium is present as a solitary immotile organelle that projects from the apical membrane (Berbari et al., 2009). Cilia have 3 distinct domains; the basal body, the transition zone and the axoneme (**Fig. 1.5**). The basal body is docked into the cell membrane and consists of 9 microtubular triplets organised in a ring structure, these microtubules extend toward the cell surface until they reach the transition zone at which they extend as a continuum of doublets into the axoneme (Beisson and Wright, 2003; Gerdes et al., 2009). Unlike motile cilia, the primary cilium does not have a central pair of microtubules and its structure is referred to as 9+0 (**Fig. 1.5**) (Berbari et al., 2009). The basal body is derived from the mother centriole following exit from the cell cycle and organises the microtubular structure of the basal body and axoneme (Nigg and Raff, 2009). The microtubule structure is surrounded by a ciliary membrane which is continuous with the plasma membrane of the cell but is molecularly distinct.

The length of the primary cilium varies between cell types, ranging from 1-9 μm , with a width of approximately 0.2 μm (Scherft and Daems, 1967). It has been proposed that variations in cilium length will lead to variations in ciliary response pathways. Increased length will require less force for the cilium to bend, decreasing the threshold of Ca^{2+} influx. It will also increase cilium volume changing the concentration of ions, molecules and proteins within the axoneme. Finally, increased length will also increase the time required for cargo to be transported by intraflagellar transport (IFT) (Dummer et al., 2016). Although cilium length varies between cell types changes in length can occur due to injury or inflammation, in these instances cilium length could have effects on cellular function (Miyoshi et al., 2011).

In general, primary cilia function appears to be conserved. Primary cilia function as a signalling centre for the cell, able to detect both mechanical and chemical changes in the extracellular environment. Using IFT of molecules and receptors along the microtubules of the axoneme, primary cilia can transduce signalling pathways including, the Hedgehog (Hh), Wnt and PDGF signalling pathways (reviewed in (Berbari et al., 2009)). Primary cilia also function as mechanoreceptors: bending of primary cilia in MDCK cells (a line of canine kidney epithelial cells) leads to an increase in calcium signalling ((Praetorius and Spring, 2001) cited by (Berbari et al., 2009)). This function is especially important in kidney epithelial cells, mutations that affect primary cilia often lead to polycystic kidney phenotypes (Berbari et al., 2009).

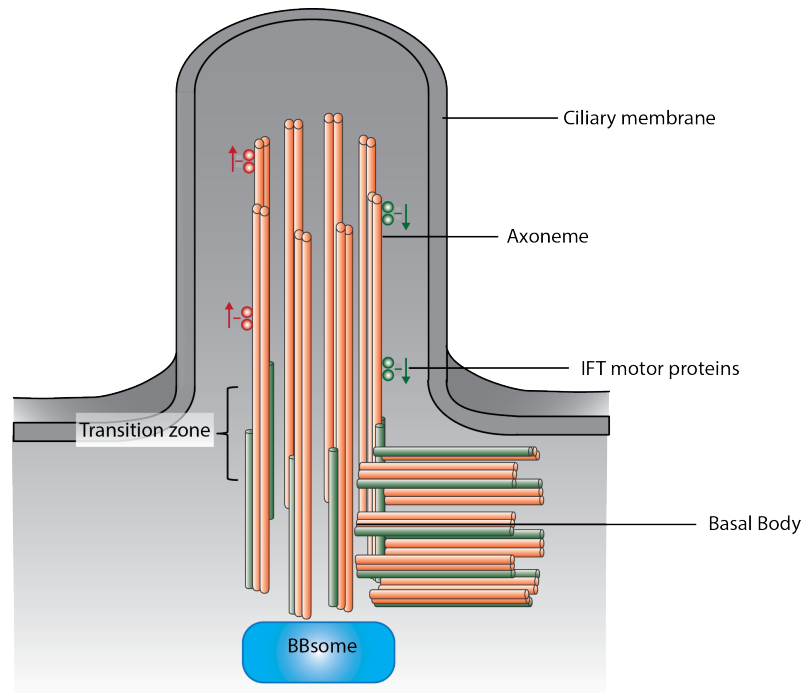


Figure 1.5 The basic structure of the primary cilium.

The primary cilium is composed of the basal body at the base of the structure, extending from this is the ciliary axoneme which is surrounded by the ciliary membrane. The region at the base of the axoneme that distinguishes the ciliary compartment from the rest of the cytoplasm is known as the Transition zone. Adapted from (Ainsworth, 2007)

1.2.2 **Ciliogenesis**

Unlike motile cilia which undergo *de novo* centriologensis, the primary cilium forms from an existing centrosome which becomes the basal body (Dirksen, 1991). The existing centrosome is composed of a mother and a daughter centriole. It is the mother centriole that contributes to the structure of the primary cilium. Because the centrosome acts as an anchor for both ciliary microtubules and mitotic spindles there are no reports of cells simultaneously having a primary cilium and mitotic spindles. Primary cilia are therefore regarded as post mitotic organelles and their assembly and disassembly occur in line with the cell cycle (Gerdes et al., 2009).

The complex mechanistic and molecular control of ciliogenesis remains to be fully understood. However, it has been established that ciliogenesis occurs synchronously with the cell cycle (reviewed in (Izawa et al., 2015)) (**Fig. 1.6**) and is initiated through de-repression of specific factors (Gerdes et al., 2009).

In brief, the assembly of the primary cilium is controlled by the loss of centriolar satellites, non-membranous electron-dense particles, which facilitates the accumulation of ciliary vesicles at the distal appendages of the mother centriole. Accumulation of more secondary vesicles leads to the production of a continuous vesicle that encapsulates the basal body and nascent axoneme (Kobayashi et al., 2014). The fusion of this vesicle to the plasma membrane creates the ciliary membrane compartment. Following the docking of the basal body the axonemal microtubules begin to extend beneath the membrane, this happens exclusively at the distal end of the cilium relying on IFT of proteins produced in the cytoplasm (Ishikawa and Marshall, 2011).

Centriolar satellites are associated with a complex of many proteins, some of which act to suppress ciliogenesis. CP110, a substrate of cyclin-dependant kinases (CDKs), strongly expressed through G₁ to S phase of the cell cycle, is one such protein that represses ciliogenesis. CP110 controls the duplication of centrosomes and its mutation or deletion leads to polyploidy (Chen et al., 2002). It has been identified that CP110 forms a complex with Cep97; the deletion of the CP110-Cep97 complex leads to the production of primary cilia in cycling cells, providing evidence for the repressive effective of this complex on ciliogenesis (Spektor et al., 2007). Other proteins that have

been identified to interact with this complex are Cep290, Kif24 and Rab8a (Kobayashi et al., 2014), the importance of which to ciliogenesis will be discussed in more detail in section 1.4.

As mentioned the outgrowth and elongation of the primary cilium is driven by IFT. After the cilium has reached full length it remains highly dynamic and continues to traffic proteins up and down the axoneme. New tubulin is continually accumulating at the distal tip of the axoneme, ciliary length is controlled however by the continued turnover of tubulin. This has been shown to be an active process that is regulated by IFT and the Kinase-13 molecular motor (Izawa et al., 2015).

The re-entry of cells into the cell cycle requires the disassembly of the primary cilium, this occurs through a shift in the balance of the dynamic assembly and disassembly of the axoneme. This process has been extensively studied in cell culture due to the ease in controlling culture conditions. Serum starved cells will arrest the cell cycle and become quiescent in G_0 allowing for the production of a primary cilium. Reintroduction of serum or particular growth factors to the medium prompts cells to re-enter the cell cycle which is accompanied by the re-absorption of the primary cilium. This process has been shown to be controlled by several proteins including human enhancer of filamentation (HEF1), Aurora A kinase, Pitchfork (Pifo) and Tctex-1. HEF1 and Aurora A kinase activate histone deacetylase 6 (HDAC6) which deacetylates microtubules allowing for cilium resorption (Kim and Tsiokas, 2011). The final stage of cilium disassembly involves the release of the basal body from the cell membrane, this is regulated in part by the Pifo protein. The release of the basal body frees up the centrosome to act as microtubule organising centre (MTOC) allowing cells to undergo mitosis (Izawa et al., 2015; Kobayashi and Dynlacht, 2011).

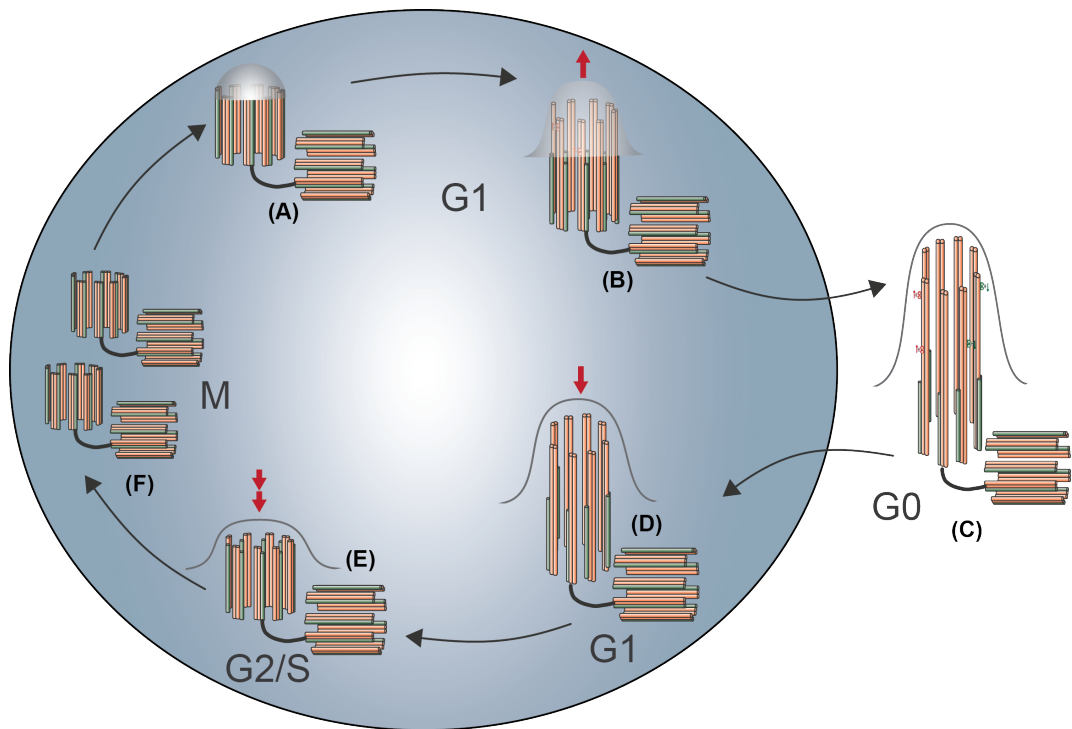


Figure 1.6 Ciliogenesis and the cell cycle.

Assembly of the primary cilia occurs during G1/G0 phases of the cell cycle. Upon cell cycle exit the centrosome migrates to the cell surface to form the basal body. Ciliary vesicles accumulate and encapsulate the mother centriole (A). Fusion of the ciliary vesicle with the plasma membrane creates the ciliary compartment and allows the assembly and elongation of the axoneme by IFT (B). Cells that have exited the cell cycle display a mature primary cilia (C). Cell cycle re-entry initiates the disassembly of the primary cilia (D, E). Finally, the basal body is released from the plasma membrane allowing the centrosome to act as a microtubule organising centre (F). Adapted from (Izawa et al., 2015)

1.2.3 *Ciliopathies*

The importance of primary cilia to normal development and homeostasis is demonstrated by the myriad of phenotypic abnormalities that arise from mutations in proteins associated with primary cilia. Syndromes that arise due to the malfunction of the cilium are collectively termed ciliopathies.

The presence of primary cilia is widespread within an organism therefore mutations in cilia genes often affect multiple tissues and organs. Common symptoms of ciliopathies include polycystic kidneys, retinal defects, changes in skeletal structure (polydactyly), infertility, liver fibrosis, situs inversus and mental retardation (Hildebrandt et al., 2011). Many of these symptoms are associated with developmental defects due to the requirement of primary cilia for normal signalling of the Shh and Wnt pathways which are essential for many developmental processes.

Due to the vast number of proteins associated with the correct structure and function of the primary cilium the genetic mutations that lead to symptoms of human syndromes often overlap (Powles-Glover, 2014). This can lead to a difficult diagnosis of the underlying genetic problem. However, syndromes have been identified that result from mutations in a single gene (summarised in **Table 1.2**) the severity of which is dependent on the type of mutation the patient has. For this reason, the severity and number of symptoms can vary greatly within the same syndrome.

Due to the high evolutionary conservation of primary cilia it is possible to utilise animal models to study their structure and function, whilst modelling mutations that lead to ciliopathies. *C. elegans*, green algae, zebrafish, *Xenopus* and mice are all extremely useful models in the understanding of primary cilia (Fry et al., 2014a).

Table 1.2 Examples of single gene ciliopathies.

Examples of ciliopathies that arise from mutations in a single gene. (Summarised from (Hildebrandt et al., 2011; Stephen et al., 2015)).

| Ciliopathy | Associated Genes | Symptoms |
|---|--|---|
| Joubert's Syndrome | NPHP3 NPHP6/CEP290 NPHP8/RPGRIP1L AHI1 MKS3 ARL13B INPP5E TMEM216 NPHP1 TALPID3 | <ul style="list-style-type: none"> • Mental Retardation • Ataxia • Retinal Coloboma • Irregular Breathing • Malformation of midbrain-hindbrain junction |
| Meckel's Syndrome | MKS1 MKS3 NPHP3 NPHP6/CEP290 NPHP8/RPGRIP1L TMEM216 CC2D2A | <p>Perinatal death due to malformation of multiple organs including;</p> <ul style="list-style-type: none"> • Lung hypoplasia • Polycystic Kidneys • Postaxial polydactyly • Situs inversus |
| Bardet Biedl Syndrome | BBS1 to BBS12 MKS1 NPHP6/CEP290 SDCCAG8 SEPT7 | <ul style="list-style-type: none"> • Retinal degeneration • Cystic kidney disease • Cognitive impairment • Diabetes mellitus • Obesity • Infertility • Polydactyly |
| Autosomal Dominant Polycystic Kidney Disease | PKD1 PKD2 | <ul style="list-style-type: none"> • End stage renal disease |
| Autosomal Recessive Polycystic Kidney Disease | PKHD1 | <ul style="list-style-type: none"> • End stage renal disease • Polycystic kidneys • Chronic liver fibrosis |

1.2.4 **Primary cilia and hedgehog signalling**

As mentioned the primary cilium is a key organelle for signal transduction within the cell. One of the pathways cilia are involved in is the sonic hedgehog (Shh) signalling pathway, which is of particular importance to this research. The discovery of its role in Shh signalling was due to phenotypic observations of mice with mutations in IFT proteins that presented very similarly to phenotypes that arise from a loss of function of *Shh*. Mutations in *wimple* (*wim*) and *flexo* (*fxo*), the mouse homologues of the intra-flagella transport genes *lft127* and *lft88* respectively, have been shown to be embryonic lethal with defects in neural tube closure, abnormal brain morphology and preaxial polydactyly; phenotypes very similar to those seen in *Shh* mutant embryos. Further analysis of these mutants showed the IFT proteins play a role in the Shh pathway at the level of GLI proteins (discussed in more detail in section 1.3) (Huangfu et al., 2003). The requirement for primary cilia to transduce hedgehog signalling is however unique to vertebrates, invertebrates with mutations in IFT proteins only exhibit phenotypes that suggest a dysfunction in cilia formation within neuronal cells (Huangfu et al., 2003).

Since the initial connection between Shh and the primary cilium was established many cilia associated proteins have been implicated in correct function of Hh signalling. These include many members of the IFT protein family (Cortellino et al., 2009; Qin et al., 2011), motor proteins such as KIF3a (Huangfu et al., 2003) and structural stability proteins such as ARL13b (Caspary et al., 2007). Analysis of these and many other mutants have confirmed the requirement of a structurally and functionally sound primary cilium for normal Shh signalling.

1.2.5 **Primary cilia function in skeletal muscle**

Primary cilia were reported to be present on CO25 myoblast cells in the 1990's ((Zeytinoglu et al., 1996) cited by (Fu et al., 2014)) however it wasn't until recently that primary cilia were functionally linked to skeletal muscle myoblast activity. Fu et al. (2014) demonstrated the dynamic presence of primary cilia on C2C12 myoblast cells during cell differentiation. They showed that primary cilia are present during the early stages of differentiation but are

gradually lost as the process occurs. By disrupting the formation of primary cilia by miRNA silencing of cilia genes they showed the requirement for a primary cilium in muscle differentiation. In cilia deficient C2C12 cells the formation of myosin heavy chain (MHC) positive fibres was significantly reduced whilst proliferation was increased. This suggests a role for the primary cilium in cell cycle exit and the initiation of differentiation.

The presence of a primary cilium on SCs has also been confirmed, however it is restricted to QSCs. Primary cilia are disassembled on entry of SCs into the cell cycle, with re-assembly of a primary cilium being restricted to those undergoing self-renewal. It appears that the presence of a primary cilium on self-renewing satellite cells is not a passive process but plays an active role in the ability of SCs to re-establish quiescence. Disruption of primary cilia leads to a reduction in the number of SCs expressing *Pax7* after 72hrs in *ex vivo* myofibre culture, suggesting a reduction in the number of SCs re-entering quiescence (Jaafar Marican et al., 2016).

1.3 Sonic Hedgehog signalling

The Hedgehog (Hh) gene mutation was first discovered and characterised in 1980 in the fruit fly, *Drosophila melanogaster*, during a large scale screen to identify genes that change or impair normal larval body plan patterning (Nusslein-Volhard and Wieschaus, 1980). Hh DNA from *Drosophila* was first cloned in 1992 (Mohler and Vani, 1992) and since then Hh homologues have been found and cloned from many vertebrate and invertebrate species including; *Hirudo medicinalis* (leech), *Diadema antillarum* (sea urchin) *Mus musculus* (mouse), *Danio rerio* (zebrafish), *Gallus gallus* (chicken) *Rattus rattus* (rat) and human (Varjosalo and Taipale, 2008).

Due to evolutionary duplication events, higher vertebrates including mammals have multiple copies of the *Drosophila* Hh gene that have been named *Desert hedgehog (Dhh)*, *Indian hedgehog (Ihh)* and the most well studied *Sonic hedgehog (Shh)* (Pathi et al., 2001). The areas of expression of these 3 proteins within the mouse embryo are largely distinct from one another (Bitgood and McMahon, 1995) and the mammalian Hh homologues have been shown to play roles in different developmental processes; *Shh* is important for the establishment of the left-right and anterior-posterior axes and the patterning of many tissues such as the limb, neural tube and somite, *Ihh* modulates chondrocyte differentiation and *Dhh* plays a role in germ-line proliferation and later stages of spermatogenesis (Pathi et al., 2001). SHH, DHH and IHH all signal through the same receptors and use the same transduction pathway, however, their potency and activity vary in different cell types, suggesting distinct roles for each protein during development (Pathi et al., 2001). From here on, this thesis will focus on Shh signaling due to its role in myogenesis.

1.3.1 Overview of the pathway

The Shh signalling pathway has been extensively studied; receptors, transduction molecules and response genes have all been classified with many fine details of their interactions being well characterised. The basic transmission of the Shh pathway is summarised in **Fig. 1.7**.

Activity of the SHH protein requires post-translational modification. This involves a cleavage event to produce the N-terminal “active” protein (SHH-N),

during this cleavage the C-terminus of SHH-N covalently binds a cholesterol moiety that allows the protein to be tethered to the plasma membrane. Tethering of SHH to the plasma membrane allows for controlled short range signalling, if unprocessed N-terminal SHH is expressed there is an expansion in cells that respond to the SHH signal suggesting it is having longer range effects (Porter et al., 1996). SHH has both short and long range activity in developing vertebrates. Dispatched (Disp) has been shown to control the short or long range activity of SHH by modifying the cholesterol anchor and releasing the active N-terminal SHH protein (Burke et al., 1999). This control allows for a gradient of SHH ligand to be produced, which is vital for the correct patterning of many embryonic structures.

Patched (PTC) is a twelve-transmembrane receptor protein that localises to the primary cilium and is the receptor for the Shh ligand. PTC has a constitutively repressive function on the Shh pathway, as demonstrated by the ectopic expression of Shh response genes when PTC is mutated (Ingham et al., 1991). In the absence of SHH ligand PTC has this inhibiting effect by repressing the function of another transmembrane receptor, smoothed (SMO) (Taipale et al., 2002). However, binding of SHH to PTC releases the inhibition on SMO. This relationship was established through observations that loss of *Shh* or *Smo* produce similar phenotypes, whereas loss of *Ptc* activity mimics an increase in *Shh* activity (Varjosalo and Taipale, 2008). The *Ptc* gene is also a target of the Shh pathway and its expression is upregulated with active Shh signalling, establishing a feedback loop that can fine tune and limit the activity of the pathway (Goodrich et al., 1996).

Following binding of SHH to PTC, the receptor is internalised sequestering SHH ligand and inactivating PTC. In the absence of active PTC, SMO is hyperphosphorylated causing a conformational change promoting the accumulation and localisation to the ciliary membrane where its activity can regulate downstream transcription factors, namely the Ci/GLI protein family (Corbit et al., 2005; Zhao et al., 2007).

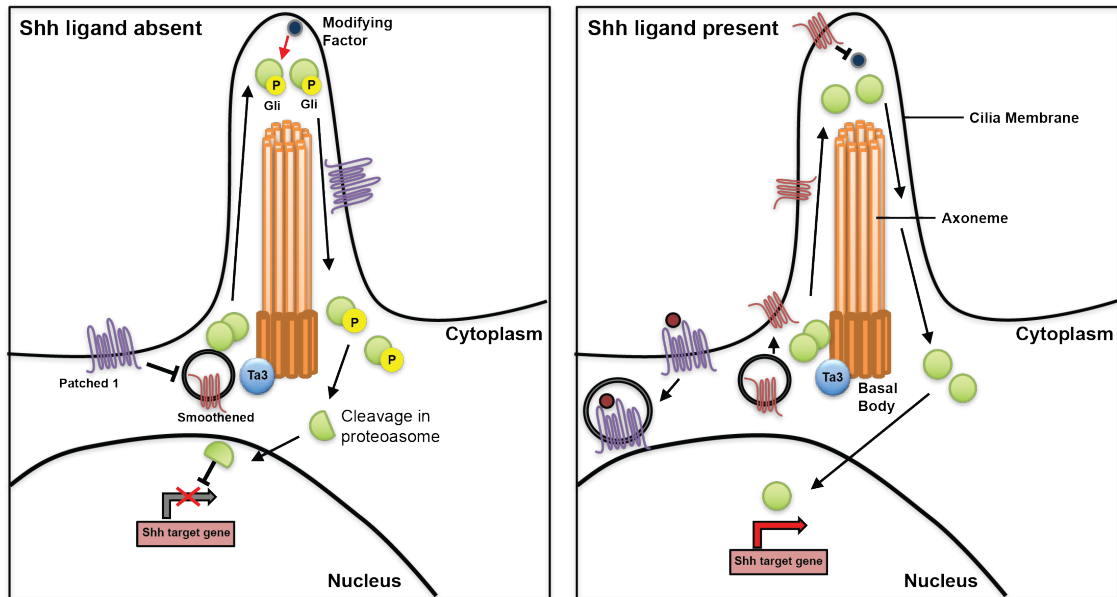


Figure 1.7 The Sonic Hedgehog pathway.

In the absence of a Hh ligand the transmembrane receptor PTC has an inhibitory effect on SMO preventing it from translocating to the cell membrane. This allows for the GLI proteins present internally in the cell to be phosphorylated, marking them for cleavage in proteasomes. When the GLI proteins are cleaved, they translocate to the nucleus and can act as repressors of gene expression. However, binding of SHH ligand to PTC causes internalisation of the complex removing the inhibition on SMO. SMO can then move to the cell membrane and inhibit the phosphorylation of the GLI proteins. Without the phosphorylation mark, the GLI proteins remain in their full-length form, translocate to the nucleus where they act as transcriptional activators. Adapted from (Varjosalo and Taipale, 2008).

1.3.2 *GLI proteins*

The Shh signalling pathway culminates in the regulation of a family of zinc finger proteins, the GLI proteins, that have dual roles as transcriptional activators/repressors of Shh response genes. *Drosophila* have one *Gli* gene, *Cubitus interruptus* (Ci) whereas, the *Gli* gene family in vertebrates consists of 3 members, *Gli1*, *Gli2* and *Gli3*. The activator/repressor function of these genes is regulated by post-translational modifications that are responsible for producing either full length activator protein (GLI^A) or cleaved repressor protein (GLI^R) (Hui and Angers, 2011).

The basic structure of GLI/Ci proteins consists of a N-terminal transcriptional repressor domain, zinc finger DNA binding sites and a C-terminal transcriptional activator domain (**Fig. 1.8**). However, it has been shown that

GLI1 contains only the C-terminal transcriptional activator domain, whilst GLI2 and GLI3 have both activator and repressor domains (Dai et al., 1999; Sasaki et al., 1999).

Due to its protein structure GLI1 has robust transcriptional activator activity, however, it has been shown to be dispensable for development and Shh signalling. *Gli1* null mice are viable and have no apparent phenotypes (Bai et al., 2002). GLI2 primarily acts as a transcriptional activator, with only a small portion of the GLI2^A being cleaved to the repressor form. GLI2^A is readily degraded in the absence of SHH, however active Shh signalling inhibits the processing and degradation of GLI2 allowing it to carry out transcriptional activation (Pan et al., 2006). GLI3, on the other hand, is readily processed into GLI3^R and therefore functions primarily as a transcriptional repressor (Wang et al., 2000). Both *Gli2* and *Gli3* have been shown to be essential for development and the transduction of the Shh pathway, mice with mutations in these genes are unable to respond to Shh and possess many developmental defects. Many mutations in the human *GLI2/3* genes have been linked to congenital malformations (reviewed in (Hui and Angers, 2011)).

Processing of GLI^A to GLI^R is mediated by phosphorylation events that mark the proteins for degradation by proteasomes. Ci, GLI2 and GLI3 all contain a processing determining domain (PDD) which appears to be critical for the partial processing to their respective repressor forms, removal of the PDD for Ci prevents the production of Ci^R (Methot and Basler, 1999). Consistent with its potent activator function GLI1 does not contain a PDD domain.

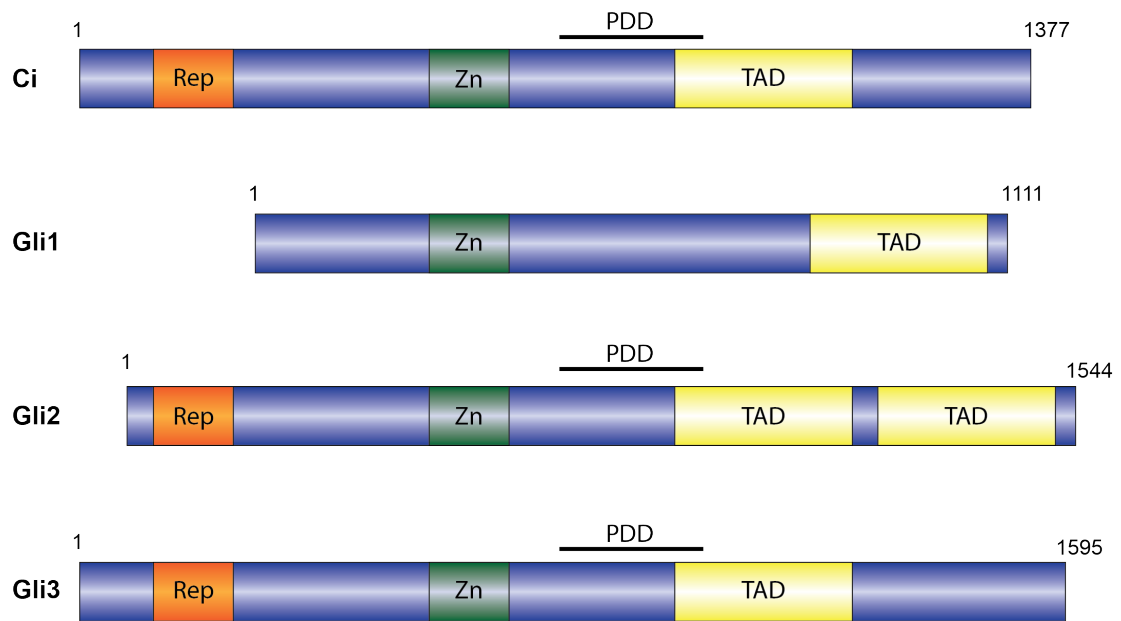


Figure 1.8 Structure of the Ci/GLI proteins.

Ci and Gli proteins are zinc finger transcription factors all containing zinc finger DNA binding domains (Zn). Ci, Gli2 and Gli3 all contain C-terminal repressor domains (Rep) and N-terminal transcription activator domains (TAD), however Gli1 only contain the TAD domain. Ci, Gli1 and Gli2 also contain a processing determining domain (PDD), crucial for processing into repressor forms. Adapted from (Hui and Angers, 2011).

The phosphorylation of GLI is carried out sequentially by Protein Kinase A (PKA), Glycogen Synthase Kinase 3 (GSK3) and Casein Kinases 1 (CK1). GLI2 and GLI3 contain six phosphorylation sites in their C-terminal end. It is the phosphorylation of the first 4 sites that leads to the processing into their repressor forms, whilst phosphorylation of the fifth and sixth sites inhibits their transcriptional activity, providing a mechanism of control of GLIA function (Niewiadomski et al., 2014) Although phosphorylation of GLI2 and GLI3 are carried out by the same kinases, these events lead to partial degradation of GLI3 and the production of GLI3^R whereas GLI2 usually gets completely degraded and very little GLI2^R is produced (Pan et al., 2006). The phosphorylation of GLI proteins is mediated in the Shh pathway by SMO, however the precise mechanism is unknown. Treatment of Shh responsive C3H10T1/2 cells with SAG, a synthetic SMO agonist, leads to the reduction of phosphorylated GLI2/3, providing evidence that it is the action of SMO within the Shh pathway that is mediating GLI^A/GLI^R levels (Li et al., 2017).

1.3.3 *Shh* role in muscle development

As previously mentioned the *Shh* pathway plays a vital role in the initial determination of myogenic precursors, sending inductive signals to the somite and promoting the specification of myogenic cells in the developing dermomyotome (Munsterberg et al., 1995; Munsterberg and Lassar, 1995). *In situ* hybridisation for *Myf5* and *MyoD* in *Shh*^{-/-} embryos provides evidence that the expression of these MRFs in the epaxial domain (dorso-medial dermomyotome) is dependent on *Shh*, however, expression in the hypaxial (ventro-lateral dermomyotome) domain is independent of *Shh* (Borycki et al., 1999). Using BrdU and TUNEL assays it was established that the loss in *Myf5* and *MyoD* is not due to a reduction in proliferative ability or an increase in apoptosis of cells in the epaxial domain, but due to the inductive role *Shh* usually plays in *Myf5* expression. The fact that *MyoD* expression is defective in cell explants from *Myf5*^{-/-} embryos even in the presence of ectopic *Shh* expression provides evidence that *Myf5* is the direct target of *Shh* induction, which in turn activates *MyoD* expression (Borycki et al., 1999).

As established, GLI proteins play an integral role in the transduction of the *Shh* pathway and in the activation or repression of *Shh* response genes. The expression of the *Gli* genes in somites has been characterised through *in situ* hybridisation. *Gli2* and *Gli3* are expressed in the anterior pre-somitic mesoderm but *Gli1* is not. *Gli1* is expressed in the ventral medial portion of newly formed somites and as the somite matures overlaps with *Pax1* expression specific to the sclerotome, *Gli1* is excluded from the dermomyotome. For a transient period at the onset of expression *Gli2* and *Gli3* are expressed throughout the somite but are soon restricted to areas of the myotome and dermomyotome (McDermott et al., 2005). This expression pattern suggests a role for *Gli2* and *Gli3* in myogenesis due to the overlap with *Myf5* (McDermott et al., 2005; Ott et al., 1991).

To confirm the role of the GLI proteins in *Myf5* expression *in situ* hybridisation for *Myf5* was carried out in various *Gli2* and *Gli3* mutants. The activation of *Myf5* in *Gli2*^{-/-} and *Gli3*^{-/-} single mutants is normal which suggests *Gli2* and *Gli3* are functionally redundant and can compensate for each other. In compound mutants of *Gli2/Gli3* however, *Myf5* expression is delayed in the epaxial domain of the dermomyotome, whilst in *Gli2*^{-/-}/*Gli3*^{+/-} or *Gli2*^{+/-}/*Gli3*^{-/-}

mutants *Myf5* expression is still present although is weaker than in wild types. These observations suggest that *Gli2* or *Gli3* is required for *Myf5* expression and one functional allele is sufficient to induce *Myf5* expression albeit to a lower level than wild types (McDermott et al., 2005).

Myf5 has been established as a direct target of long range Shh signalling. GLI proteins bind directly to its enhancer in cells of the epaxial somite, as demonstrated by its complete inactivity in *Shh* null embryo and partial activity in *Shh* heterozygous embryos (Gustafsson et al., 2002). Taken together this provides evidence for Shh signalling being vitally important for skeletal muscle development.

1.3.4 ***Shh* role in muscle regeneration**

The function of the Shh signalling pathway has been recognised as vital in normal embryonic development but was thought to have a very minimal role within the adult organism. However, over the past decade the importance of Shh in maintenance and proliferation of adult stem cells and its role in the development of some cancers has started to become apparent. This thesis will focus on investigating the role of Shh in adult skeletal muscle stem cells.

Shh has been shown to play a role in the normal development of skeletal muscle, both through promoting proliferation of muscle precursor cells and by directly targeting muscle specific transcription factors. It is therefore reasonable to assume that *Shh* may play a similar role in muscle regeneration as the two processes follow very similar molecular and morphological pathways.

In vitro studies using isolated SCs from mouse and chick provided the first link that Shh signalling could be involved in muscle regeneration. SCs and primary myoblasts cultured with SHH showed an increase in *Ptc1* and *Gli1* transcripts, this increase was not seen if the cells were also cultured with cyclopamine, a SMO inhibitor, showing these cells are able to specifically respond to SHH signals (Koleva et al., 2005). These culture experiments have also shown Shh signalling can increase proliferation and promote differentiation. Incubation with SHH results in increased incorporation of BrdU and the expression of *Mgn* and *MHC* (Elia et al., 2007; Koleva et al., 2005), again these effects can be blocked with cyclopamine. This provides evidence

that Shh signalling is playing a role in the proliferation and differentiation of SCs and myoblasts *in vitro*.

Some of the first *in vivo* evidence of the involvement of the Shh pathway in skeletal muscle regeneration came in the late 2000's. Following injury through mechanical crush or cardiotoxin injection, Straface et al. (2009) showed there is a significant upregulation of *Shh* and *Ptc1* in skeletal muscle suggesting the pathway is active after injury. The normal regeneration pathway includes upregulation of *Myf5* and *MyoD* to induce differentiation of satellite cells into myoblasts. However, if the Shh pathway is blocked in regenerating muscle by administration of cyclopamine, this up-regulation is diminished, suggesting that Shh may play a role in the activation of *Myf5* and *MyoD* to allow for muscle regeneration (Straface et al., 2009).

Further evidence of the activity of the Shh pathway in skeletal muscle regeneration has been gathered using the *mdx* mouse, a disease model of human Duchenne Muscular Dystrophy (DMD). In DMD skeletal muscle is unstable due to the lack of dystrophin, leading to repeated rounds of muscle necrosis, degeneration and regeneration. As the disease progresses the ability of the muscle to regenerate declines and eventually leads to fibrosis of the muscle (Manning and O'Malley, 2015). Interestingly, the pattern of Shh signalling activity changes with the progression of the disease. *Ptc1* and *Gli1* expression is increased in 1 month old *mdx* mice compared to wild types, by 6 months expression is the same and by 12 months expression is significantly lower in *mdx* mice. This correlates with the amount of regeneration occurring at these stages of the disease, with the most occurring at a young age and very little as the mouse ages (Piccioni et al., 2014b). Treatment with plasmid DNA encoding for *Shh* has been shown to improve the ability of *mdx* mice and mice with age associated impairment of SCs to regenerate after injury (Piccioni et al., 2014a; Piccioni et al., 2014b), providing evidence that the Shh pathways plays a vital role in muscle regeneration.

1.4 Talpid 3 (Ta3)

1.4.1 *Discovery of the Talpid3 mutant*

The Talpid mutants are a group of 3 chicken mutants that are characterised by a distinct set of phenotypes including polydactyly, craniofacial abnormalities and shortened spinal column (Cole, 1942; Ede and Kelly, 1964a, b). The 3 mutants were independently discovered and are autosomal recessive mutations. The Talpid lethal was first described by Cole (1942), in which he observed fowl embryos to have shortened limbs, with a duplication in digits on both the forelimb and hindlimb which appeared to resemble the forelimb of a mole, which in latin is *Talpa*, leading to the group referring to these mutants as “Talpid lethals”. This discovery was followed closely by the *talpid2* and *talpid3* mutants (Abbott et al., 1959; Ede and Kelly, 1964a) Cole’s Talpid mutant has since become extinct, but experimental *talpid2* and *talpid3* flocks have been maintained which has allowed the identification of the genes responsible for these mutations as *C2CD3* (Chang et al., 2014) and *KIAA0586* (Davey et al., 2006) respectively.

1.4.2 *The Talpid3 gene (KIAA0586)*

Using the chick *talpid3* (*Ta3*) mutant in comparison with wild type chick DNA, the *Talpid3* mutation was mapped to the *KIAA0586* gene on chromosome 5 of the chicken genome. *KIAA0586* is ubiquitously expressed in wild type embryos, explaining the widespread phenotypic disruptions seen in *ta3* mutant embryos. Further analysis of *KIAA0586* orthologues across a number of vertebrate species including; Human, Dog, Mouse and *Xenopus*, revealed homology of all 30 exons however homologues were not found in the *Drosophila*, *C. elegans* or *Ciona intestinalis* invertebrate species (Davey et al., 2006). This analysis also revealed the *ta3* chick mutant arose due to a frame shift mutation following the insertion of a single thymine residue resulting in a premature in-frame stop codon. This premature stop produces a truncated protein of 366 amino acids rather than the 1524 amino acid protein produced in wild type embryos (Davey et al., 2006).

KIAA0586 was experimentally confirmed as the *talpid3* gene through complimentary rescue experiments in the chicken neural tube. Ectopic

expression of SHH in wild type neural tube induces ectopic expression of *Nkx2.2* and *Islet1*, dorsalises *Pax6* expression, induces *Ptc1* throughout the neural tube and reduces the ventral expression of *Pax7*. However, these changes do not occur in the *ta3* mutant, with only weak expression of *Ptc1*. When *ta3* neural tube was exposed to ectopic SHH and was also electroporated with a construct expressing KIAA0586 some misexpression was observed in line with ectopic SHH expression in wild types (Davey et al., 2006).

1.4.3 ***The Talpid3 protein***

KIAA0586 encodes a 1524 amino acid protein that when mapped to other vertebrate species revealed a highly conserved region between amino acids 498-585, downstream of the mutation that results in a truncated 366 amino acid protein and encoded by exons 11 and 12. This region is predicted to contain a single coiled-coil domain. Rescue experiments using the chick neural tube and various expression constructs revealed the need for the coiled-coil domain for the function of the protein. The highly conserved region (498-585 amino acids) that contains the coiled-coil domain is not sufficient to rescue *ta3* neural tube mis-patterning, however, it is absolutely required for the rescue to occur (Yin et al., 2009).

1.4.4 ***Talpid3 functions elucidated by studying Talpid3 mutants***

Talpid3 mutants of all species examined show a pleiotropic embryonic phenotype, mutants have widespread developmental defects in seemingly unrelated systems of the embryo (Ede and Kelly, 1964b). These phenotypes include unpatterned polydactyly, craniofacial defects including hypoteleorism, loss of endochondral bone formation, vascular defects and abnormal dorsoventral patterning of the neural tube, all leading to embryonic lethality (Buxton et al., 2004; Davey et al., 2007; Davey et al., 2006; Ede and Kelly, 1964a, b).

The phenotypes of all species with *Talpid3* mutations studied so far show very similar phenotypes. The only difference being the *ta3* chick does not show any abnormalities in left-right asymmetry, whereas *Ta3* mice and zebrafish do. The reason for this is still not fully understood, however a recent discovery that

very early stage *ta3* chick embryos have functional cilia is surprising, but a possible explanation. It has been hypothesised that there is potentially maternal TA3 protein present in the egg that allows the initial formation of primary cilia in the early embryo, resulting in normal functional cilia that then play a role in breaking the symmetry of the embryo. This idea is also supported by evidence from the *Ta3* zebrafish mutant (MZTalp3), which has maternal TA3 present and does not show a disruption in organ asymmetry, however when the maternal TA3 is not present the embryo shows a similar left-right phenotype as mice (Stephen et al., 2014).

From looking at the range of phenotypes that *ta3* mutant embryos present the conclusion was drawn that all the developmental defects were similar to phenotypes of embryos with defective Shh signalling.

By examining the phenotypes presented in the *ta3* mutant embryos and using in-depth molecular analysis, the role of *Ta3* in developmental processes is being unravelled. As previously mentioned the presentation of phenotypes such as polydactyly and hypoteleorism, point towards a role for *Ta3* in the Shh pathway. This being later confirmed by Lewis et al. (1999) who showed that components of the Shh signalling pathway were abnormally expressed in the limb of *ta3* mutants. They also further explained the pleiotropic phenotype by showing that some genes regulated by the Shh pathway are unresponsive to Shh signals such as *Gli1*; whilst other genes, namely *Ptc*, are significantly upregulated in *ta3* mutant limb bud tissue. This paper confirmed that the expression of SHH protein is normal in *ta3* mutants and began to explore the idea that *ta3* mutants have abnormal processing of Shh signals and downstream effectors (Lewis et al., 1999).

Another observation of phenotypic similarities of *ta3* mutants was with mouse embryos with mutations in intraflagellar transport (IFT) proteins, these mutants lack primary cilia. It has since been shown that *ta3* mutants also lack primary cilia which explains the disruption of Shh signalling. Using rescue experiments in *ta3* mutant chicken embryos, by electroporation of a construct encoding the full length chicken *Ta3*, it was confirmed that the loss of *Ta3* is what causes the lack of primary cilia. Furthermore, using an antibody against chicken TA3 it was identified that the gene encodes a centrosomal protein that is required for normal primary cilia assembly (Yin et al., 2009). More specifically

TA3 appears to play a role in vesicle fusion to the basal body, which allows for growth of the axoneme (as described in section 1.2.2). In *ta3* mutants migration of the centrioles to the apical region and maturation to basal bodies is not affected, however the basal body fails to dock into the apical membrane, resulting in failure of axoneme extension (Yin et al., 2009) (**Fig. 1.9**).

It is not only primary cilia, but all cilia that fail to form in *ta3* mutants. Formation of motile cilia is different to primary cilia in that the cell must undergo de novo centriologensis to form the basal bodies in these multi-ciliated cells. In *ta3* mutants multiple basal bodies form but again they fail to dock into the plasma membrane, it has been reported that centrosomes of normally multi-ciliated cells, in *ta3* mutants, are rarely seen near the apical surface (Stephen et al., 2013).

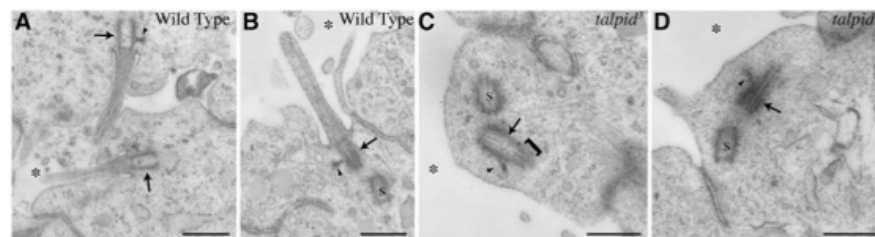


Figure 1.9 Ciliogenesis fails in Ta3 mutants.

TEM sections show basal body and mature ciliary axoneme of mature primary cilium in wild type embryos (**A-B**) whilst in *Taplid3* mutants basal bodies are still present but they have failed to dock into the membrane and there is an absence of the ciliary axoneme (**C-D**). Adapted from Yin et al. (2009)

The specific role of *Ta3* and the reason why the basal body fails to dock remains speculative. A couple of hypotheses were proposed by Yin et al. (2009) including a role for *Ta3* during the fusion of vesicles to the basal body. There is a complex of centrosomal proteins known as the BBSome that functions to activate Rab8, a GTP-ase that traffics ciliary membrane proteins to the base of the primary cilium (Nachury et al., 2007). It has been speculated that TA3 may be part of the BBSome. Rab8a is mislocalised when there is a depletion of *Ta3* in RPE1 cells (human retinal pigment epithelial cells) suggesting a potential involvement of TA3 in this complex (Kobayashi et al., 2014). However, there may be some problems in using this cell model to determine the function of *Ta3*, other aspects of cilium formation studied in this paper show different results

from the *ta3* chick model. For example, in *Ta3* depleted cells there is an accumulation of centriolar satellites around the centrosomes, which is thought to play a role in preventing ciliogenesis. This is not seen in *ta3* chicken embryos (Kobayashi et al., 2014). The precise role of *Talpid3* therefore, remains to be established.

1.4.5 **Creation of the *Talpid3* mutant mouse**

Since *Ta3* null embryos show lethality relatively early in development, the generation of a *ta3* mouse model that enables conditional knock-out of the *Ta3* gene is very useful to study the effects on later embryonic development. This has been achieved following the discovery that exons 11 and 12 of the *Ta3* gene are essential for TA3 protein function (Yin et al., 2009). Based on this a mouse line was created that contained loxP sites flanking exon 11 and 12 allowing for conditional deletion of *Ta3* function by Cre-recombinase (Bangs et al., 2011).

A classical approach using homologous recombination was used to create the targeting vector (**Fig. 1.10**), which was transfected into C57BL/6 ES cells. Successfully transfected cells were transferred to pseudopregnant NMRI mice. Chimeric mice were bred to C57BL/6 females and mice with successful germline transmission were identified by black coat colour. Confirmation of the presence of floxed *Ta3* (*Ta3^{ff}*) alleles was carried out by PCR.

Ta3^{ff} mice were crossed with a mouse line that ubiquitously expressed Cre-recombinase (Cre) to generate *ta3^{-/-}* mice. Analysis of *ta3* null mice confirmed the requirement of exons 11 and 12 for normal TA3 function, reminiscent of what had been seen in the chick mutant. *Ta3^{-/-}* mice show embryonic lethality at E10.5, have abnormal Shh signalling and lack primary cilia (Bangs et al., 2011).

With the generation of the *Ta3^{ff}* mouse it became possible to explore the role of *Ta3*, and subsequently primary cilia and Shh signalling, in later developmental and adult processes in a tissue specific manner. The first conditional knock out (CKO) of *Ta3* to be generated was limb specific using a *Prrx1-Cre* mouse strain, *Prrx1* is expressed in limb mesenchyme from E9.5 in the forelimb and E10.5 in the hindlimb. Examination of *Ta3* CKO limb

mesenchyme at E10.5 showed loss of primary cilia, however, endothelial cells retained their cilia, demonstrating specific loss of TA3 function in the mesenchyme. Fore- and hindlimbs of the CKO mutants showed polydactyl and soft tissue syndactyly. Skeletal formation also appeared to be affected as bones of the limbs were shorter with less ossification. Demonstrating the importance of TA3 to later stages of limb development (Bangs et al., 2011).

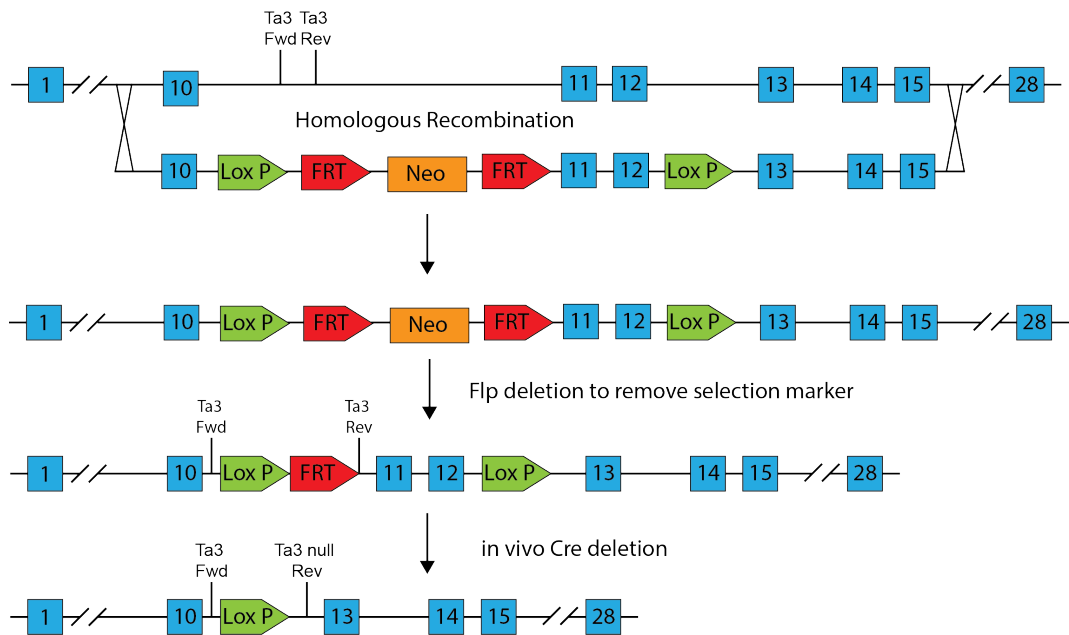


Figure 1.10 Cloning strategy for the generation of a *Ta3^{ff}* allele.

Homologous recombination was used to insert LoxP sites (green) flanking exons 11 and 12 of the mouse *Ta3* gene. Flp recognition target (FRT) sites (red) allowed for Flp deletion of the neomycin selection cassette (orange). Forward (*Ta3* Fwd) and Reverse (*Ta3* Rev) primer binding sites are shown, used to identify WT, *Ta3^f* and *Ta3⁻* alleles by PCR. Adapted from (Bangs et al., 2011)

1.4.6 *Sonic hedgehog* signalling in *Talpid3* mutants

Due to the failure of ciliogenesis in *ta3* mutants there are severe disruptions in the signalling cascade of the Shh pathway. As the release of the Shh ligand is not dependent on the presence of primary cilia it is not surprising that Shh expression in *ta3* mutants is relatively normal. There are slight variations between wildtypes and *ta3* mutants however, for example in the limb bud of *ta3* chick mutants there is an expansion of Shh expression into the middle portion of the bud, whereas Shh is restricted to the posterior portion in

wildtypes. This expansion coincides with an expansion in *Hoxd13* expression, a gene regulated by the Shh pathway. However, using cyclopamine to block Shh transduction, the expansion of *Hoxd13* is still present, showing this expansion is ligand independent (Davey et al., 2006). This observation combined with the fact that expression of *Ptc*, a component of the Shh receptor and a direct target of Shh, is significantly reduced in *ta3* mutants (Lewis et al., 1999), points to the possibility that disruption of Shh signalling is due to a disruption somewhere downstream in the pathway, potentially with the GLI proteins. A disruption in the GLI proteins would also explain the mix of gain of function and loss of function like phenotypes observed in the *ta3* mutants, possibly due to an increased level of GLI^A or GLI^R proteins.

In wildtype embryos the presence of both GLI3^A and GLI3^R is detected in the limb buds, with GLI3^R being expressed in a gradient, with maximum levels at the anterior (Wang et al., 2000). However, in the *ta3* chick mutant there is a significant increase in the expression of GLI3^A protein and a loss of the graded expression of GLI3^R, explaining the expansion of *Hoxd13* expression, and also explaining how there is still *Hoxd13* expression even after Shh is removed using cyclopamine (Davey et al., 2006).

The processing of GLI3 is affected in the majority of cilia gene mutations (Goetz and Anderson, 2010) however, there is very little evidence that the processing of GLI2 is also affected. Li et al. (2017) have begun to address this issue with the generation of a *Ta3* mutant mouse containing a *Gli2*^{FLAG} allele, revealing that GLI2^R protein levels were significantly reduced in *Ta3* mutant embryos. Confirming earlier findings by Davey et al. (2006), they also showed a reduction in the levels of GLI3^R in *Ta3* embryos. The reduction of GLI2^R and GLI3^R was due to a reduction in the phosphorylation of these proteins.

As previously mentioned, the phosphorylation of GLI is carried out in part by PKA. Co-immunoprecipitation of TA3 and two of the four subunits of PKA, PKAR1 α and PKAR1 β , showed that these proteins interact *in vitro*, more specifically using various *Ta3* mutant constructs it was shown that the C-terminal region of the TA3 protein is required for PKA interaction but not the middle or N-terminal regions. PKAR1 β and TA3 co-localize to the centrosome in wild type fibroblast cells lines however in about 25% of *ta3* mutant cells PKAR1 β was not localised to the centrosome which could account for some of

the reduction in GLI phosphorylation. Different regions of the TA3 protein appear to have different functional roles during TA3 ciliogenesis. Using *Ta3* mutant constructs it was shown that the N-terminal region allows centriolar localisation whilst the C-terminal region is required for ciliogenesis (Li et al., 2017).

1.5 Project Aims and Hypotheses

Multiple lines of research have shown the involvement of primary cilia and Shh signalling in the development and regeneration of skeletal muscle. *Ta3* mutants have been shown to display multiple phenotypes linked to the loss of primary cilia and a disruption in Shh signalling. However, to date there is very little data that shows the role *Ta3* plays in skeletal muscle development or regeneration. Therefore, this project aims to:

1. Investigate the effects of SC specific *Ta3* mutations on skeletal muscle regeneration after injury.
2. Investigate the effects of SC specific *Ta3* mutations on the ability of SCs to migrate, proliferate and differentiate.
3. Investigate the effects of SC specific *Ta3* mutations on the expression of MRFs during SC differentiation and self-renewal.

Hypothesis:

A SC specific loss of *Ta3* will disrupt normal SC function and the ability of skeletal muscle to efficiently regenerate following injury.

Chapter 2 Materials and Methods

2.1 Mouse lines

All mouse lines used in this study were obtained from collaborators and were bred on a C57BL/6 background. Breeding strategies were used to obtain mice that had the *Ta3* gene removed in adult SCs to study the role of *Ta3* in muscle regeneration and SC maintenance, differentiation and self-renewal.

For injury experiments female mice were used aged between 12-18 weeks. For myofibre isolation experiments both male and female mice were used that were at least 12 weeks of age.

2.1.1 *Conditional Talpid3 mutant mice*

The conditional *Ta3* mutant mice were a gift from Prof. Cheryl Tickle (University of Bath). These mice have exons 11 and 12 of the *Ta3* gene flanked by lox P sites (discussed in section 1.4.5). Homozygous *Ta3* floxed (*Ta3^{ff}*) mice were crossed with a mouse line expressing a Cre recombinase – ERT2 fusion protein that had been knocked into the *Pax7* locus obtained from The Jackson Laboratory (B6;129-*Pax7^{tm2.1(cre/ERT2)Fan/J}*). The resulting genotypes from the F1 generation, *Ta3^{f/+}//Pax7^{CreERT2/+}* mice were crossed with *Ta3^{ff}* mice to produce an F2 generation containing both *Ta3* heterozygous and homozygous mutants that are also *Pax7^{CreERT2/+}*. The line was maintained by crossing *Ta3^{ff}//Pax7^{CreERT2/+}* mice with *Ta3^{ff}//Pax7^{+/+}* or *Ta3^{f/+}//Pax7^{+/+}* to ensure mice remained heterozygous for *Pax7* expression. These mice were used in all experiments to study the effect of removing *Ta3* from SCs. Cre-mediated recombination of floxed alleles was induced by intraperitoneal (IP) injection of tamoxifen (Sigma, UK; T5648) at a dose of 3mg/40g body weight on 5 consecutive days followed by one rest day and a final injection. Tamoxifen was administered every other day during regeneration protocols.

2.1.2 **Reporter mouse lines**

Several reporter mouse lines were crossed with the $Ta3^{ff}/Pax7^{Cre-ERT2/+}$ mice to assess recombination efficiency and to visualise and track Pax7+ SCs. To assess recombination efficiency $Ta3^{ff}/Pax7^{Cre-ERT2/+}$ mice were crossed with *Rosa26-LacZ* mice; used for staining with β -galactosidase on muscle sections, or with *Rosa26-tdTomato* mice (Madisen et al., 2010); used for fluorescence imaging of SCs on single myofibres. To allow for ex vivo visualisation of WT and *Ta3* mutant SCs a $Pax7^{ZsGreen}$ mouse line was used (Bosnakovski et al., 2008).

2.1.3 **Animal maintenance**

All mice were maintained in accordance with Home Office regulations under specific pathogen free conditions in individually ventilated cages. Mice were weaned at approximately 3 weeks of age and separated by gender. Soon after weaning mice were ear tagged/notched and ear biopsies were taken for genotyping.

Experimental animals were sacrificed by cervical dislocation. Maintenance animals that were no longer required were sacrificed by exposure to increasing CO₂, in line with Home Office, Schedule 1 guidelines.

2.2 **Molecular biology techniques**

2.2.1 **Genotyping PCR**

Mouse genotypes were determined by PCR on genomic DNA extracted from ear biopsies. Biopsy samples were incubated in 50 μ l lysis buffer (0.1M TrisHCl pH8.5, 0.25M NaCl, 0.2% SDS, 5mM EDTA, 0.1mg/ml Proteinase K, Sigma H₂O) overnight at 55°C. Lysate was diluted 1:20 for PCR.

The product size of each band is detailed in **Table 2.1**. PCR primers are detailed in **Table 2.2**.

Table 2.1 Expected PCR product size for genotyping PCR

| Allele | PCR product size (bp) |
|-----------------------------|-----------------------|
| Talpid3 floxed | 470 |
| Talpid 3 wild type | 351 |
| Talpid 3 null | 273 |
| Cre/ Cre-ERT2 | 650 |
| ROSA26 – LacZ wild type | 600 |
| ROSA26 – LacZ mutant | 320 |
| ROSA26 – tdTomato wild type | 297 |
| ROSA 26 – tdTomato mutant | 196 |
| Pax7 ZsGreen | 300 |

Table 2.2 Genotyping primer sequences

| | | |
|-----------------|-------------------|------------------------------|
| Talpid3 | Forward | 5'-TGCCATGCAGGGATCATAGC-3' |
| | Reverse | 5'-GCTAGTACATTGCTGCAAGC-3' |
| | Null Reverse | 5'-GAGCACACTGGAGGAAAGC-3' |
| Cre | Forward | 5'-ATCCGAAAAGAAAACGTTGA-3' |
| | Reverse | 5'-ATCCAGGTTACGGATATAGT-3' |
| Rosa26 Lac Z | Mutant | 5'-AAGACCGCGAAGAGTTTGTGTC-3' |
| | Wild type | 5'-AAAGTCGCTCTGAGTTGTTAT-3' |
| | Wild type Reverse | 5'-GGAGCGGGAGAAATGGATATG-3' |
| Rosa26 tdTomato | | 5' -AAGGGAGCTGCAGTGGAGTA- 3' |
| | | 5' -CCGAAAATCTGTGGGAAGTC- 3' |
| | | 5' -GGCATTAAAGCAGCGTATCC- 3' |
| | | 5' -CTGTTCTGTACGGCATGG- 3' |
| Pax7 ZsGreen | Forward | 5' -CTGCATGTACCACGACTCCA- 3' |
| | Reverse | 5' -GTCAGGTGCCACTTCTGGTT- 3' |

PCR reagents were added to a master mix (**Table 2.3**) and aliquoted, 3 μ l of lysate was added to each reaction

Table 2.3 Master mix for genotyping PCR

| Reagent | Concentration | Volume per reaction |
|--------------------------|---------------|---------------------|
| Biomix Red (Bioline) | N/A | 12.5 μ l |
| Forward Primer | 10mM | 0.5 μ l |
| Reverse Primer | 10mM | 0.5 μ l |
| Sterile H ₂ O | N/A | 7-8.5 μ l |
| Final Volume | - | 25 μ l |

PCR reactions were subject to the following conditions;

Table 2.4 Conditions for genotyping PCR

| Stage | Temperature (°C) | Time | Cycles |
|-----------------|------------------|------------|---------------|
| Denaturation | 94 | 3 minutes | } X 30 cycles |
| Denaturation | 95 | 40 seconds | |
| Annealing | 58 | 40 seconds | |
| Extension | 72 | 30 seconds | |
| Final extension | 72 | 5 minutes | |

2.2.2 *Agarose gel electrophoresis*

Agarose (Sigma, UK) gels were made at a 1.5% concentration in 1x TAE buffer by warming. Ethidium Bromide (Sigma, UK) was added to the gel at a concentration of 0.5 μ g/ml. Electrophoresis was carried out at 90-100V for 30-60 minutes, depending on gel size. DNA was visualised using a UV trans-illuminator (BIO-RAD).

2.3 Cardiotoxin (CTX) injection

Mice were anaesthetised by isoflurane inhalation and muscle injury was induced with a 50µl intramuscular injection of cardiotoxin (100µM) into the right Tibialis Anterior (TA) muscle. The contralateral un-injured TA muscle was used as a control.

2.4 Dissection of mice

2.4.1 *Tibialis anterior (TA) isolation*

Following CTX induced injury and after the required period of regeneration (5, 10, 15 or 25 days) mice were sacrificed by cervical dislocation and the TA muscle was collected, pinned in a physiologically stretched position and frozen in isopentane cooled in liquid nitrogen. Muscles were stored at -80°C until required.

2.4.2 *Single myofibre isolation*

Following administration of Tamoxifen according to the schedules detailed in Chapter 3, Extensor Digitorum Longus (EDL) muscles were isolated from 8-14 week old mice and incubated in Collagenase I (2mg/ml, Sigma, UK) for 60-90 minutes at 37°C. After collagenase treatment muscles were transferred to BSA (Sigma, UK) coated dishes with deactivation medium (DMEM Glutamax media (Gibco), 1% PenStrep (Gibco)). EDL muscles were subjected to repeated trituration through descending diameter glass Pasteur pipettes until single myofibres separated from the isolated muscle. Single myofibres were selected and cultured in the conditions detailed in **Table 2.5** depending on their downstream use.

Table 2.5 Culture conditions of single myofibres

| Use | Culture Medium | Culture time |
|--------------------------------------|---|---------------------|
| Time-lapse imaging of live myofibres | DMEM, 20% FBS, 1% Chick embryo extract (CEE), 1% PenStrep | Up to 110 hrs |
| Immunofluorescence staining | DMEM, 10% Horse Serum, 0.5% CEE, 1% PenStrep | 24-96 hrs |
| Outgrowth of Satellite Cells | DMEM, 20% FBS, 10% Horse Serum, 1% CEE, 10ng/ml bFGF, 1% PenStrep | 72+ hrs |

2.5 Histology

2.5.1 *Cryosectioning*

Frozen TA muscles were mounted using a small amount of OCT (Tissue Tek – Agar Scientific) and sectioned at a thickness of 10 μ m. Sections were collected on Superfrost Plus slides and stored at -80°C until required.

2.5.2 *Immunolabelling on muscle sections*

Frozen sections were equilibrated to room temperature for 10-15 minutes before beginning the staining protocol. All washes were carried out at room temperature unless otherwise stated. Slides were washed in PBS for 10 minutes and fixed in 1% PFA for 10 minutes. Brief wash in 0.1% PBST and placed in ice cold methanol for 8 minutes followed by a brief wash in PBST. Slides were blocked in 5% Normal Goat Serum (NGS, Gibco) for 90 minutes at 37°C, then rinsed in PBST. Slides were incubated in Nidogen primary antibody (**Table 2.7**) in 2% NGS for 60 minutes at 37°C. Then washed x3 in PBST for 5 minutes. Slides were incubated in Alexa Fluor 488 secondary antibody (**Table 2.8**) in 2% NGS for 60 minutes. Slides were washed x3 in PBST for 5 minutes, incubated with DAPI (0.5 μ g/ml) for 5 minutes and washed x3 in PBST for 5 minutes. Slides were mounted with hydromount (National Diagnostics).

2.5.3 *Immunolabelling on single myofibres*

Single myofibres were fixed in 4% PFA for 8 mins at room temperature and then washed x3 in 1x PBS for 5 minutes. Fibres were permeabilized in 0.5% Triton-X (Sigma, UK) in PBS for 6 minutes at room temperature, washed in 1x PBS and incubated in blocking solution (10% NGS in 0.1% TBST) at 37°C for 90 minutes. Primary antibodies (**Table 2.7**) in 5% NGS were applied to fibres and incubated over night at 4°C. Following 3 washes in TBST for 15 minutes each, fibres were incubated in secondary antibodies (**Table 2.8**) in 5% NGS and DAPI (0.5µg/ml) for 1 hour at room temperature. Fibres were washed twice in TBST for 15 minutes followed by 1 wash in TBS only. Fibres were then mounted using gelvatol (**Table 2.6**)

Table 2.6 Gelvatol recipe

| Reagent | Amount | Final Concentration |
|---|--------|---------------------|
| 0.01M KH ₂ PO ₄ (pH to 7.2 with Na ₂ HPO ₄ .H ₂ O) | 80ml | 0.01M |
| NaCl | 0.65g | 0.14M |
| Polyvinylalcohol (Gelvatol, Type II, Sigma P-1836) | 20g | |
| Glycerin (Sigma) | 40ml | |

2.5.4 *Immunolabelling on satellite cells in culture*

SCs were fixed in 4% PFA for 15 minutes at room temperature and then washed x3 in 1x PBS for 5 minutes. SCs were permeabilized in 0.1% Triton-X (Sigma, UK) in PBS for 10 minutes at room temperature and incubated in blocking solution (10% NGS in PBS) at 37°C for 2 hours. SCs were incubated in MF20 primary antibody (**Table 2.7**) in 5% NGS over night at 4°C. Following 3 washes in PBS for 5 minutes each, SCs were incubated in secondary antibodies (**Table 2.8**) in 5% NGS and DAPI (0.5µg/ml) for 1 hour at room temperature. SCs were washed x3 in 1x PBS for 5 minutes and then stored at 4°C in PBS. Images were taken within 48 hours of immunostaining.

2.5.5 *Immunolabelling on C2C12 cells*

C2C12s were fixed in 4% PFA for 15 minutes at room temperature and then washed x3 in 1x PBS for 5 minutes. C2C12s were stored in PBS at 4°C or processed immediately as follows. C2C12s were permeabilized in 0.1% Triton-X (Sigma, UK) in PBS for 10 minutes at room temperature and incubated in blocking solution (10% NGS in PBS) at 37°C for 2 hours. C2C12s were incubated in Arl13b/ Acetylated alpha tubulin primary antibody (**Table 2.7**) in 5% NGS overnight at 4°C. Following 3 washes in PBS for 5 minutes each, C2C12s were incubated in secondary antibodies (**Table 2.8**) in 5% NGS and DAPI (0.5µg/ml) for 1 hour at room temperature. C2C12s were washed x3 in 1x PBS for 5 minutes and then stored at 4°C in PBS. Images were taken within 48 hours of immunostaining.

Table 2.7 Primary antibodies used for immunolabelling

| Antibody Target | Host Species | Dilution | Supplier | Catalogue code |
|-------------------------------|------------------------|-------------------|-----------------|-----------------------|
| Acetylated α -Tubulin | Mouse (monoclonal) | 1:100 | Sigma, UK | T7451 |
| Arl13b | Rabbit (polyclonal) | 1:100 | Proteintech | 17711-1-AP |
| Myosin (MF20) | Mouse (monoclonal) | 1:200 | DSHB | AB 2147781 |
| Myf5 | Rabbit (polyclonal) | 1:50 | Santa Cruz | SC-302 |
| MyoD | Mouse (monoclonal) | 1:50 | Santa Cruz | SC-377460 |
| Myogenin | Mouse (monoclonal) | 1:100 | DSHB | AB 2146602 |
| Nidogen 1 | Rabbit (polyclonal) | 1:2000 | U.Mayer | (Willem et al., 2002) |
| Pax7 | Mouse (monoclonal) | 1:100 | DSHB | AB 528428 |
| Talpid3 | Rabbit (polyclonal) | 1:1000/ 1:2000 | Proteintech | 24421-1-AP |
| α -Smooth Muscle Actin | Mouse (monoclonal) | 1:400 | Sigma, UK | C6198 |

Table 2.8 Secondary antibodies used for immunolabelling.

All secondary antibodies were used at a dilution of 1:500.

| Fluorophore name | Specificity | Supplier | Catalogue number |
|-------------------------|--------------------|-----------------|-------------------------|
| Alexa Fluor 488 | Goat anti-mouse | Invitrogen | A32723 |
| Alexa Fluor 488 | Goat anti-rabbit | Invitrogen | A-11034 |
| Alexa Fluor 568 | Goat anti-mouse | Invitrogen | A-11004 |
| Alexa Fluor 568 | Goat anti-rabbit | Invitrogen | A-11036 |
| Alexa Fluor 647 | Goat anti-mouse | Invitrogen | A32728 |
| Alexa Fluor 647 | Goat anti-rabbit | Invitrogen | A32733 |

2.5.6 Haematoxylin and Eosin (H&E) staining

Fresh 0.1% Eosin Y (Acros Organics) was prepared with distilled water and a few drops of glacial acetic acid. Mayers Hemalum (Merck/EMD millipore) was diluted 1:1 in distilled water. All solutions were filtered before use. Frozen sections were equilibrated to room temperature for 10-15 minutes before staining. All washes were carried out at room temperature. Slides were stained with Mayers Hemalum for 1-7 minutes with a brief wash in H₂O then 'blued' in running tap water for 15 minutes. Slides were stained with 0.1 % Eosin-Y for 30 seconds – 3 minutes, followed by a brief wash in H₂O. Slides were dehydrated through ascending concentrations of ethanol (70, 80, 95, 2x 100%) and placed in histoclear (National Diagnostics) for 7 minutes (x2). After staining slides were mounted with Depex (Fisher Scientific) mounting medium and left to air dry for 10-15 minutes.

2.5.7 X-gal staining for the detection of LacZ

Frozen sections were equilibrated to room temperature for 10-15 minutes before staining. Muscle sections were washed in 0.1M Phosphate buffer (**Table 2.9**) for 10 minutes, fixed in X-Gal fixation buffer (**Table 2.9**) and washed twice in Wash buffer (**Table 2.9**) for 5 minutes. Fresh staining solution was prepared from Core X-Gal buffer (Table 2.9) and X-Gal stock solution (Table 2.9). Staining solution was filtered before use on sections. Muscle sections were incubated in staining solution until LacZ staining was visible, approximately 24 hours. Following staining, muscle sections were washed twice in Wash buffer for 5 minutes, allowed to dry and mounted in hydromount (National Diagnostics).

Table 2.9 Reagents for X-Gal Staining

| Reagent | Ingredients |
|-----------------------|---|
| 0.1M Phosphate Buffer | NaH ₂ PO ₄ , Na ₂ HPO ₄ , H ₂ O |
| Fixation buffer | 5mM EGTA, 2mM MgCl ₂ , 0.2% Glutaraldehyde, 0.1M Phosphate Buffer |
| Wash Buffer | 2mM MgCl ₂ , 0.1M Phosphate Buffer |
| Core X-Gal Buffer | 2mM MgCl ₂ , 5mM K ₄ Fe (CN) 6-3H ₂ O, 5mM K ₃ Fe (CN) 6-3H ₂ O, 0.1M Phosphate Buffer |
| X-Gal Stock Solution | 500mg X-Gal, 10ml Dimethylformamide |

2.6 Tissue culture

2.6.1 Culture of single myofibres in Collagen I gels

Following isolation, single myofibres were plated on ice in a collagen I gel (Table 2.10 and Table 2.11) with 2 fibres per well of the inner 24 wells of a 48 well plate. The plate was then incubated at 37°C for 60 minutes for the gel to set. 200µl of medium was added to each well and incubated at 37°C for 60 minutes.

Table 2.10 Reagents used for 4x Media to make collagen gels

| Reagent | Volume |
|-------------------------|--------|
| 10X DMEM | 4ml |
| 100x pyruvate | 0.4ml |
| 0.5M NaHCO ₃ | 2ml |
| H ₂ O | 3.6ml |

Table 2.11 Reagents used to make collagen gels

| Reagent | Final Concentration | Volume |
|--------------------|---------------------|--------|
| 4x Media mix | - | 1.5ml |
| FBS | 20% | 1.2ml |
| H ₂ O | - | 720µl |
| 5 mg/ml Collagen I | 2mg/ml | 2.4ml |
| 0.1M NaOH | 230µl/ml | 480µl |
| Final Volume | | 6ml |

2.6.2 Outgrowth and culture of satellite cells

Following isolation, single myofibres were plated on Matrigel-coated (Scientific lab supplies) 12 well plates. Matrigel was briefly washed over the surface of each well and excess was removed. Matrigel was left to set at 37°C for 30 minutes before plating. Approximately 100-150 myofibres were plated per well in proliferation medium (Table 2.5). Myofibres were cultured for 72hrs to allow SCs to migrate from the myofibres, after which myofibres were removed. The remaining proliferation medium was removed, SCs were washed in PBS and treated with trypsin for approximately 5 minutes. SCs were re-suspended in

proliferation medium and re-plated on Matrigel. SCs were then cultured in proliferation medium for 9 days. Fresh medium was given every 3-4 days.

2.6.3 **Culture of C2C12 myoblasts**

C2C12 myoblast cells were cultured in growth medium (**Table 2.10**) in a 75cm² flask. Cells were maintained at a confluency no higher than 70% to prevent spontaneous differentiation. During maintenance, fresh medium was given every other day.

C2C12 cells were used for differentiation once they reached 80-90% confluency. They were then washed x2 with PBS to remove all growth medium and then exposed to differentiation medium (**Table 2.12**). During the differentiation process, fresh medium was given every day. Cells used for immunostaining were seeded onto poly-l-lysine-coated glass cover slips and grown in the conditions stated above.

Table 2.12 Reagents used for C2C12 myoblast media

| Media type | Reagent | Final Concentration |
|-----------------------|-----------------|----------------------------|
| Growth media | DMEM (GlutaMAX) | - |
| | Pen/Strep | 1% |
| | FBS | 10% |
| Differentiation media | DMEM (GlutaMAX) | - |
| | Pen/Strep | 1% |
| | Horse Serum | 2% |

2.6.4 **Transfection of C2C12 cells**

E. coli cells containing a pDEST-Arl13b12 plasmid (Addgene) were grown on LB medium over night at 37°C. DNA was extracted using a QIAGEN Plasmid Mini Kit (Qiagen, UK) according to manufacturer's instructions. DNA quantity and purity was measured using a nanodrop.

Proliferating C2C12 cells were plated on 6 well tissue culture plates and grown until 70% confluency at which point they were transfected with 4µg of pDEST-Arl13b12 plasmid per well using lipofectamine (Life Technologies) according to manufacturer's instructions.

Following transfection cells were washed twice in PBS and fixed in 4% PFA for 15 minutes at room temperature and then washed x3 in 1x PBS for 5 minutes.

2.7 Microscopy

2.7.1 *Imaging of muscle sections, single myofibres and C2C12 cells*

Brightfield and fluorescent images of muscle sections were taken using a Zeiss AxioPlan 2ie microscope. Images were captured using 20x PlanNeofluar objective (0.6NA) and a Zeiss AxioCam HRm CCD camera.

2.7.2 *Time lapse imaging*

Brightfield and fluorescent images were captured using a Zeiss Axiovert 200M inverted microscope. Images were captured using a 10x PlanNeofluar objective and a Zeiss AxioCam HRm CCD camera. An image was captured every 20 minutes for a duration of 94-96hrs.

2.7.3 *Imaging of satellite cells in culture*

Multiple phase 1 and fluorescent images were captured that represented areas in the middle and towards the edge of the culture dish using a Zeiss AxioVert 2 microscope. Images were captured using a 10x PlanNeofluar objective and a Zeiss AxioCam HRm CCD camera.

2.8 Image analysis – Image J

2.8.1 *Muscle fibre diameter*

Images of muscle sections stained with Nidogen antibody to visualise the basement membrane and DAPI to visualise the nuclei were used to analyse fibre diameter post injury.

Images were processed in Fiji (ImageJ) to subtract background, then converted to a binary image for better visualisation of fibre basement membranes. Areas of Nidogen staining that were lost when converting the image to binary were filled in using the paint tool. Minimum ferret diameter was measured using the Analyse Particles tool (further details in **Fig. 3.4**)

2.8.2 *Analysis of time lapse movies*

Migration speed of satellite cells on myofibres was analysed using the MTrackJ plugin (Meijering et al., 2012) with Fiji (ImageJ) software. In brief, SCs were followed frame by frame as they migrated along the fibre between divisions. MTrackJ produces data on distance between two points between frames, this was used to calculate the distance individual SCs had migrated over time, i.e. speed of migration.

Proliferation data was gathered by manually counting the number of divisions occurring during the time lapse movies.

2.9 Statistics and Graphs

2.9.1 *Statistical analysis*

All statistical analysis was carried out using Graphpad Prism 6 software. For all experiments, multiple data points were collected for each mouse which were used to generate the population mean. The population mean values were used for statistical analysis to compare between control and mutant mice.

Data was tested for Gaussian distribution using a Shapiro-Wilk test and was also analysed visually by histograms.

For each experiment an n number of 3 mice was used unless otherwise stated. Due to the small n number non-parametric statistical analysis is not appropriate, therefore a parametric analysis was used. Unpaired, two tailed students T-tests carried out pairwise were used to calculate statistical significances. p value interpretations for this thesis are detailed in Table 2.13.

Table 2.13 Interpretation of p value to assess statistical significance

| p value | Interpretation |
|-----------------------|---------------------------|
| $p \leq 0.05$ | Statistically significant |
| $p > 0.05 - \leq 0.1$ | Data trend |
| $p > 0.1$ | Not significant |

2.9.2 **Graphs**

All graphs were produced using Graphpad Prism 6 software. Appropriate graphs were selected depending on the data being displayed. Histograms were used to visualise data distribution and analyse shifts in distribution. Bar graphs were used to compare mean values.

Chapter 3 The loss of *Talpid3* in muscle satellite cells impairs muscle regeneration following injury

3.1 Introduction

To investigate the role of primary cilia in SCs and their contribution to muscle regeneration we used a tamoxifen inducible, SC specific, *Talpid3* KO mouse line subjected to a muscle injury and regeneration protocol. *Ta3* mutants are known to have defects in primary ciliogenesis, which leads to disrupted Shh signalling. Both functional primary cilia and Shh signalling have been shown to be important for normal satellite cell function, most recently for self-renewal, and normal skeletal muscle regeneration (Fu et al., 2014; Jaafar Marican et al., 2016; Straface et al., 2009). Therefore, this chapter aims to explore the effects of *Ta3* mutations in SCs on the ability of skeletal muscle to regenerate after injury.

We generated a tamoxifen inducible, SC conditional *Ta3* mutant mouse line by crossing *Ta3^{ff}* and *Pax7^{Cre-ERT2}* mice, which allowed for normal development and growth of skeletal muscle during embryonic, foetal and post-natal periods but removed *Ta3* function in the adult animal upon the administration of tamoxifen.

To investigate the role of *Ta3* function in SCs during muscle regeneration, a muscle injury protocol was adopted (detailed in **Fig. 3.3A/3.7A/3.9A**). Tamoxifen was administered to all experimental mice. *Ta3^{ff}Pax7⁺* or *Ta3^{ff/+}Pax7^{Cre-ERT2/+}* were used as WT, whilst *Ta3^{ff}Pax7^{Cre-ERT2/+}* were used as *Ta3* mutants.

Injury was induced in the Tibialis Anterior (TA) muscle by injection of Cardiotoxin (CTX), a potent toxin isolated from Cobra venom, on one or two occasions. CTX causes contracture of skeletal muscle by releasing membrane Ca^{2+} inducing injury (Lin Shiau et al., 1976). Morphology of regenerating muscle was assessed by H&E staining of muscle sections. Regeneration efficiency was assessed by measuring myofibre diameter after 10, 15 and 25 days of regeneration or after double injury and compared to contralateral uninjured control muscle. We also assessed the effects of a deletion of *Ta3* in

SCs on homeostasis of muscle structure by inducing recombination of *Ta3* and allowing mice to live normally for 4 months before injury was induced.

3.2 Generation of *Talpid3* conditional knockout in skeletal muscle satellite cells

3.2.1 *Breeding strategies to generate tamoxifen inducible conditional Talpid3 mutants*

To generate a Cre-recombinase inducible line to remove *Ta3* function specifically in satellite cells, *Ta3^{ff}* females, that have loxP sites flanking exons 11 and 12, were crossed with *Pax7^{Cre-ERT2/+}* males to generate *Ta3^{f/+}Pax7^{Cre-ERT2/+}* F1 generation (**Fig. 1A, B**). F1 mice were then crossed with a *Ta3^{ff}* mouse to generate *Ta3^{ff}Pax7^{Cre-ERT2/+}*, *Ta3^{f/+}Pax7^{Cre-ERT2/+}* and *Ta3^{ff}Pax7^{+/+}* F2 generation (hereafter referred to as *Pax7-Ta3^{ff}*, *Pax7-Ta3^{f/+}* and *Ta3^{ff}* respectively). The *Pax7^{Cre-ERT2/+}* line used was generated as a knock-in mutant therefore the *Pax7* allele was maintained as heterozygous to ensure *Pax7* remained functional in SCs.

3.2.2 *Genotyping of Talpid3 cKO mice*

To confirm the generation of mice with *Pax7-Ta3^{ff}*, *Pax7-Ta3^{f/+}* and *Ta3^{ff}* genotypes, genomic PCR was carried out on ear clippings of weaned pups. Previously published primers (See **Table 2.2**) were used that can distinguish the *Ta3* floxed and *Ta3* WT alleles along with the presence of *Cre-recombinase* gene. PCR results confirmed the presence of the *Ta3* floxed (470bp), the *Ta3* WT (351bp) and *Cre* (650bp) in F2 generation pups (**Fig. 3.1C**), confirming the generation of an inducible, SC conditional *Ta3* KO mouse line.

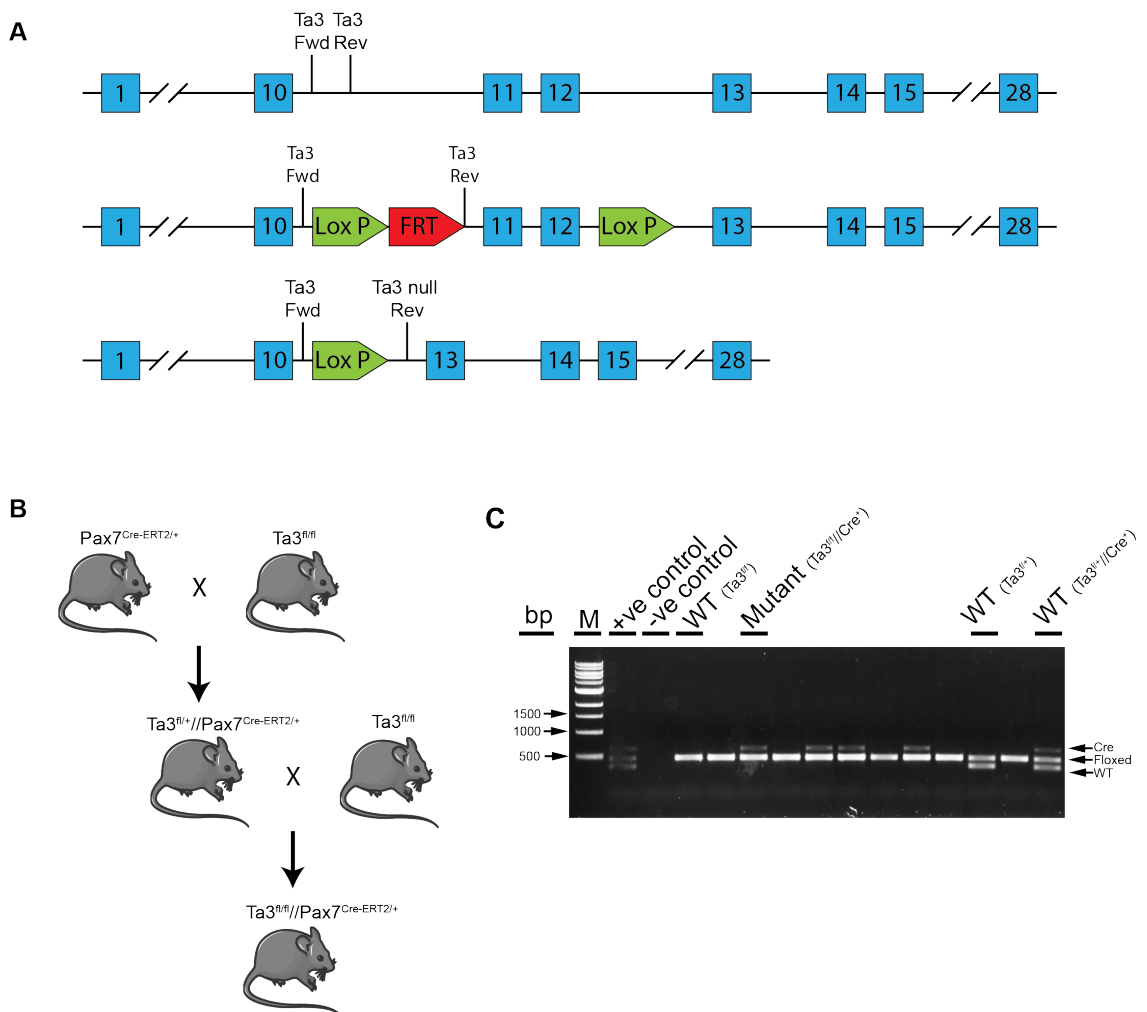


Figure 3.1 Generation of a tamoxifen inducible, satellite cell specific *Talpid3* KO mouse line.

(A) Schematic of the wildtype, floxed and null alleles of *Talpid3*, including primer binding sites for genotyping PCR. (B) Breeding strategy to generate *Talpid3* mutant mice. (C) Example electrophoresis gel following genotyping PCR. Positive Cre-recombinase band at 650bp, *Talpid3* floxed allele at 470bp and *Talpid3* wild typed (WT) band at 351bp. M= Base pair ladder.

3.2.3 **Confirming the efficient recombination of the *Talpid3* locus**

To assess recombination of the floxed *Ta3* allele three approaches were used, two indirectly assessed the recombination of reporter genes and one directly assessed the presence of a *Ta3* null allele.

Ta3^{ff}Pax7^{Cre-ERT2/+} (*Pax7-Ta3^{ff}*) and *Ta3^{ff}Pax7⁺* (*Ta3^{ff}*) mice were crossed with Rosa26-LacZ (*R26R^{LacZ}*) reporter mice, which contain a loxP-STOP-loxP-LacZ cassette targeted to the ubiquitously expressed *R26R* gene. Presence of the reporter allele was confirmed by genomic PCR (data not shown). Pax7 driven expression of a Cre-ERT2 fusion protein, that undergoes a conformational change upon tamoxifen induction allowing Cre-recombinase to translocate to the nucleus, was used to recombine the loxP-STOP-loxP and drive expression of the LacZ gene. Following tamoxifen induction and cardiotoxin injury muscle sections were tested for β -galactosidase activity, positive fibres were seen in muscle sections from *Pax7-Ta3^{ff}* mutant mice but not *Ta3^{ff}* control mice (**Fig. 3.2A**) confirming the recombination of the *R26R* locus upon administration of tamoxifen in *Pax7-Ta3^{ff}* mutant mice containing the *Pax7^{Cre-ERT2}* allele, but no recombination of in the *Ta3^{ff}* control mice due to the absence of Cre-recombinase. It was assumed that successful recombination of the *R26R* allele would coincide with the successful recombination of the *Ta3* allele. The presence of β -galactosidase positive fibres following CTX injury indicated that *Pax7-Ta3^{ff}* mutant SCs are still able to fuse to myofibres (**Fig. 3.2A**).

To quantify the efficiency of recombination by *Pax7^{Cre-ERT2}*, *Pax7-Ta3^{ff}* mutant or *Pax7-Ta3^{ff/+}* control mice were crossed with *Rosa26-tdTomato* (*R26R^{tdTom}*) reporter mice, which contain loxP-STOP-loxP cassette downstream of a CAG promotor that drive a fluorescent tdTomato gene. These were also crossed with *Pax7^{ZsGreen}* mice which express green fluorescent protein under the control of the Pax7 promotor to allow for the identification of SCs. Presence of the reporter alleles was confirmed by genomic PCR (data not shown). Pax7 driven expression of a Cre-ERT2 fusion protein was used to recombine the loxP-STOP-loxP and drive expression of the tdTomato gene. Single myofibres were isolated and fixed at T0 from *Pax7-Ta3^{ff}* mutant or *Pax7-Ta3^{ff/+}* control mice following 3 consecutive tamoxifen injections. SCs were identified by the presence of ZsGreen fluorescence and recombination was confirmed by the

presence of tdTomato fluorescence (**Fig. 3.2B**). Recombination efficiency was calculated as the percentage of ZsGreen positive SCs that were also tdTomato positive, 92% in *Pax7-Ta3^{f/+}* controls (calculated from 37 SCs on 19 myofibres from 2 mice) and 94% in *Pax7-Ta3^{ff}* mutants (calculated from 81 SCs on 22 myofibres from 2 mice) (**Fig. 3.2C**). Again, it was assumed that recombination of the *R26R* locus would coincide with recombination of the *Ta3* allele.

Finally, the presence of the *Ta3* null allele was directly assessed through PCR. Whole muscle samples from uninjured TA muscles of *Pax7-Ta3^{f/+}*, *Ta3^{f/+}* and *Ta3^{ff}* mice that were used for injury experiments were subjected to genomic PCR with primers that can identify WT, floxed and null alleles of the *Ta3* gene. The null allele was present only in *Pax7-Ta3^{ff}* samples, floxed allele remains present in all samples due to the presence of myonuclei which do not undergo Pax7 specific Cre recombination (**Fig. 3.2D**).

Taken together these data show that *Pax7^{Cre-ERT2}* recombines LoxP sites with approximately 93% efficiency after 3 consecutive tamoxifen injections, and this recombination generates a null allele in *Ta3* floxed SCs. All experimental mice were subject to 6 tamoxifen injections prior to being exposed to experimental conditions, it was therefore assumed that recombination of the floxed *Ta3* locus would be more than 93% by start of any experiment.

We were able to demonstrate that our mutation causes a loss of *Talpid3* function on a genomic level, which according to previously published research results in the production of a non-functional protein (Yin et al., 2009). However, by removing *Ta3* within adult SCs there will be a period in which functional protein will still be present after recombination has occurred. The half-life of TA3 remains unknown, we therefore wanted to confirm the presence/ absence of TA3 protein following recombination by tamoxifen. We attempted to use a commercially available Talpid3 antibody for immunolabelling in C2C12 cells. Unfortunately, we were not able to detect TA3 using this method. Ideally, we would have used the antibody for western blott detection of the TA3 protein from isolated SCs from *Ta3^{f/+}* controls and *Pax7-Ta3^{ff}* mutants, however we were not able to culture enough SCs for protein extraction. Therefore, we were unable to confirm the amount of time functional TA3 protein is present after induction of recombination with tamoxifen.

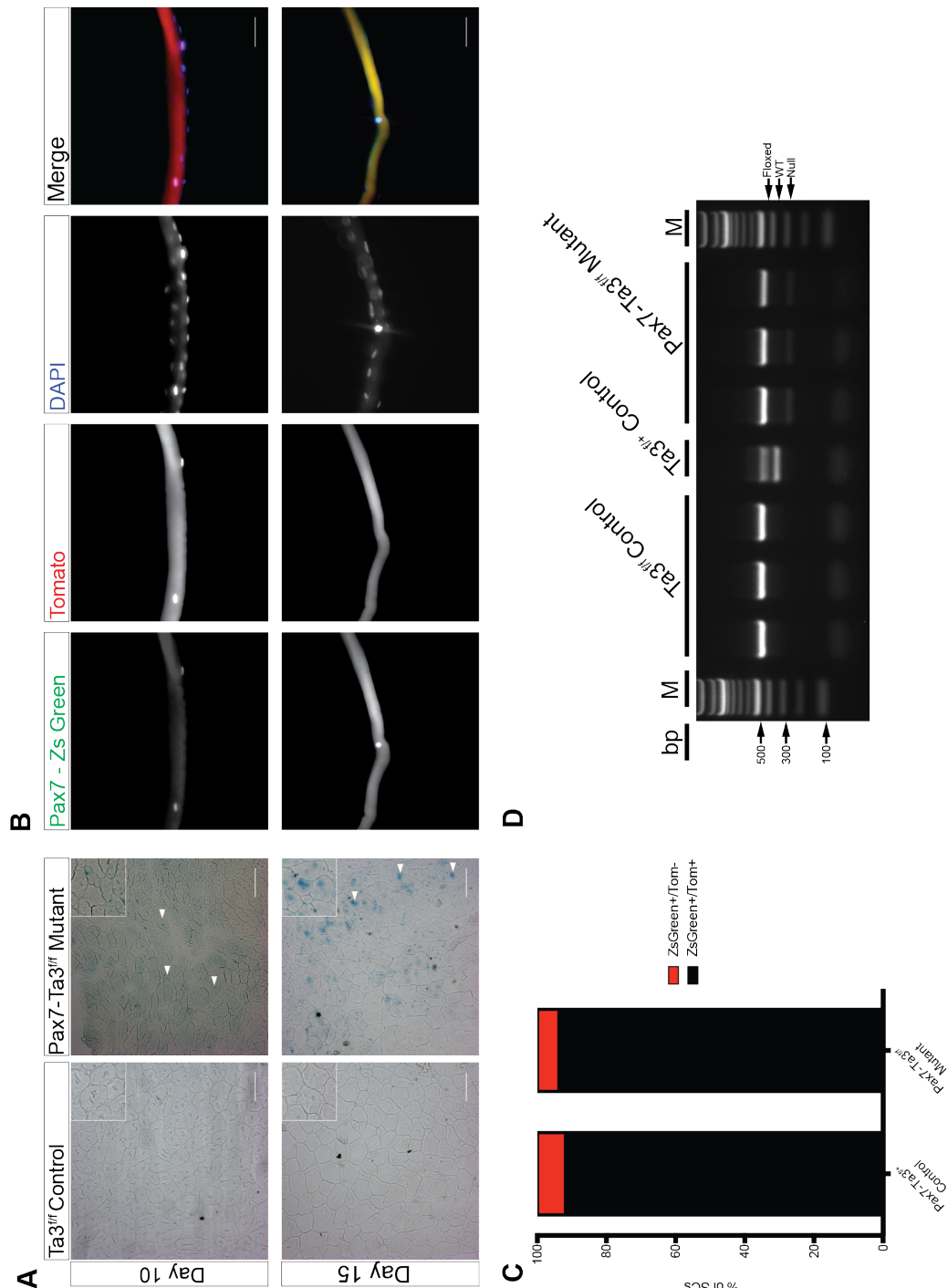


Figure 3.2 The Talpid3 locus is efficiently recombined in satellite cells upon induction with tamoxifen in $Ta3^{ff}Pax7^{Cre-ERT2}$ mice.

(A) Tamoxifen induced recombination of the *Talpid3* locus was measured indirectly by LacZ staining in $Ta3^{ff}Pax7^{Cre-ERT2}Rosa-LacZ$ injured muscle sections. (B) Zs-Green and Tomato positive SCs in $Ta3^{ff}Pax7^{Cre-ERT2}Rosa-tdTomato$ myofibres indicate successful tamoxifen induced recombination of the *Rosa-26* locus and an indirect measurement of *Talpid3* recombination. (C) Quantification of efficiency of recombination by the administration of tamoxifen. $Pax7-Ta3^{ff/+}$ controls = 37 SCs on 19 myfibres from 2 mice, $Pax7-Ta3^{ff}$ mutants = 81 SCs on 22 myofibres from 2 mice. (D) Direct confirmation of recombination of the floxed *Ta3* allele by PCR. M= base pair ladder. Floxed allele = 470bp, WT allele = 351bp, null allele = 273bp.

3.2.4 ***The effect of a *Talpid3* mutation on the presence of primary cilia in satellite cells***

In all cell types studied to date, mutations within *Ta3* cause the loss of primary cilia (Bangs et al., 2011; Yin et al., 2009). When this project started the presence of primary cilia on SCs had yet to be confirmed. We therefore set out to detect primary cilia on SCs by immunolabelling isolated myofibres.

Primary antibodies against Arl13b and Acetylated α -tubulin were successful in immunolabelling primary cilia on undifferentiated C2C12 cells (**Fig 3.3A**). However, we were not successful when using the same combination of antibodies for immunolabelling primary cilia on SCs.

Transfection of a GFP tagged Arl13b plasmid (pDEST47-Arl13b12, Addgene) was also successful in labelling primary cilia in C2C12 cells (**Fig 3.3B**). This technique however was not used in SCs. Over expression of *Arl13b* by this plasmid has been shown to increase ciliary length in cultured MEFs (Larkins et al., 2011), we were therefore concerned that transfection could lead to artificial false positives.

The presence of primary cilia on SCs was later confirmed by Jaafar Marican et al. (2016), we therefore changed our focus for this project away from the detection of primary cilia. However, this still leaves the question of when is the primary cilium removed from SCs in our model? Due to the quiescent, non-cycling state of SCs at the time of recombination of the *Ta3* locus it is possible that the primary cilium remains intact until the SC is activated and begins to progress through the cell cycle. There is no evidence to date that *Ta3* is required for the maintenance of the primary cilium, only that it is required for its assembly. It is therefore essential that future experiments in this project are conducted to analyse the presence of primary cilia on SCs from *Pax7-Ta3^{fl/fl}* mutants immediately after isolation and then again after SCs have been activated and are cycling. This could be achieved by immunolabelling with Arl13b or by culturing SCs and performing western blott analysis for the presence of proteins associated with the primary cilium such as IFT88 or Arl13b.

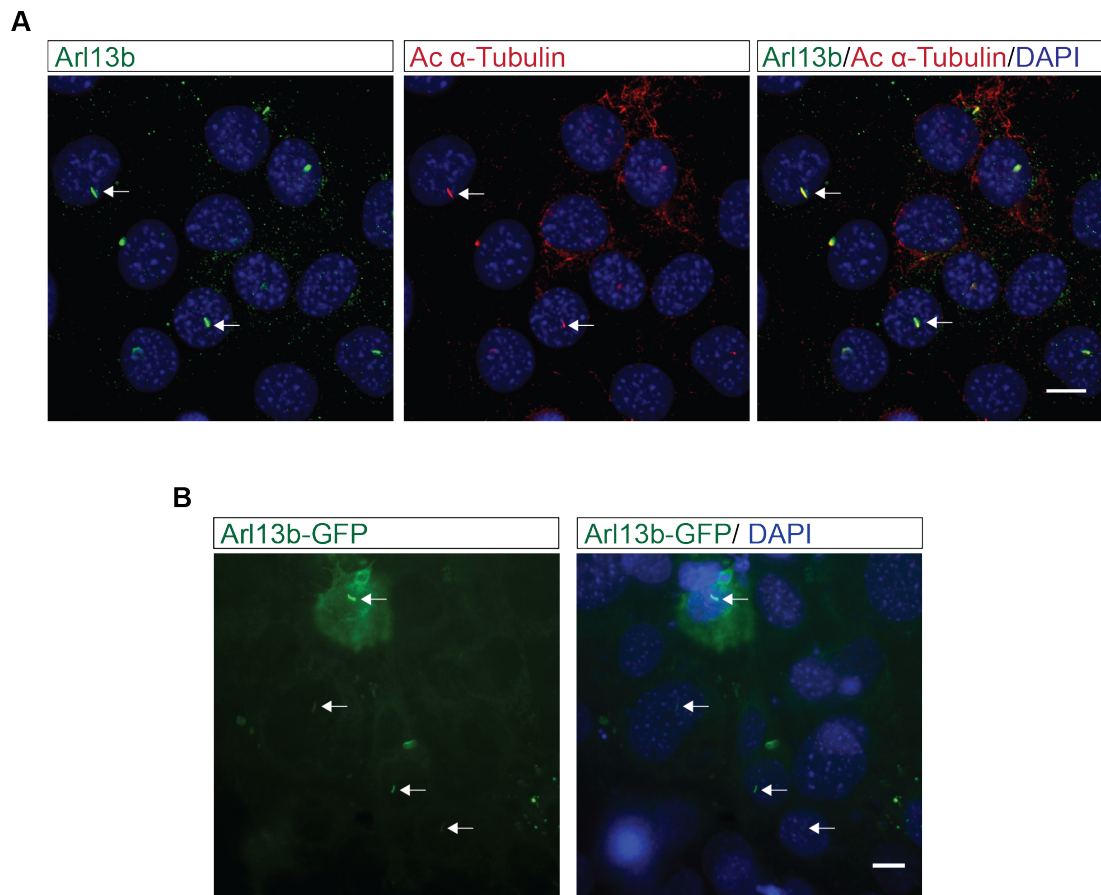


Figure 3.3 Primary cilia on C2C12 cells

(A) Positive immunostaining for primary cilia on C2C12 cells at T0 +6hrs in differentiation media (white arrows). Arl13b (green) and Acetylated α -Tubulin (red) co-localise to the primary cilium. (B) Positive labelling of primary on C2C12 cells (white arrows) by transfection with Arl13b-GFP plasmid. Scale bar = 10 μ m.

3.3 Analysis of muscle regeneration following short-term removal of *Talpid3* in skeletal muscle satellite cells

Short term removal of *Talpid3* refers to tamoxifen induced recombination being carried out directly before injury with CTX and was used for all experiments in this section.

3.3.1 Tamoxifen induction and injury experiment protocol

To investigate the role of *Ta3* in skeletal muscle regeneration *Pax7-Ta3^{ff}* mutants and *Ta3^{ff}* controls were subject to the protocol detailed in **Fig. 3.4A**. This included a seven-day period of SC DNA recombination through the IP administration of tamoxifen (with one rest day on day 6). On day 8 injury to the right TA muscle was carried out by intramuscular injection of CTX, the contralateral limb was left as an uninjured control. Mice were allowed to recover and sacrificed 5, 10, 15 or 25 days post injury. During the recovery and regeneration period tamoxifen was administered every other day to minimise contribution from SCs that may have escaped recombination during the initial period of tamoxifen induction. The number of mice used from each genotype and time point are detailed in **Table 3.1**

Table 3.1 Mice used for short term regeneration experiments

| Experimental Time Point | Genotype | Number of mice |
|-------------------------|------------------------------|----------------|
| 5 days | <i>Ta3^{ff}</i> | 3 |
| | <i>Pax7-Ta3^{ff}</i> | 3 |
| 10 days | <i>Ta3^{ff}</i> | 3 |
| | <i>Pax7-Ta3^{ff}</i> | 3 |
| 15 days | <i>Ta3^{ff}</i> | 3 |
| | <i>Pax7-Ta3^{ff}</i> | 3 |
| 25 days | <i>Ta3^{ff}</i> | 4 |
| | <i>Pax7-Ta3^{ff}</i> | 4 |

3.3.2 ***Histological analysis of regenerating skeletal muscle following CTX injury***

Following the specified period of regeneration TA muscle was isolated, frozen and cryosectioned. 12 sections from each TA muscle from each mouse were selected that sampled multiple locations throughout the length of the muscle and subjected to H&E staining. In both *Pax7-Ta3^{ff}* mutant and *Ta3^{ff}* control mice centrally located nuclei were present at all time points, indicating the muscle had been injured and was undergoing regeneration. Five days after injury the presence of numerous regenerating myofibres was seen in *Ta3^{ff}* controls (**Fig. 3.4B**) whereas there were far fewer present in *Pax7-Ta3^{ff}* mutants (**Fig. 3.4C**), those that were present were visibly smaller. After 10, 15 and 25 days of regeneration the number of regenerating myofibres in *Pax7-Ta3^{ff}* muscle had increased compared to 5 days (**Fig. 3.4D-I**) however, myofibres in *Pax7-Ta3^{ff}* mutant muscle still appeared visibly smaller than *Ta3^{ff}* controls (**Fig. 3.4D-I**).

Non-injected control muscles from *Pax7-Ta3^{ff}* mutants and *Ta3^{ff}* controls showed no signs of centrally located nuclei, confirming the muscle had not been injured. There was no difference in myofibre size, number and organisation in non-injured muscle (**Fig. 3.4J, K**).

Due to the visual differences in myofibre size between *Pax7-Ta3^{ff}* mutants and *Ta3^{ff}* controls observed in H&E stained sections of CTX injected muscle quantification of myofibre size was carried out to confirm the observed differences.

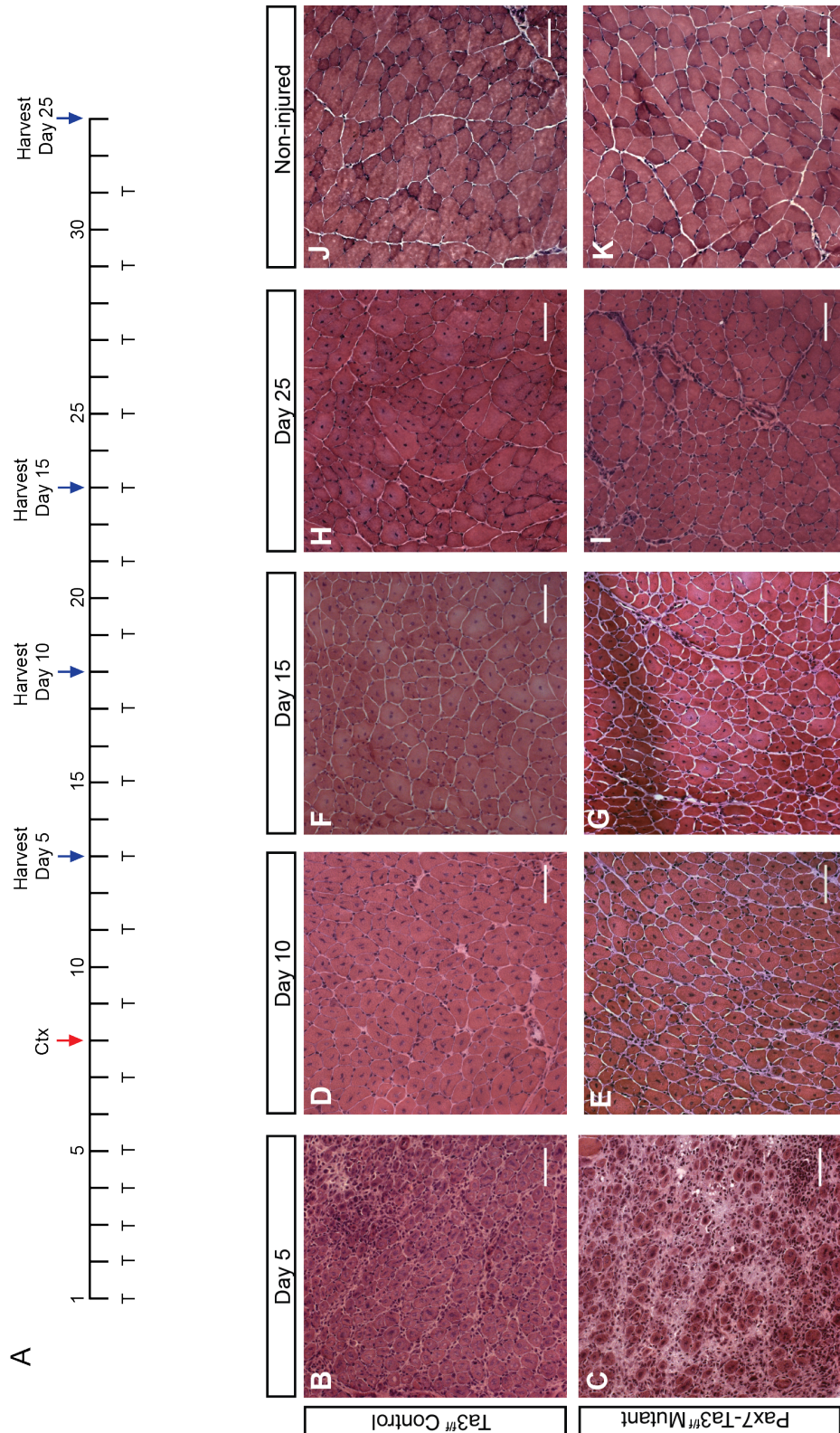


Figure 3.4 Satellite cell specific deletion of *Ta3* impairs muscle regeneration after CTX injury.

(A) Schematic of tamoxifen and CTX treatment. (B-K) TA muscle sections from *Pax-Ta3^{ff}* mutant and *Ta3^{ff}* control mice were analysed by H&E staining on days 5, 10, 15 and 25 after injury. Representative images from 12 TA sections from each mouse at each time point. $n \geq 3$ mice for each time point. (Scale bars = 50 μ m).

3.3.3 **Quantitative analysis of regenerating skeletal muscle following CTX injury**

To more accurately understand the differences in progression of muscle regeneration in *Pax7-Ta3^{ff}* mutants and *Ta3^{ff}* controls a quantitative approach was used to measure the size of regenerating myofibres. The basement membrane (BM) surrounding individual myofibres was visualised by immunostaining against Nidogen, a BM protein that connects collagens and laminins, on muscle sections taken from injured and non-injured TA muscles. Up to 5 images were taken from different areas of each muscle section (**Fig 3.5A**) to ensure that representation of the whole injured area was sampled. Myofibre size was measured using ImageJ software to calculate the minimum feret diameter (Detailed in **Fig. 3.5B**). A measurement of minimum feret diameter was taken to reduce the error associated with a non-transverse section through myofibres. Minimum feret diameter is calculated by measuring the diameter between every possible pair of parallel tangents and taking the smallest distance, which should always be the same irrespective of the plane of sectioning, assuming myofibres are cylindrical (**Fig. 3.5C**).

Quantitative analysis was carried out on muscle sections after 10, 15 and 25 days of regeneration but not after 5 days of regeneration. At this early time point the integrity of the BM is very weak making Nidogen staining of distinct basement membrane and measurement using ImageJ very difficult and inaccurate.

Quantitative data was collected from an average of 1706 myofibres from 16 areas across 6 muscle sections for each TA muscle analysed. The exact number of myofibres, areas and sections analysed for each mouse is detailed in **Appendix 1.1**.

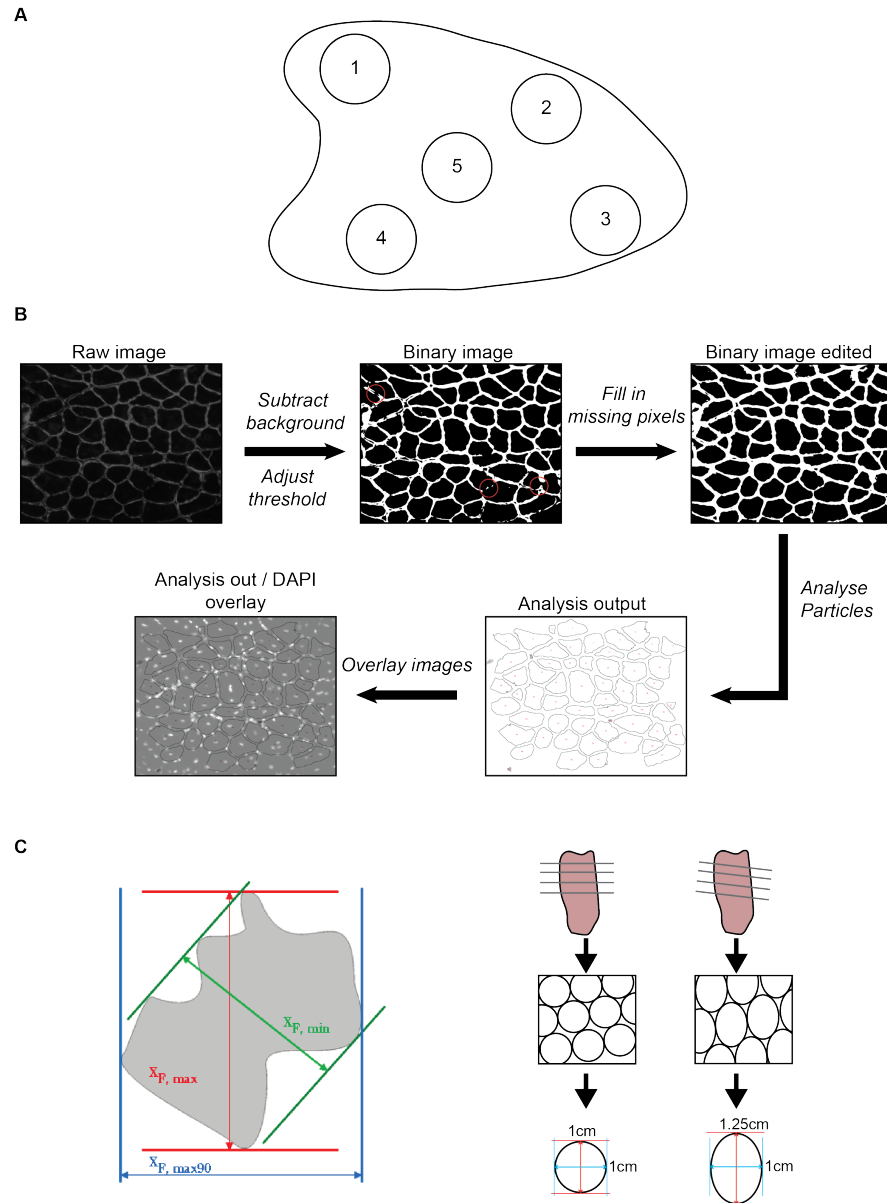


Figure 3.5 Method of quantitative analysis of minimum feret diameter using ImageJ software.

(A) Schematic representation of imaged areas within TA muscle sections. (B) Work flow of ImageJ software. Raw images of Nidogen immunostaining were opened with ImageJ. Background subtraction was applied and the threshold of the image adjusted to create a binary image. Missing pixels (indicated by red circles) were filled in using the paintbrush tool. Analyse particles function was used to measure minimum feret diameter of each myofibre, producing an outline overview of each fibre and a related data point in a spreadsheet. DAPI stained image was overlaid with the outline image and non-regenerating fibres were discarded. (C) Schematic representation of minimum feret diameter.

Nidogen immunostaining revealed similar phenotypic results to the H&E staining. Five days after injury the presence of numerous regenerating myofibres was seen in *Ta3^{ff}* controls (**Fig. 3.6A'**) whereas there were far fewer regenerating myofibres present in *Pax7-Ta3^{ff}* mutants (**Fig. 3.6A''**), those that were present were visibly smaller with a less well defined surrounding membrane. After 10, 15 and 25 days of regeneration there was a normal distribution of fibre diameter in both *Pax7-Ta3^{ff}* mutants and *Ta3^{ff}* controls, however, there was a shift in the distribution towards a smaller feret diameter in *Pax7-Ta3^{ff}* mutants (**Fig. 3.6G-J**). At all time points quantified, the mean minimum feret diameter was significantly smaller in *Pax7-Ta3^{ff}* mutants compared to *Ta3^{ff}* controls ($p < 0.005$, $n \geq 3$) (**Fig. 3.6F**), suggesting regeneration is impaired in *Pax7-Ta3^{ff}* mutant mice. There was no difference in fibre size in non-injured myofibres (**Fig. 3.6E', E'', F, J**)

In *Ta3^{ff}* controls at 10 and 15 days of regeneration average myofibre size was significantly smaller than non-injured muscle (10 days $p = 0.0007$, 15 days $p = 0.0028$, $n = 3$) (**Fig. 3.6F**). By 25 days of regeneration myofibres in *Ta3^{ff}* controls had increased in size and were not significantly different to non-injured myofibres ($p = 0.1523$, $n \geq 3$) (**Fig. 3.6F**) indicating full recovery from injury. This gradual increase in myofibre size is to be expected during muscle regeneration. However, in *Pax7-Ta3^{ff}* mutants myofibre size was significantly smaller compared to non-injured muscle at all time points including 25 days ($p < 0.0001$, $n \geq 3$) (**Fig. 3.6F**) suggesting that a mutation in *Ta3* in SCs leads to impaired muscle regeneration preventing myofibre recovery.

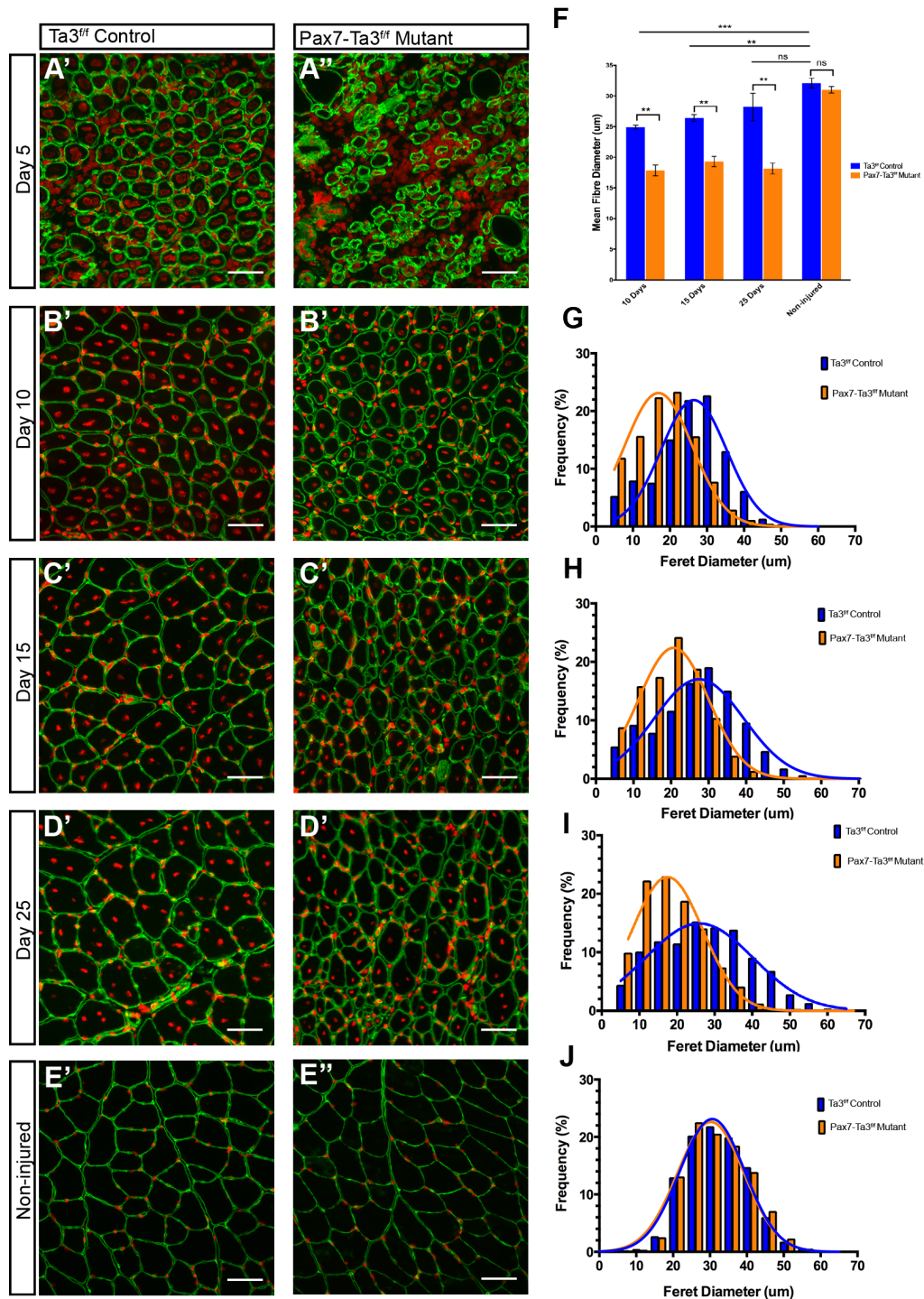


Figure 3.6 Myofibre size is significantly smaller after injury with CTX in satellite cell specific *Ta3* mutants.

(A'-E'') Representative images of TA Muscle sections from CTX injured and non-injured *Pax7-Ta3^{ff}* mutant and *Ta3^{ff}* control mice were analysed by Nidogen (green) immunostaining and DAPI (red) at 5, 10, 15 and 25 days after injury. (F) Mean minimum feret diameter of myofibres, calculated from population mean of each mouse from *Pax7-Ta3^{ff}* mutant and *Ta3^{ff}* control mice at 10, 15 and 25 days after injury and non-injured muscle. ** indicates $p \leq 0.005$, *** indicates $p \leq 0.0005$, ns indicates $p > 0.05$, calculated by unpaired, two tailed t-test. $n \geq 3$ mice for each time point. Error bars = SEM. (G-J) Minimum feret diameter distribution of myofibres from *Pax7-Ta3^{ff}* mutant and *Ta3^{ff}* control mice at 10 (G), 15 (H), 25 (I) days after regeneration and from non-injured muscle (J).

3.3.4 α -Smooth Muscle Actin expression is prolonged in *Pax7-Ta3^{ff}* mutants

Pax7-Ta3^{ff} mutant mice showed impaired muscle regeneration after injury with CTX. Myofibres remained significantly smaller than both time matched controls and non-injured muscle. To assess whether these fibres were stuck at an early stage of regeneration or were just simply smaller in size we utilised the dynamic expression of α -smooth muscle actin (α -SMA) throughout regeneration in adult skeletal muscle.

α -SMA was expressed in myofibres during early stages of regeneration, until approximately 8 days after injury, but expression was down-regulated in later stages (**Fig. 3.7A**). In myofibres from *Ta3^{ff}* control TA muscles there was no expression of α -SMA after 10 or 15 days of regeneration (**Fig 3.7 B, D**) however in *Pax7-Ta3^{ff}* mutant TA muscles many myofibres were positive for α -SMA after 10 days of regeneration (**Fig. 3.7C**). This was true of all sections analysed, 12 sections from 3 mutants and 12 sections from 2 control mice. This suggests myofibres at 10 days after injury are at an earlier stage of regeneration in mutants compared to the controls. Myofibres from *Pax7-Ta3^{ff}* mutant TA muscles appeared to progress past this early stage of regeneration as 15 days after injury the majority of myofibres were α -SMA negative (**Fig 3.7E**). This suggests that *Pax7-Ta3^{ff}* mutants do have some capacity for muscle regeneration but the process is delayed.

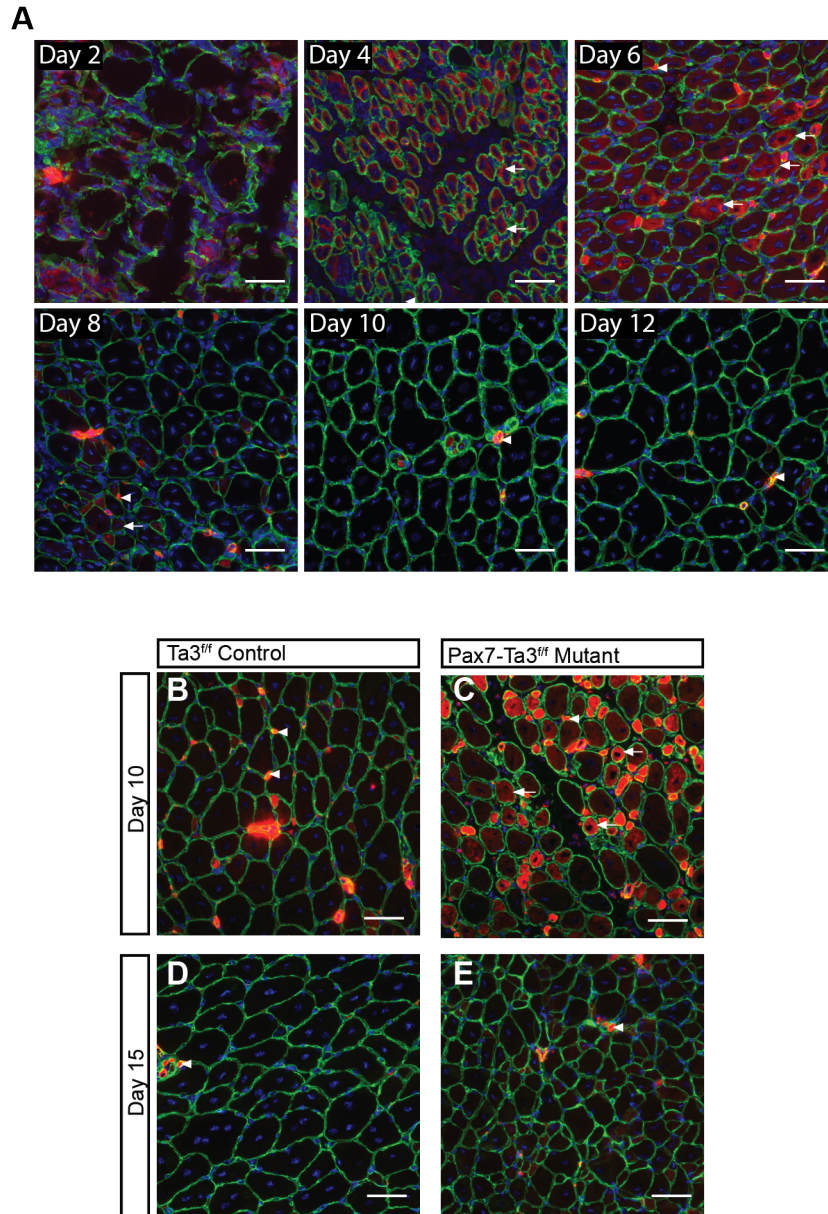


Figure 3.7 Satellite cell specific KO of *Ta3* leads to prolonged expression of α -SMA.

(A) Representative images of time course of α -SMA expression during muscle regeneration in WT mice from 2-12 days after injury (n=2 mice for each time point). α -SMA positive myofibres (white arrows) are present 4-8 days after injury. (B-D) Representative images of α -SMA expression in myofibres from *Pax7-Ta3^{ff}* mutants and *Ta3^{ff}* controls 10 and 15 days after injury (n \geq 2 mice for each time point). α -SMA positive fibres are present in *Pax7-Ta3^{ff}* mutants (100% of images analysed showed 10+ α -SMA positive fibres) (C) at 10 days of regeneration but not in *Ta3^{ff}* controls (100% of images analysed showed less than 10 α -SMA positive fibres) (B). All images are immunostaining on TA muscle sections for Nidogen (green), α -SMA (red) and DAPI (blue). Arrow heads indicate positive staining of blood vessels. Scale bars = 50 μ m.

3.4 Analysis of muscle regeneration following long-term removal of *Talpid3* in skeletal muscle satellite cells

Short term injury experiments showed *Pax7-Ta3^{ff}* mutants have impaired muscle regeneration due to *Ta3* being knocked out in SCs. It has been reported that SCs not only activate following injury but also play a role in general homeostasis and turnover of skeletal muscle (Pawlikowski et al., 2015). We therefore designed another set of experiments (referred to as long term (LT)) in which *Ta3* was knocked out of SCs and mice were left to live normally for almost 4 months, before injury with CTX. We hypothesised that if SCs are contributing highly to the homeostasis of skeletal muscle we would observe defects in myofibres in non-injured muscle from *Pax7-Ta3^{ff}* mutants and possibly a more severe phenotype after injury due to evidence that the loss of primary cilia impairs SCs ability to self-renew (Jaafar Marican et al., 2016).

3.4.1 Tamoxifen induction and injury experiment protocol

To investigate the role of *Ta3* in SCs during muscle homeostasis and general wear and tear *Pax7-Ta3^{ff}* mutants and *Ta3^{ff}* controls were subject to the protocol detailed in **Fig. 3.8A**. Similar to the ST protocol recombination of *Ta3* was induced by 5 consecutive days of tamoxifen IP injections, followed by another 10 days of tamoxifen administered every second day. Following this, mice were left to live normally for 17 weeks. Ctx injury was induced in the right TA muscle, contralateral limbs were left as non-injured controls. TA muscles were harvested after 10 days of regeneration as this was the time point during the ST experiment in which we saw the biggest discrepancy between stage of regeneration between *Pax7-Ta3^{ff}* mutants and *Ta3^{ff}* controls. 4 *Pax7-Ta3^{ff}* mutant and 4 *Ta3^{ff}* control mice were used for this analysis.

3.4.2 ***Histological analysis of regenerating skeletal muscle following CTX injury***

Following 10 days of regeneration at the end of the protocol, TA muscle was isolated, frozen and cryosectioned. 12 sections from each TA muscle from each mouse were selected that sampled multiple locations throughout the length of the muscle and subjected to H&E staining.

In non-injured muscle of both *Ta3^{ff}* controls and *Pax7-Ta3^{ff}* mutants myofibres looked healthy with no centrally located nuclei. Myofibres appeared to be of similar size and organisation (**Fig. 3.8F, G**).

Ten days after injury with CTX the presence of many regenerating fibres was seen in *Ta3^{ff}* control (**Fig 3.8D**) and *Pax7-Ta3^{ff}* mutant (**Fig. 3.8E**) muscles, however similar to what was seen in the ST experiment, myofibres from *Pax7-Ta3^{ff}* mutants were observed to be visibly smaller than in controls (**Fig 3.8B-E**).

Due to the visual differences in myofibre size between *Pax7-Ta3^{ff}* mutants and *Ta3^{ff}* controls observed in H&E stained sections of CTX injected muscle quantification of myofibre size was carried out to confirm the observed differences.

A

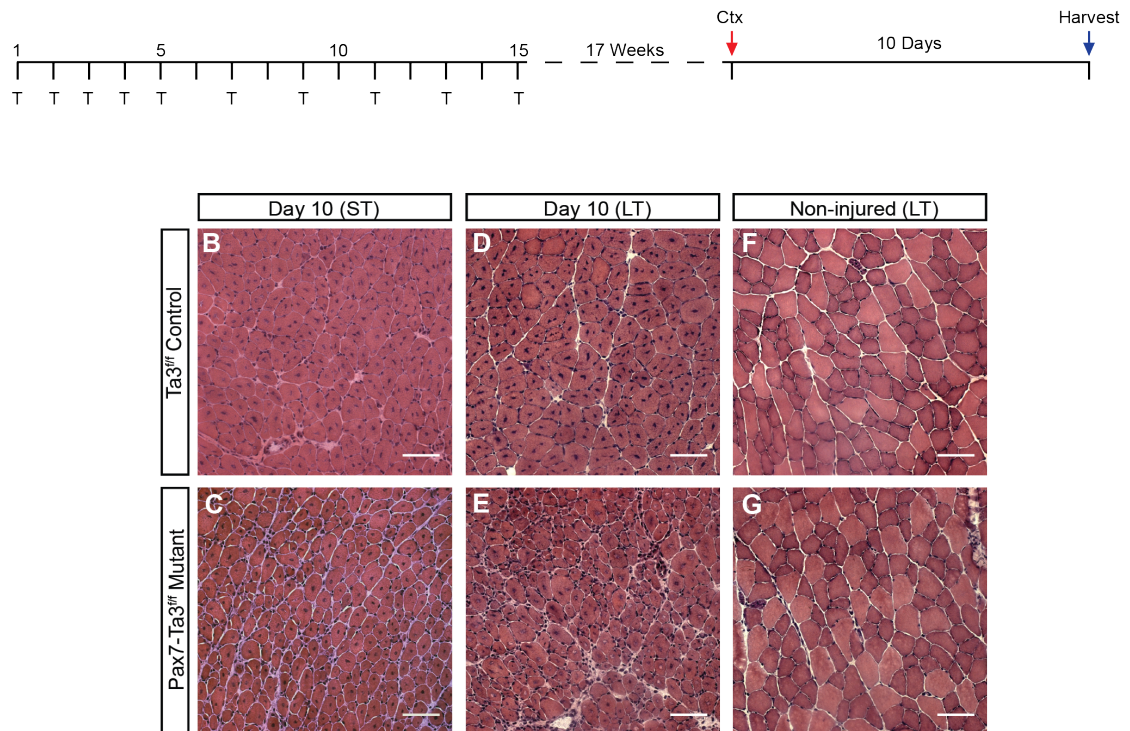


Figure 3.8 Satellite Cell specific deletion of *Ta3* for an extended period impairs muscle regeneration following injury with CTX but does not affect muscle homeostasis.

(A) Schematic of tamoxifen and CTX treatment. (B-G) TA muscle sections from *Pax-Ta3^{ff}* Mutant and *Ta3^{ff}* Control mice were analysed by H&E staining 10 days after injury and in non-injured muscle. Representative images from 12 sections from each TA muscle, n=4 mice. ST= short term, tamoxifen induced recombination immediately prior to CTX injury. LT= long term, tamoxifen induced recombination 4 months prior to CTX injury. (Scale bars = 50 μ m)

3.4.3 **Quantitative analysis of regenerating skeletal muscle following CTX injury**

As with the short-term experiments, myofibre size was quantified using ImageJ software (explained in **section 3.3.3** and **Fig. 3.5**). Quantitative data was collected from an average of 4291 myofibres from 34 areas across 7 muscle sections for each TA muscle analysed. The exact number of myofibres, areas and sections analysed for each mouse can be found in **Appendix 1.2**

Nidogen immunostaining revealed similar phenotypic results to the H&E staining. Ten days after injury the presence of numerous regenerating myofibres was seen in $Ta3^{ff}$ controls (**Fig. 3.9A'**) and $Pax7-Ta3^{ff}$ mutants (**Fig. 3.9A''**). Similar to the ST experiments, after 10 days of regeneration in LT experiments there was a normal distribution of fibre diameter in both $Pax7-Ta3^{ff}$ mutants and $Ta3^{ff}$ controls, however there was a shift in the distribution towards a smaller feret diameter in $Pax7-Ta3^{ff}$ mutants (**Fig. 3.9C**). In LT experiments, 10 days after injury mean minimum feret diameter was significantly smaller in $Pax7-Ta3^{ff}$ mutants compared to $Ta3^{ff}$ controls ($p < 0.05$, $n \geq 3$) (**Fig. 3.9E**) suggesting regeneration is impaired in $Pax7-Ta3^{ff}$ mutant mice. There was no difference in fibre size in non-injured myofibres (**Fig. 3.9B', B'', D, E**).

To understand the contribution of SCs to homeostasis of the muscle and to see if this is impaired with the long-term removal of $Ta3$, the mean minimum feret diameter of myofibres from $Pax7-Ta3^{ff}$ mutants and $Ta3^{ff}$ controls in the ST experiments was compared to those in the LT experiments. There was no significant difference in fibre size depending on whether $Ta3$ was removed immediately prior or 4 months prior to injury in controls ($p = 0.6898$, $n = 3$) or mutants ($p = 0.4715$, $n = 3$) (**Fig 3.9F**) suggesting there is not more of a detrimental effect when removing $Ta3$ for a longer period of time before injury.

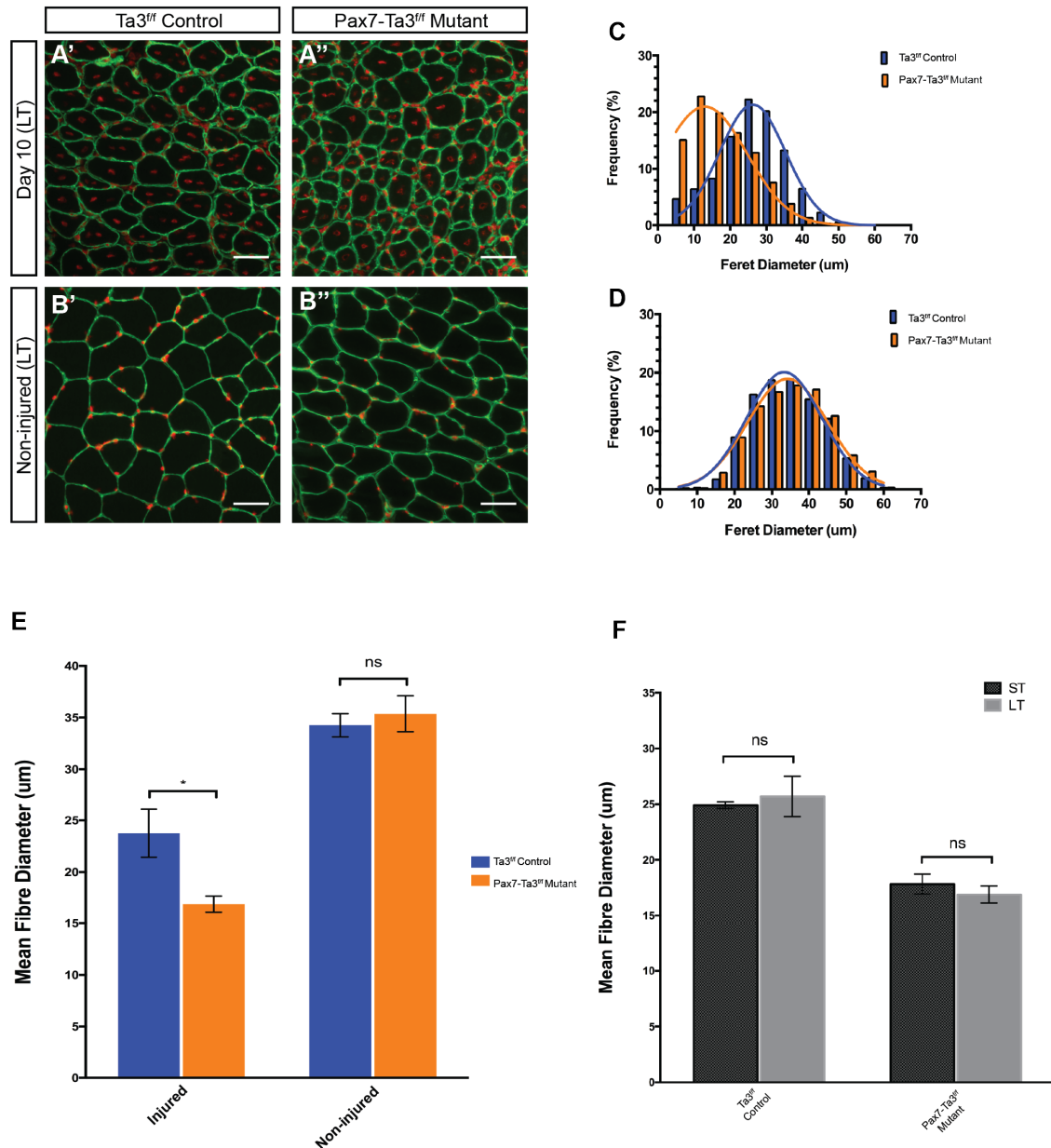


Figure 3.9 Muscle regeneration is not further impaired by the removal of *Ta3* for an extended period before injury.

(A'-B'') Representative images from TA muscle sections from CTX injured and non-injured *Pax7-Ta3^{ff}* mutant and *Ta3^{ff}* control mice were analysed by Nidogen (green) immunostaining and DAPI (red) at 10 days after injury. (C, D) Minimum feret diameter distribution of myofibres from *Pax7-Ta3^{ff}* mutant and *Ta3^{ff}* control mice at 10 days (C) after injury and in non-injured muscle (D). (E) Mean minimum feret diameter of myofibres, calculated from population mean of each mouse from *Pax7-Ta3^{ff}* mutant and *Ta3^{ff}* control mice at 10 days after injury and non-injured muscle. (F) Mean minimum feret diameter of myofibres, calculated from population mean of each mouse from *Pax7-Ta3^{ff}* mutant and *Ta3^{ff}* control mice at 10 days after injury in short term (ST) and long term (LT) experiments. * indicates $p \leq 0.05$, ns indicates $p > 0.05$, calculated by unpaired, two-tailed t-test. $n \geq 3$ mice.

3.5 Analysis of *Talpid3* mutant satellite cells ability to self-renew.

We have already shown that a SC specific loss of *Ta3* impairs muscle regeneration as hypothesised based on evidence that primary cilia and Shh signalling are required for the normal proliferation and differentiation of muscle progenitors. However, SCs being stem cells must also be able to self-renew to maintain the stem cell pool and allow for multiple rounds of muscle repair and regeneration following injury. Recent evidence indicated that primary cilia play a vital role in this process. Jaafar Marican et al. (2016) showed that removing the primary cilium from SCs, using treatment with nocodazol or taxol which destabilise microtubules, or with forchlorfenuron which inhibits a family of proteins that regulate cilium length, reduced the number of cells that re-express Pax7 following 72hrs in ex vivo culture, suggesting a reduced number were re-entering quiescence. We therefore hypothesised that *Pax7-Ta3^{ff}* mutants, which we assume to not possess a primary cilium on SCs, would have impaired self-renewal and should therefore have more severe impairment of muscle regeneration following double injuries.

3.5.1 *Tamoxifen induction and injury experiment protocol*

To investigate the role of *Ta3* in the self-renewal of SCs after injury *Pax7-Ta3^{ff}* mutants and *Ta3^{ff}* controls were subject to the protocol detailed in **Fig. 3.11A**. This included a seven-day period of SC DNA recombination through the IP administration of tamoxifen (with one rest day on day 6). On day 8 injury to the right TA muscle was carried out by intramuscular injection of CTX, the contralateral limb was left as an uninjured control. After 25 days of regeneration a second injury to the TA muscle was carried out by CTX injection. Mice were allowed to recover and sacrificed 10 days post 2nd injury. During the recovery and regeneration period tamoxifen was administered every other day to minimise contribution from SCs that may have escaped recombination during the initial period of tamoxifen induction.

3.5.2 Analysis of myofibres after double CTX injury

Following 10 days of regeneration at the end of the protocol, TA muscle was isolated, frozen and cryosectioned. 12 sections from each TA muscle from each mouse were selected that sampled multiple locations throughout the length of the muscle and subjected to H&E staining. Visual analysis of the full muscle section revealed variability in the size of the area injured in each TA muscle (Fig 3.10). In all $Ta3^{ff}$ control mice more than approximately 50% of the muscle has been injured whereas in 3/4 $Pax7-Ta3^{ff}$ mutants only approximately 25-30% of the muscle is injured. Closer analysis of these regenerating areas must therefore be done with the caveat that the area of injury was different in control compared to mutant mice.

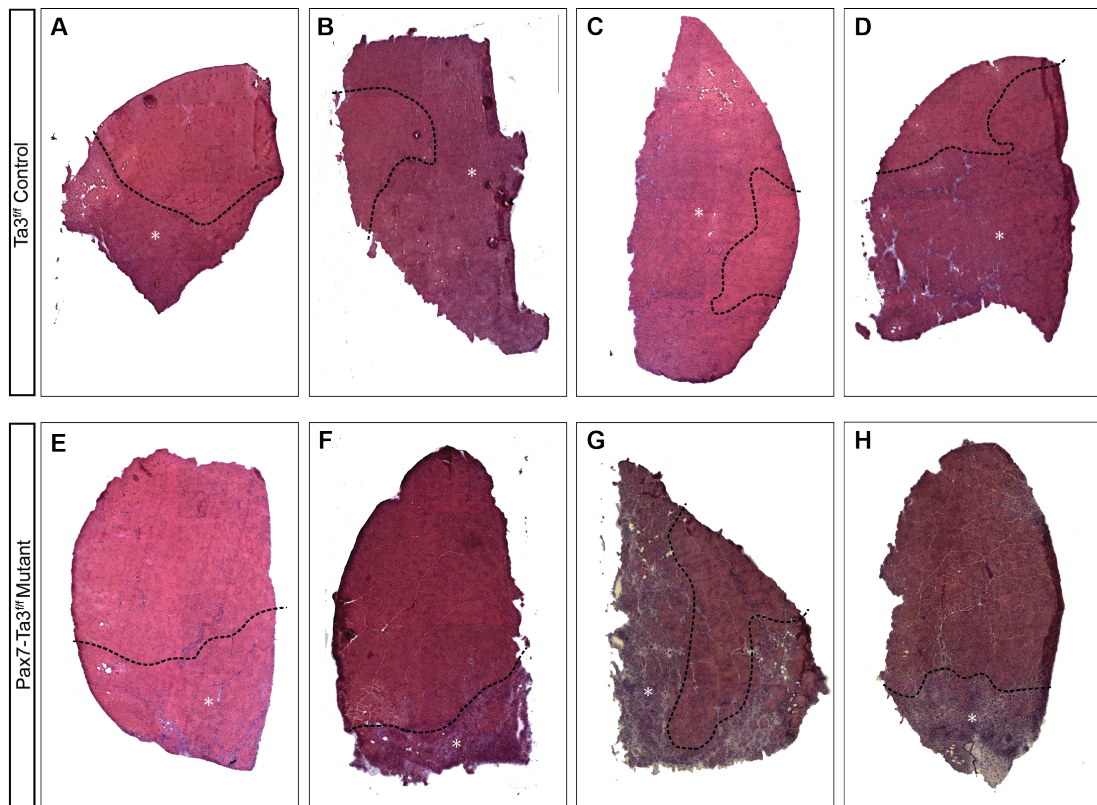


Figure 3.10 Whole muscle sections following double cardiotoxin injury.

(A-D) Whole TA muscle sections from $Ta3^{ff}$ control mice following double injury with CTX. (E-H) Whole TA muscle sections from $Pax7-Ta3^{ff}$ mutant mice following double injury with CTX. Representative images from 12 muscle sections from each mouse. Dotted line indicates border of injury site. * indicates injured region. Images not to scale.

H&E staining showed the presence of regenerating fibres in all $Ta3^{ff}$ control mice samples. The morphology and size of regenerating fibres in $Ta3^{ff}$ controls appeared to be as expected 10 days post CTX injury (**Fig. 3.11B-E**). Quantification of myofibre size in $Ta3^{ff}$ controls by measuring minimum ferret diameter showed a normal distribution of myofibre sizes. There was no significant difference in myofibre size in $Ta3^{ff}$ controls 10 days after a single injury or 10 days after a second injury ($p=0.5129$, $n=3$) (data not shown). These data show that in control mice SCs were still able to efficiently regenerate the muscle after a second injury, suggesting the SC pool had been maintained, following the first injury, through self-renewal.

The results from $Pax7-Ta3^{ff}$ mutants were somewhat inconclusive. H&E staining revealed areas within the injured TA muscle that showed no sign of regeneration, the presence of myofibres with centrally located nuclei was very low in these areas in 3 TA muscles (**Fig. 3.11G-I**), only one muscle had many regenerating fibres (**Fig 3.11F**). Quantification of myofibre size was not possible in $Pax7-Ta3^{ff}$ mutants due to the severity of the injury site and disruption to the BM.

These data suggest there could be a defect in self-renewal of SCs from $Pax7-Ta3^{ff}$ mutants, which led to the SC pool being depleted after the first injury leaving too few SCs to be able to regenerate the muscle after a second injury. However, there were limitations to this technique (discussed in section 3.6), thus conclusions from this data need to be strengthened with increased n numbers.

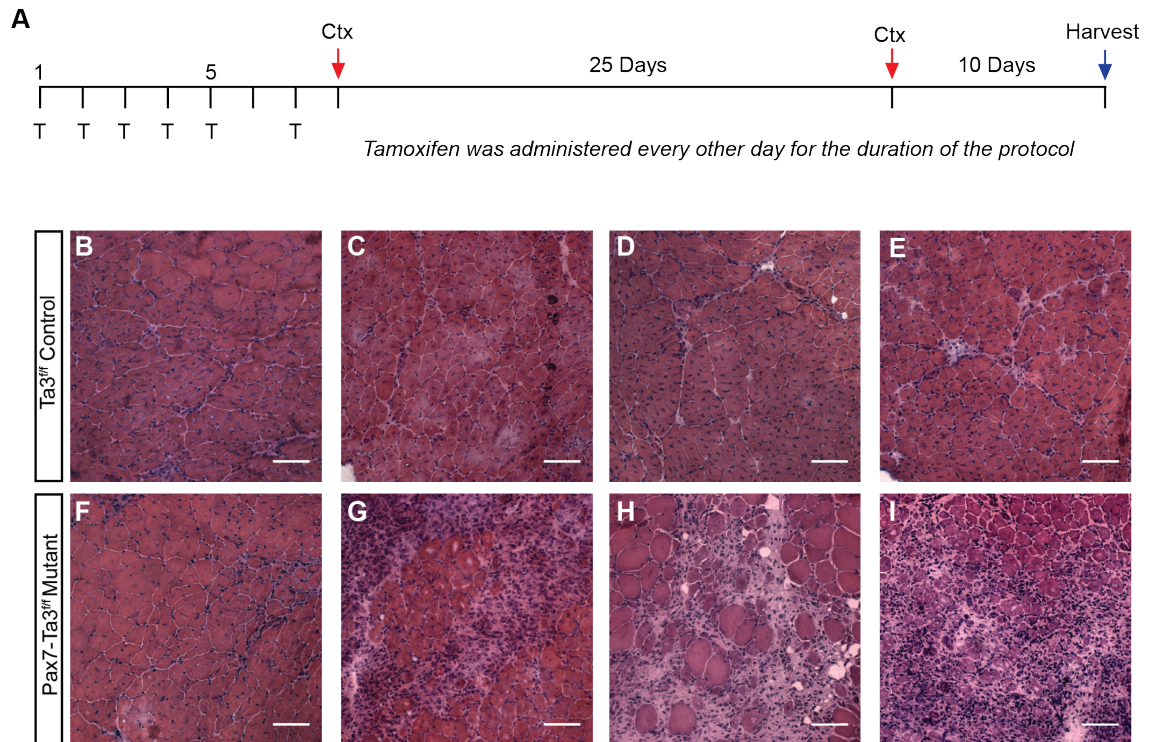


Figure 3.11 Satellite cell specific loss of *Ta3* results in limited SC self-renewal and loss of muscle regeneration after repeated CTX injuries.

(A) Schematic of tamoxifen and CTX treatment. (B-I) Representative images of 12 TA muscle sections from each *Pax-Ta3^{ff}* Mutant and *Ta3^{ff}* Control mouse were analysed by H&E staining on days 10 days after 2nd injury. (Scale bars = 50 μ m)

3.6 Discussion

The aim of this chapter was to investigate the requirement of *Ta3* in SCs for muscle regeneration after injury. Published research has shown that mutations in *Ta3* lead to the loss of primary cilia and disruption in Shh signalling, both of which have been shown to play vital roles in normal SC function during muscle regeneration (Fu et al., 2014; Jaafar Marican et al., 2016; Koleva et al., 2005).

The experiments in this chapter utilised the generation of a tamoxifen inducible, SC specific *Ta3* mutant mouse line. We successfully generated *Ta3^{ff}Pax7^{Cre-ERT2}* mice that also expressed one or more reporters (*R26R^{LacZ}*, *R26R^{td-Tomato}*, *Pax7^{ZsGreen}*). Cre-recombinase mediated recombination in these mice was at least 93% efficient after 3 consecutive tamoxifen injections, in line with previously published data on the *Pax7^{Cre-ERT2}* mouse (Lepper et al., 2009). Caution has to be applied when using the Cre-loxP system in SCs however, due to the ability of very few SCs to repopulate the whole muscle after injury if they have escaped recombination (von Maltzahn et al., 2013). Therefore, we administered tamoxifen by IP injection every second day throughout the regeneration period.

SC specific KO of *Ta3* caused a deficiency in muscle regeneration after CTX injury as indicated by significantly smaller myofibres at all time points studied (5, 10, 15 and 25 days). It was evident that muscle regeneration was delayed in *Pax7-Ta3^{ff}* mutants due to the prolonged expression of α -SMA 10 days after injury. However, this expression was downregulated again by 15 days. This, along with the fact that there were regenerating fibres present in *Pax7-Ta3^{ff}* mutants suggested a deficiency in regeneration but not a complete loss or inability of SCs lacking cilia to contribute to the process. In *Ta3^{ff}* control mice, by 25 days of regeneration, myofibres had regenerated to a point where their size was not significantly different to the non-injured myofibres. This is consistent with published observations that regeneration restores muscle to homeostasis by 28 days post injury (Hardy et al., 2016). However, in the *Pax7-Ta3^{ff}* mutants myofibres were still significantly smaller than the non-injured muscle. It is possible that this is as far as the myofibres are able to recover, however it would be interesting to assess the muscle at an additional later time

point, maybe 30-35 days post injury, to determine if the myofibres are able to make a full recovery or not.

The delayed/ deficient phenotype but not complete loss of regenerative ability fits well with a cilium mutation. As previously discussed, Shh signalling in *Ta3* mutants is not simply a KO of Shh signalling. *Ta3* mutants show many pleiotropic phenotypes due to the mis-regulation of $GLI^A:GLI^R$ ratio. It is therefore possible that the low level of regeneration that is occurring is due to a low level of Shh signalling still taking place in *Pax7-Ta3^{ff}* SCs, however the highest levels of Shh signalling are perturbed which are required for normal and effective SC function after injury. It would therefore be interesting to determine the Shh signalling status in *Ta3* mutant SCs, for example by sorting cells and examining expression of GLI isoforms.

From these injury experiments it is not possible to deduce at what stage in the regeneration process SCs from *Pax7-Ta3^{ff}* mice are defective. It could be a problem with SC activation, proliferation, differentiation or apoptosis that cause a regeneration phenotype. This will be addressed in Chapters 4 and 5.

After confirming a phenotype for *Pax7-Ta3^{ff}* mutant SCs during muscle regeneration we were interested to investigate their role during muscle homeostasis and everyday wear and tear. There is still much discussion in the field as to the contribution of SCs to the turn-over of adult skeletal muscle. It is largely accepted that SCs contribute greatly to post-natal and juvenile muscle growth (Mesires and Doumit, 2002; Oustanina et al., 2004). However, there is conflicting evidence regarding the contribution of SCs to myonuclear turnover in uninjured muscles. Some studies show that up to 20% of myofibres in adult mice hind limbs are tdTomato⁺ 2 weeks after SC labelling (Pawlikowski et al., 2015). Whilst others have found that skeletal muscle is still able to undergo hypertrophy in the absence of SC in the short term (McCarthy et al., 2011). However, a follow up study revealed that growth does plateau in the absence of SCs (Fry et al., 2014b). We hypothesised that if SCs are contributing to myonuclear turnover and cilium deficient SCs have reduced self-renewal, that there would be a depletion in the SC number in *Pax7-Ta3^{ff}* mutant mice that had been treated with tamoxifen and then allowed to live normally. Due to a potential reduction in SC number we anticipated a more severe muscle regeneration phenotype following CTX injury in *Pax7-Ta3^{ff}* mutant mice that

had been treated with tamoxifen 4 months prior to injury (LT experiment) compared to those treated with tamoxifen 1 week prior to injury (ST experiment). However, there was no significant difference in myofibre size 10 days after injury in *Pax7-Ta3^{ff}* mutant mice in the ST experiment compared to the LT experiment. Suggesting the pool of SCs was similar in both circumstances. This is likely due to a low turnover of SCs leaving enough to partially recover the muscle after injury. To exacerbate any potential phenotype, it would be interesting to repeat these experiments incorporating an exercise regime. Causing stress and small injuries to the muscles would require the contribution of some SCs for low level repair. It would be interesting to see how *Pax7-Ta3^{ff}* mutants would then respond to a severe injury with CTX.

To understand further if *Pax7-Ta3^{ff}* mice have a defect in self-renewal, as would be expected from evidence from cilia depleted SCs (Jaafar Marican et al., 2016), we carried out double injury experiments. Initial results appear to suggest that muscle regeneration is severely compromised in *Pax7-Ta3^{ff}* mutant mice after a second CTX induced injury. In 3/4 *Pax7-Ta3^{ff}* mutants there were areas of injured muscle that appeared to be completely devoid of regenerating fibres, this was not seen in any of the *Ta3^{ff}* control mice. However, there are some limitations to these experiments. One of the *Pax7-Ta3^{ff}* mice showed levels of regeneration that were similar to the regeneration seen in other *Pax7-Ta3^{ff}* mutants after a single injury. It is possible that either the first or second CTX injection in this mouse missed the TA muscle and therefore the muscle was only subjected to a single injury. Unfortunately, with the technique used it is not possible to determine that the same part of the muscle has been injured twice.

Another limitation of the CTX injury technique is possible differences in diffusion of the toxin throughout the muscle with each injection. Every care was taken to try to direct the injection to the same place each time however on some occasions the CTX may only hit a small area on the edge of the muscle, which sometimes leads to less diffusion of CTX throughout the muscle. This could lead to a large volume of CTX concentrating in a small area of the muscle, causing a far more severe injury in this localised area. This would then result in more necrosis than if the CTX had diffused throughout the whole muscle, potentially requiring full *de novo* regeneration of muscle fibres rather than just

repair. Unfortunately, analysis of images of the full area of the TA muscle from the double injury experiments indicates that the area of damage in some of the *Pax7-Ta3^{ff}* mutants was quite small (**Fig 3.10F, H**). This seemed to coincide with a severe regeneration phenotype, compared to *Ta3^{ff}* controls, in which the area of injury was quite extensive (**Fig 3.10A-D**). It is therefore possible that the lack of regeneration was due, at least in part, to the very localised injury. This was observed in a couple of mice after single injury with small areas of muscle damage (data not shown). To draw more definitive conclusions, this double injury experiment should be repeated to increase the probability that both CTX injections cover the same, widespread area of the TA muscle.

To summarise, in this chapter we have shown that SC specific mutations in *Ta3* cause a delay in regeneration following injury with CTX and that there is potentially a defect in SC self-renewal with preliminary evidence suggesting that double injury with CTX may cause a very severe regeneration defect. The molecular mechanism through which this occurs is still not clear but will be investigated in Chapters 4 and 5.

Chapter 4 The loss of *Talpid3* in muscle satellite cells on their ability to migrate, proliferate and differentiate

4.1 Introduction

The results obtained in Chapter 3 suggest that the loss of *Ta3* from SCs impairs their ability to efficiently repair and regenerate skeletal muscle following injury. This chapter will explore in more detail the phenotypic differences between WT and *Ta3* mutant satellite cells to try to understand the reason for the deficiency in regeneration.

The proliferation and migration of satellite cells after activation is vital to their ability to efficiently regenerate injured skeletal muscle. Following activation, SCs must migrate along their associated myofibre or between myofibres to the site of injury. They must be able to proliferate to produce a pool of myoblasts that will differentiate to repair and repopulate damaged myofibres.

To investigate if the loss of *Ta3* from SCs affects their ability to migrate or proliferate we used time-lapse microscopy to visualise the behaviour of WT and *Ta3* mutant satellite cells whilst still associated with their resident myofibre. Previously published research using this technique has shown that SCs move from beneath the basal lamina of their myofibre to the exterior within 12-24hrs of activation (Siegel et al., 2009). Proliferation of SCs has been shown to be asynchronous, with the first division happening anytime from 24-48hrs after activation, subsequent division happens anytime from 5-17hrs after the first division with an average of 10hrs (Siegel et al., 2011).

As previously discussed, *Ta3* mutations leads to a loss of primary cilia formation which subsequently causes a disruption of Shh signalling. Primary cilia are present on quiescent SCs and are disassembled within the first 24hrs of activation, we therefore wanted to capture this period during our time-lapse recording and imaging was started 4-5hrs after myofibre isolation. The primary cilium begins to appear in SCs again between 72-96hrs in those cells destined

to re-enter the stem cell niche, we therefore continued our imaging for 90hrs after isolation.

Myogenic progenitor cells that are generated following SC proliferation must differentiate and fuse to each other or the damaged myofibre in order to repair damaged muscle. Myogenic progenitors generated from SCs in culture will begin to spontaneously differentiate when the level of serum in the culture media is low. To investigate the effects of a *Ta3* mutation on differentiation we cultured SCs isolated from *Ta3^{ff}* controls and *Pax7-Ta3^{ff}* mutants, following tamoxifen induction, on matrigel and observed morphological changes that are associated with myogenic differentiation. Once the presence of mature myotubes was evident in *Ta3^{ff}* control cultures, cells were fixed and immunostained to detect Myosin Heavy Chain (MHC) protein.

4.2 Analysis of migration of *Talpid3* mutant satellite cells

To assess any changes in migration due to the loss of *Ta3* myofibres from the EDL, composed predominately of type II fast twitch myofibres, were used. At starting number of 81 SCs on 48 myofibres from 4 *Ta3^{ff}* control mice and 97 SCs on 55 myofibres from 4 *Pax7-Ta3^{ff}* mutant mice were analysed using the MTrackJ plugin for ImageJ. Each SC was manually tracked in each frame and migration distance was recorded until the SC divided or to the end of the video, one daughter cell was then picked at random and analysed in a new track unless they separated and migrated in different directions, in which case both were analysed (**Fig. 4.1A', A''**). Including F1 and F2 daughter cells in total migration of 228 SCs from *Ta3^{ff}* controls and 266 SCs *Pax7-Ta3^{ff}* mutants were tracked.

4.2.1 Migration speed

Migration speed was calculated from the distance recorded for each track and the number of frames over which the cell was tracked (converted to time in hours). The average migration speed of all SCs tracked from *Ta3^{ff}* controls and *Pax7-Ta3^{ff}* mutants was 8.7µm/hr for both (**Fig. 4.1B**). Within the first 24hrs following isolation SCs are activated and begin to move through the basal lamina to the surface of the myofibre, migration during this period is

usually slower than after the SC has reached the exterior. Therefore, the migration speeds were re-calculated within the first 24hrs and 24+hrs to represent these different migration phases. *Ta3^{ff}* controls showed an average migration speed of 8.6 and 12.1µm/hr between 0-24hrs and 24+hrs respectively whilst in *Pax7-Ta3^{ff}* mutants migration speeds were 7.1 and 9.4µm/hr (**Fig. 4.1C**). For both time periods, there was no significant difference between *Ta3^{ff}* controls and *Pax7-Ta3^{ff}* mutants. The appearance that *Ta3^{ff}* controls migrate slightly faster than *Pax7-Ta3^{ff}* mutants both between 0-24hrs and 24+hrs but not when the average migration speed is taken over all (**Fig. 4.1C** vs **Fig. 4.1B**) is due to only F0 cells being analysed in the split time periods, whilst the total average was determined from all SC generations. This difference led to the analysis of migration speed of each generation of cells, again there was no significant difference between *Ta3^{ff}* controls and *Pax7-Ta3^{ff}* mutants (**Fig. 4.1D**).

It appears that the loss of *Ta3* does not affect the ability of SCs or their daughter cells to migrate along their host myofibre. One thing of note is the migration speed of all cells analysed was much slower than previously published data (maximum average of 12µm/hr compared to 30-40µm/hr). The timelapse interval of 20 minutes assumes linearity of migration however SCs do not always migrate in a linear fashion, therefore using smaller intervals may improve accuracy of migration data, this will be discussed further in section 4.6.

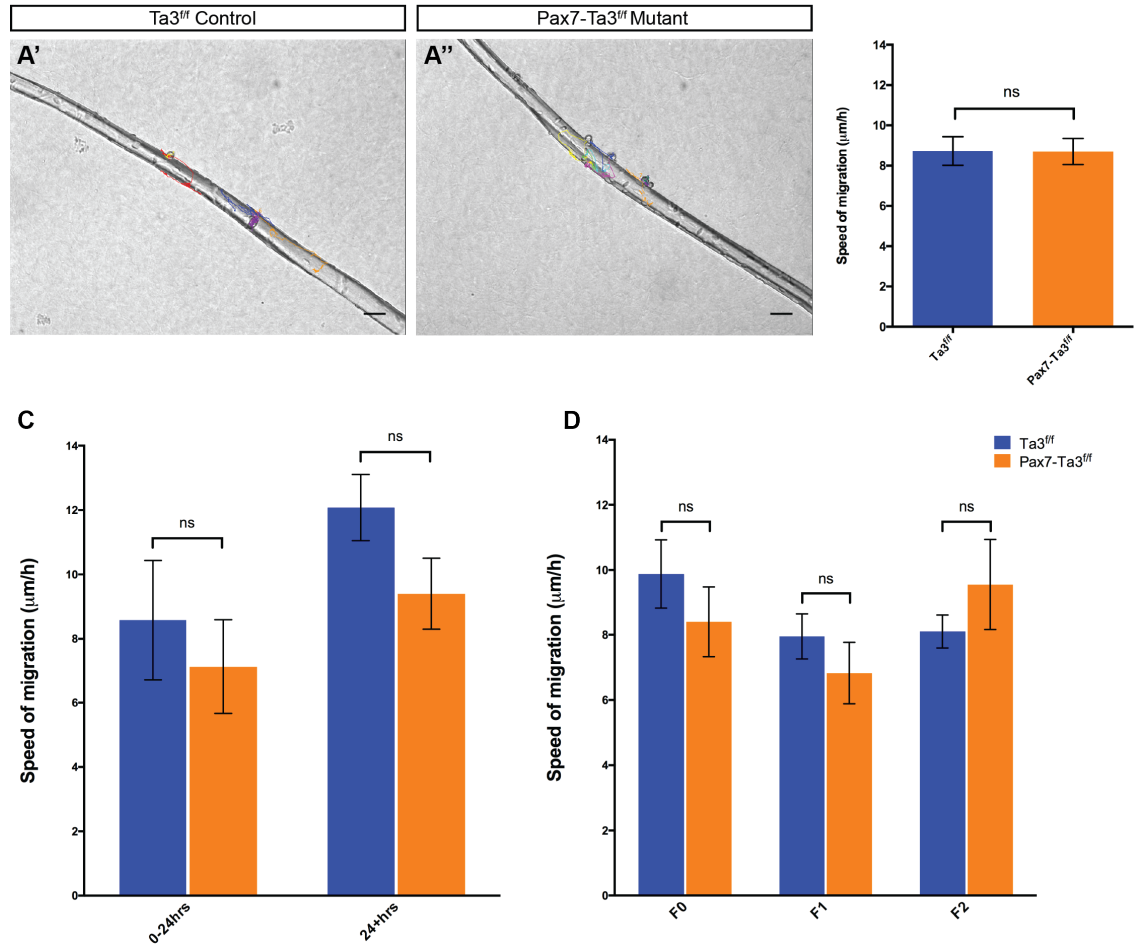


Figure 4.1 Satellite cell specific loss of *Ta3* does not affect satellite cell migration speed.

(A', A'') Example tracks from migration analysis using MTrackJ plugin for ImageJ. Scale bars = 50μm. (B) Average migration speed of all SCs analysed calculated as average of population mean from each mouse. (C) Average migration speed of F0 SCs within the first 24hrs of time-lapse recording and 24+hrs until first division calculated as average of population mean from each mouse. (D) Average migration speed of SCs and their daughter cells, F0 = SCs, F1= daughters from first division, F2 = daughters from second division calculated as average of population mean from each mouse. ns indicates $p > 0.05$ calculated by unpaired, two-tailed t-test. Error bars = SEM.

4.3 Analysis of proliferation of *Talpid3* mutant satellite cells

To assess the effects of the loss of *Ta3* on SC proliferation we analysed both the number of divisions that occurred and the time taken for the first and subsequent divisions to occur. Divisions were manually observed during the time-lapse video and the frame number of the division was noted, this was then converted to give the time of division.

4.3.1 Timing of proliferation

Published data suggests that once activated, SCs will undergo their first division within 24-48hrs. In this study time to first division ranged from 27-70hrs and 24-71hrs from the beginning of recording in *Ta3^{ff}* controls and *Pax7-Ta3^{ff}* mutants respectively, with an average time of 43 and 45hrs, which is not significantly different ($p=0.8$, $n=4$) (**Fig. 4.2**). Average time to first division was calculated by averaging the population mean of each mouse. In total 74 SCs from *Ta3^{ff}* controls and 82 SCs *Pax7-Ta3^{ff}* mutants were used in this analysis. The large range in time to first division is in line with the observation that SC divisions occur at irregular intervals. This continued with subsequent division happening anywhere from 2-50hrs and 9-30hrs after the first division in *Ta3^{ff}* controls and *Pax7-Ta3^{ff}* mutants respectively. The average cycling time to the next division in *Ta3^{ff}* controls was 17hrs and in *Pax7-Ta3^{ff}* mutants was 15hrs, again not significantly different ($p=0.5$, $n=4$) (**Fig. 4.2**). Average time between first division and second divisions was calculated by averaging the population mean of each mouse. In total 73 SCs from *Ta3^{ff}* controls and 51 SCs *Pax7-Ta3^{ff}* mutants were used in this analysis.

The exact timing of any further divisions was not calculated due to the formation of cell clusters in the majority of videos analysed which made it very hard to determine the exact frame in which a division occurred.

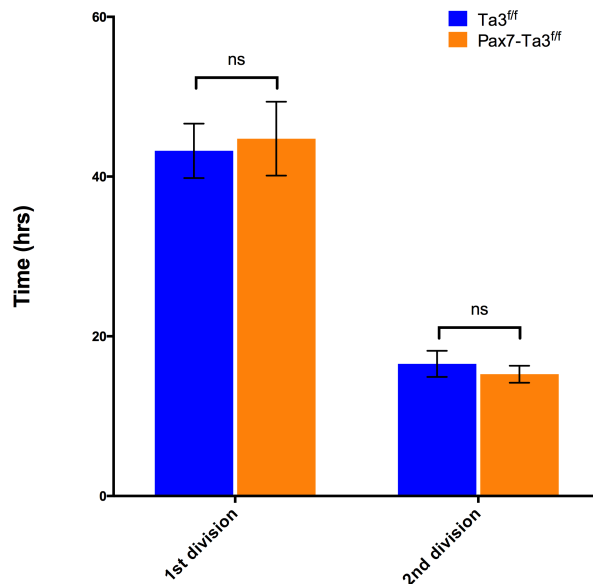


Figure 4.2 Satellite cells specific loss of *Ta3* does not affect the time taken for SCs to divide after activation.

Graph showing the average time taken for SCs to undergo their 1st division and time between their 1st to 2nd division, calculated by averaging the population means from each mouse. Error bars = SEM. $p > 0.05$, $n = 4$ calculated by unpaired, two-tailed t-test.

4.3.2 **Number of divisions**

There appeared to be no difference in the timing of divisions between *Ta3^{ff}* controls and *Pax7-Ta3^{ff}* mutants. Next, we analysed SC proliferation to see if there was any difference in the number of divisions SCs went through between controls and mutants.

In 3 out of the 4 *Ta3^{ff}* control mice all SCs divided at least once compared to *Pax7-Ta3^{ff}* mutant mice in which each mouse had at least one SC that did not divide. The average percentage of cells that did not divide was 7% and 13% in *Ta3^{ff}* controls and *Pax7-Ta3^{ff}* mutants respectively (**Fig. 4.3**). This is not statistically significant ($p = 0.5$, $n = 4$). This is likely due to the large SEM associated with the *Ta3^{ff}* control data due to the one mouse in which 5/19 (26%) SCs did not divide at all whilst all other control SCs did divide.

There was no significant difference in the percentage of SCs that went through 1, 2 or 3+ divisions in *Pax7-Ta3^{ff}* mutants compared to *Ta3^{ff}* controls (**Fig. 4.3**) (p=0.5, 0.07, 0.1 respectively, n=4). There is a possible trend in fewer *Pax7-Ta3^{ff}* mutant SCs going through 2 divisions compared to *Ta3^{ff}* controls (p= 0.07). Again, this is likely due to the large differences between individual animals. A higher number of experimental animals is needed to increase the statistical power of these results.

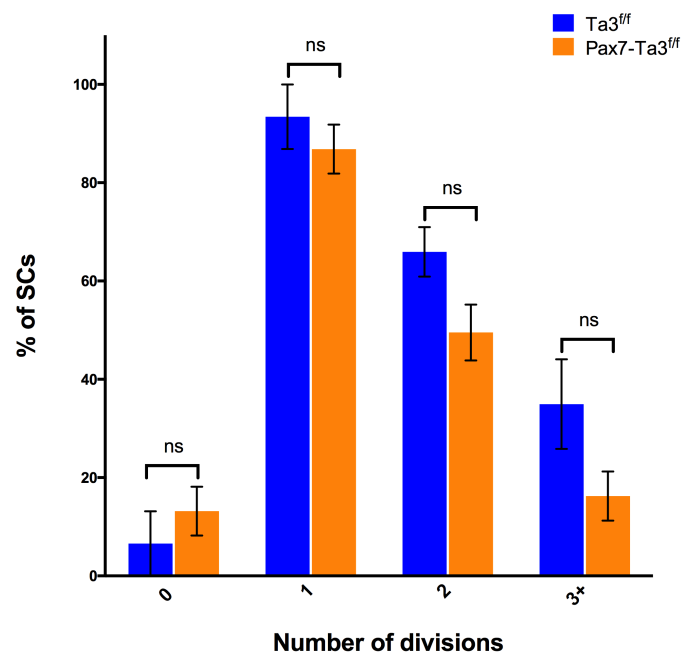


Figure 4.3 Satellite specific loss of *Ta3* does not affect the number of divisions activated SCs go through.

Graph showing the average percentage of SCs that divide 0, 1, 2 or 3+ times during the time-lapse movie (90-92hrs after isolation) from *Ta3^{ff}* controls (n=4) and *Pax7-Ta3^{ff}* mutants (n=4), calculated by averaging population mean from each mouse. Error bars = SEM. ns indicates p>0.05, calculated by unpaired, two-tailed t-test.

4.4 Analysis of differentiation of *Talpid3* mutant satellite cells

We found that SCs with mutated *Ta3* appeared to have no defect in migration compared to WT SCs. It remains unclear as to whether proliferation is affected. We also wanted to investigate how a SC specific loss of *Ta3* affects isolated SCs ability to differentiate. To isolate SCs, myofibres were dissected and plated on matrigel coated 12 well plates. Unfortunately, isolation of SCs was not efficient enough to obtain a high enough cell number to accurately count using a haemocytometer. To try to ensure a similar number of cells were seeded, at the time of plating myofibres were counted and between 100-120 were plated in each well. After 3 days of incubation SCs had migrated onto the matrigel plate and myofibres were removed. Cells were re-plated on fresh matrigel, at this stage all cells from one well were transferred together to a new well, cells were not diluted or split. SCs were incubated for up to 14 days post isolation. Images of the cells were taken every other day to assess differentiation and finally cells were fixed and stained with MF20 to visualise mature myotubes.

At 6 days post isolation (dpi), which is 2 days after re-plating, there were a similar number of cells present in both *Ta3^{ff}* control and *Pax7-Ta3^{ff}* mutant cultures upon visual assessment (**Fig. 4.4A', A''**). Unfortunately, reporter mice were not available for these experiments so it was not possible to determine the proportion of SCs compared to other types of cells that may be present in the culture. Due to the limited number of culture wells it was not possible to identify myogenic cells by immunolabelling with Pax7 or MyoD as this would have required fixing cultures at early time points before terminal differentiation had occurred.

At 8dpi many elongated myoblasts were present that had started to orientate themselves parallel to each other in *Ta3^{ff}* controls (**Fig. 4.4B'**) whereas only a few cells from *Pax7-Ta3^{ff}* mutants had an elongated shape and cells were orientated more randomly (**Fig. 4.4B''**). By 12dpi long multinucleated myotubes had formed in *Ta3^{ff}* control cultures and by 14dpi filled the majority of the field of view (**Fig. 4.4C', D'**). This was in stark contrast to *Pax7-Ta3^{ff}* mutant cultures in which only a few short myotubes had begun to form. Even by 14dpi,

these were only bi-nucleated suggesting fusion was limited to only 2 myoblast (**Fig. 4.4C''**, **D''**).

Immunostaining with an MF20 antibody that recognises Myosin Heavy Chain (MHC) protein, a component of mature myofibres, revealed all cells in $Ta3^{ff}$ control cultures were MHC positive and myofibres were multinucleated (**Fig. 4.4E'**) whereas very few cells were MHC positive in $Pax7-Ta3^{ff}$ mutant cultures (**Fig. 4.4E''**). Staining with DAPI revealed that there were many cells present in $Pax7-Ta3^{ff}$ mutant cultures, but they were not MHC positive and had not fused to form mature myotubes. This suggests that the loss of $Ta3$ in SCs impairs their normal differentiation and fusion to form mature myotubes.

The intention with this experiment was to first determine optimal culture conditions for SC culture and differentiation and then repeat the experiment with a more accurate count of the number of SCs plated with the intention of quantifying the number of SCs per field of view every second day throughout the culture period or assessing proliferation through analysis of BrdU or Edu incorporation. Unfortunately, we were not able to obtain sufficient SCs to carry out this quantification. Therefore, it was not possible to assess whether SCs from $Pax7-Ta3^{ff}$ mutants were proliferating at a similar rate to SCs from $Ta3^{ff}$ controls. This means it is possible that the differences in the number of multinucleated myotubes is due to there being few SCs present in the $Pax7-Ta3^{ff}$ mutant cultures.

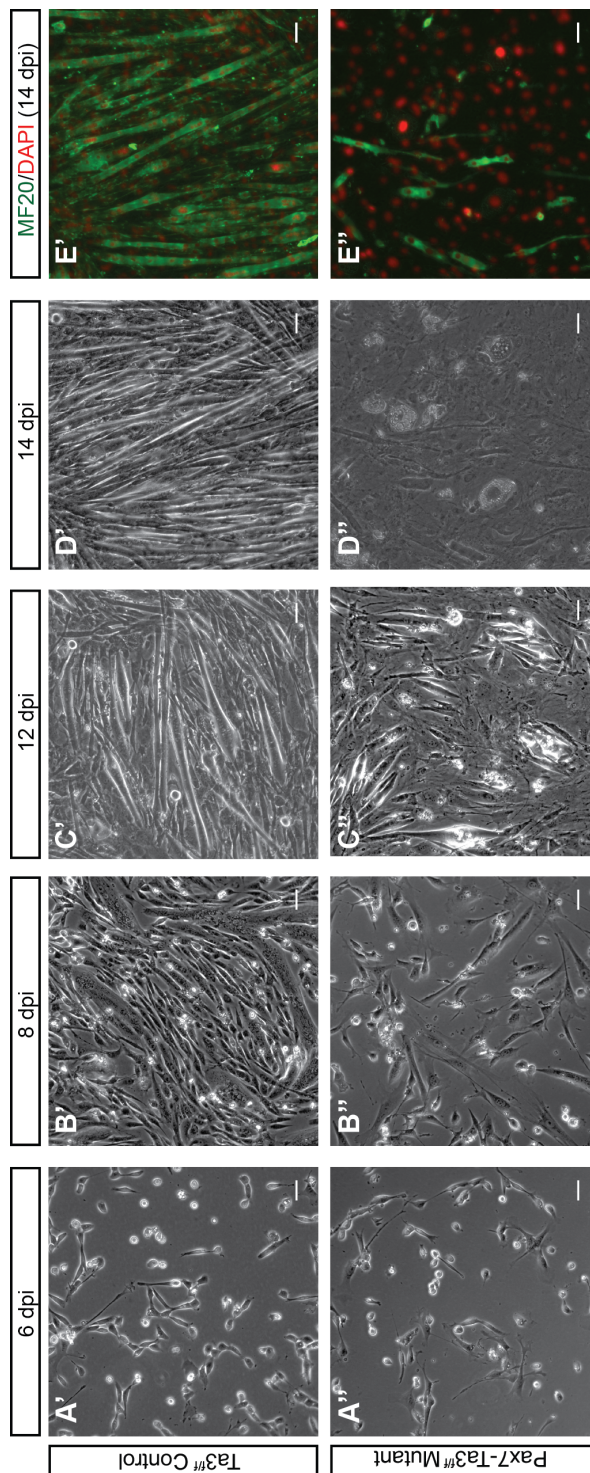


Figure 4.4 Satellite specific loss of *Ta3* disrupts differentiation ability of SCs in culture.

(A-D) Representative phase 1 images of SCs cells in culture isolated from myofibres from *Ta3^{ff}* control (A'-E') and *Pax7-Ta3^{ff}* mutant (A''-E'') mice and allowed to spontaneously differentiate (n=2). (E', E'') Immunostaining against MF20 (green) and DAPI staining (red) of differentiated SCs. Scale bars = 50 μ m.

4.5 Discussion

The aim of this chapter was to investigate the effects that the loss of *Ta3* has on SCs ability to migrate along their host myofibre, proliferate and differentiate. These steps are all vital for normal muscle regeneration following injury, which was found to be impaired in mice with *Ta3* deficient SCs.

Migration defects have been reported in fibroblasts isolated from *Ta3*^{-/-} mouse limb. In a scratch assay *Ta3*^{-/-} cells migrated more slowly and with less directionality compared to WT cells and therefore took longer to close the scratch (Bangs et al., 2011). We did not observe this defect in the SCs from *Pax7-Ta3*^{ff} mutants, which migrated at the same speed as SCs from *Ta3*^{ff} controls. The speed of migration of SCs in these experiments was much slower than previously published. Three studies of note have measured SCs migration speed using time lapse imaging of SCs on their associated myofibre. These showed an average migration speed of 30-40µm/hr in WT SCs (Collins-Hooper et al., 2012; Otto et al., 2011; Siegel et al., 2009). The technique used to isolate the myofibres was the same in all experiments and was identical to the method used here. The culture media used to culture the myofibres was also the same. Siegel et al. (2009) cultured myofibres in suspension for 24hrs prior to transferring into collagen matrix for time lapse imaging, it is not clear when or if myofibres in the other experiments were transferred into collagen.

The major discrepancy of these published studies with our research was the frequency of images taken, every 10-15 minutes compared to every 20 minutes. SCs do not migrate in a linear fashion and often move back and forth, it is therefore possible that some movements of the SCs were missed due to fewer images. However, it seems unlikely that this would account for migration speeds being around a quarter the speed of those previously published (8.7µm/hr compared to 30-40µm/hr).

Otto et al. (2011) detailed the dynamic nature of migration speed following isolation, showing that migration is much slower whilst the SC is still under the basal lamina (27µm/hr), then once it has emerged migration speed increases (50µm/hr). Our observations followed a similar trend with migration speed in the first 24hrs being slower, however speed only increased marginally and did not double as in Otto's study.

Another key property of SCs is their ability to proliferate upon activation to generate a large enough population of MPCs to repair and regenerate damaged muscle. Shh has been implicated as a mediator of cell proliferation in a number of cell types including SCs. Koleva et al. (2005) reported an increase in BrdU incorporation in SCs cultured in the presence of Shh, but this increase was halved with the addition of cyclopamine, providing evidence that the increase in proliferation was dependent on the Shh pathway. Shh has also been proposed as a possible therapy for muscular dystrophies following the discovery that Shh can increase the proliferative capacity of SCs isolated from *mdx* mice (Piccioni et al., 2014b). It is therefore possible that *Pax7-Ta3^{ff}* mutant SCs may show proliferation defects due to disruptions in Shh signal transduction. Although we did not observe any statistically significant differences in the number of divisions *Pax7-Ta3^{ff}* mutant SCs went through compared to *Ta3^{ff}* controls, there was an observable trend that fewer mutant SCs made it to each round of proliferation and an increased proportion did not divide at all during the 85+hrs of recording. This would be in line with findings from Bashford (2015) that mutations in *Ta3* lead to reduced proliferation in granule neuron progenitor (GNP) cells. Loss of another protein, Cep120, also produces a reduced proliferation phenotype in GNP cells. Cep120 mutants also fail to form primary cilia. It has been shown that *Ta3* and Cep120 directly interact, with Cep120 being dependant on *Ta3* for its correct localisation and distribution between mother and daughter centrioles (Wu et al., 2014). Therefore, it is reasonable to propose that mutations in *Ta3* may lead to reduced proliferation due to effects on Cep120 distribution. Bringing these findings together it appears that *Ta3*, primary cilia and Shh signalling are all required for normal proliferation. It is therefore important that proliferation in *Pax7-Ta3^{ff}* mutant SCs is re-assessed with a greater number of biological replicates to conclude if proliferation is affected in our model.

The data collected from the analysis of time-lapse imaging of *Ta3^{ff}* control and *Pax7-Ta3^{ff}* mutant SCs appears to show that a *Ta3* mutation does not affect SCs ability to migrate compared to controls or their ability to proliferate. However, there were multiple technical problems that occurred during the collection of the data, in order to draw unambiguous conclusions, the experiments need to be repeated. Here, this experiment was conducted on 8

separate occasions in which myofibres from 7 $Ta3^{ff}$ control mice and 8 $Pax7-Ta3^{ff}$ mutant mice were isolated and set up for time-lapse imaging. On 2 occasions the experiment ran as planned, while on other occasions some wells had bacterial infections or myofibres died before the end of the experiment. Much of this data was disregarded, however some myofibres used for the analysis were in the same plate as others that had become infected. Despite these difficulties there are still trends within the data which will be useful for informing future experiments.

We have shown that $Pax7-Ta3^{ff}$ mutant SCs are not able to regenerate myofibres as efficiently as those from $Ta3^{ff}$ controls. In an *in vivo* setting of skeletal muscle injury there are however other cell types that might be contributing in part to the repair of damaged muscle, therefore we isolated SCs to try to reveal any direct phenotypic traits that are present in the mutant SCs themselves. The involvement of Shh signalling in myogenic differentiation has been well studied. Shh signalling has been shown to be vital in the control of MRFs that allow MPCs to progress through differentiation (Borycki et al., 1999). Evidence is also present for the role of Shh in the reactivation of the myogenic pathway in adult skeletal muscle following injury through the control of Myf5 and MyoD (Straface et al., 2009). These previous studies are consistent with the striking defect observed in the differentiation ability of $Pax7-Ta3^{ff}$ mutant SCs, with reduced number of MHC positive myofibres compared to $Ta3^{ff}$ controls cultured for the same amount of time. This could be due to inability of mutant SCs to sufficiently upregulate Myf5 or MyoD and therefore a reduced ability to enter the myogenic programme. Unfortunately, due to time constraints it was not possible to directly analyse the expression of the MRFs during the differentiation time course. It would be very interesting to compare the expression of Myf5 and MyoD in the first couple of days of differentiation and then later the expression of Mgn and MRF4 by immunostaining of mutant and control SCs in culture.

There were also some technical difficulties encountered during these experiments. In our hands, the isolation technique did not harbour enough SCs to accurately count them. Therefore, an indirect approach was used to ensure

that a similar number of *Ta3^{ff}* control and *Pax7-Ta3^{ff}* mutant cells were plated. However, this allows for the possibility that there were more SCs present in control cultures compared to mutant cultures and could have limited the possibility for mutant SCs to fuse and differentiate. Efforts were made to plate the same number of myofibres in each culture and visual assessment showed a similar coverage of cells in each culture. It was also observed that in the control cultures, even in areas where cell coverage was sparse formation of myotubes still occurred. This was not the case in the mutant cultures, where few myotubes were seen even in areas of dense cell coverage. It is possible that differentiation was impaired due to presence of non-SC cell types. The purity of the cell population plated could not be accurately assessed, as reporter mice were not available for these experiments. It is therefore possible that even though the cell density of control and mutant cultures appeared the same, there may have been much higher proportion of SCs in control cultures, allowing for the generation of more myotubes. It would be ideal to repeat these experiments using *R26R^{tdTom}* reporter mice crossed with *Pax7-Ta3^{ff}* mutant and *Pax7-Ta3^{f/+}* control mice to enable visualisation of tdTomato positive SCs and calculate the purity of SC cultures. It would also be possible to use a marker of other cell types that could possibly be in the culture, for example fibroblast or adipocytes to negatively assess purity.

To summarise, in this chapter we have shown that the loss of *Ta3* from SCs does not appear to affect their ability to migrate but may reduce their ability to proliferate. It is also likely that SC specific mutations of *Ta3* leads to a reduction in myogenic differentiation and the formation of myotubes. This could explain the reduced capacity of *Ta3* mutant SCs to support muscle regeneration following injury that was observed in chapter 3. It is possible the reduction of differentiation is due to a reduced upregulation of MRF members following SC activation, this will be explored in more detail in Chapter 5.

Chapter 5 The effect of *Talpid3* loss in satellite cells on their expression of myogenic regulatory genes

5.1 Introduction

In chapters 3 and 4 we have shown that a SC specific loss of *Ta3* impairs their ability to efficiently repair and regenerate skeletal muscle following localised injury and that this impairment appears to be due to a decreased ability of the satellite cells to differentiate and possibly a decreased ability to proliferate. In chapter 4 we showed that *Pax7-Ta3^{ff}* SCs were not able to form mature myotubes *in vitro*. This chapter will investigate if this is due to an inability to correctly re-activate the myogenic differentiation pathway by analysing the expression of MRFs (Myf5, MyoD and Mgn) in *Pax7-Ta3^{ff}* mutant SCs compared to *Ta3^{ff}* controls at 0, 24, 48 and 72hrs after myofibre isolation (hereafter referred to as T0, T24, T48 and T72). The number of SCs and myofibres analysed at each time point is summarised in **Table 5.1**. We thought measuring fibres from 3 mice of each genotype would be sufficient for determining the differences between controls and mutants, but from the data it is clear a greater n number is required. Therefore, this chapter serves as a pilot study that needs to be repeated to strengthen the results.

Table 5.1 Number of SCs and myofibres analysed at each time point.

| Time point | Number of SCs | | Number of Myofibres | | Number of Mice | |
|------------|-------------------------|------------------------------|-------------------------|------------------------------|-------------------------|------------------------------|
| | <i>Ta3^{ff}</i> | <i>Pax7-Ta3^{ff}</i> | <i>Ta3^{ff}</i> | <i>Pax7-Ta3^{ff}</i> | <i>Ta3^{ff}</i> | <i>Pax7-Ta3^{ff}</i> |
| T0 | 90 | 96 | 22 | 20 | 4 | 4 |
| T24 | 80 | 109 | 14 | 21 | 3 | 4 |
| T48 | 149 | 168 | 17 | 22 | 3 | 4 |
| T72 | 322 | 295 | 32 | 31 | 3 | 4 |

The timing and expression of Pax7, Myf5, MyoD and Mgn in SCs following activation has been well studied (summarised in **Fig. 5.1**) and their roles have been well defined.

Quiescent SCs robustly express Pax7 and therefore 100% of SCs are Pax7⁺ immediately after myofibre isolation. Of these Pax7⁺ SCs approximately 90% are also Myf5⁺ whilst approximately 12% are also MyoD⁺ (Beauchamp et al., 2000). At this stage Mgn is not expressed in SCs. Within 24hrs MyoD⁺ SCs become much more common with approximately 65% of SCs expressing either Myf5, MyoD or both together (Cornelison and Wold, 1997). By 48hrs approximately 85% of SCs are Pax7⁺/MyoD⁺ with the expression of Mgn starting between 48 and 72hrs. By 72hrs approximately 40% of SCs are Pax7⁺/MyoD⁺. At this stage SCs appear to make a fate decision, those that begin to express Mgn are destined for terminal differentiation whilst those that maintain Pax7 expression will re-enter the stem cell niche (Zammit et al., 2006).

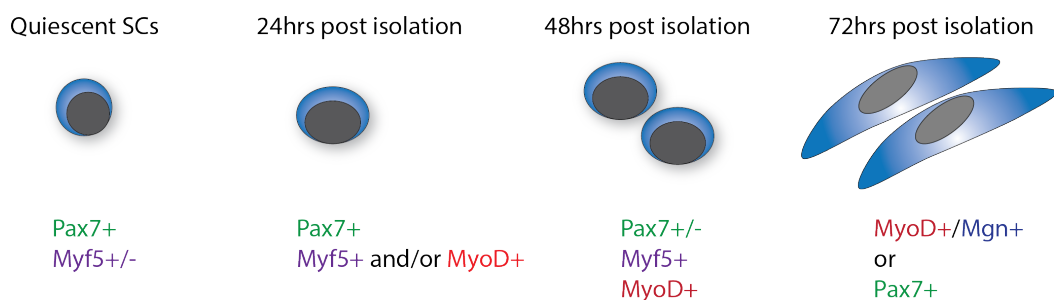


Figure 5.1 Expression of MRFs during SC activation and differentiation

Quiescent SCs express Pax7, a large proportion also express Myf5. Following activation by isolation almost all begin to express either Myf5/MyoD or both. By 48hrs post isolation all SCs will be expressing either Myf5 or MyoD and many will have down regulated Pax7. 72hrs post isolation a proportion of SCs will express Mgn, these are destined for terminal differentiation whilst a smaller population will re-express Pax7, destined to re-enter the stem cell niche.

To investigate if there are any changes in Pax7 or MRF expression in SCs with a mutation in *Ta3* EDL myofibres were isolated from *Ta3^{ff}* control and *Pax7-Ta3^{ff}* mutant mice that had been exposed to the tamoxifen scheme detailed in **Fig 5.2**. All mice used also contained *Pax7^{ZsGreen}* reporter to visualise Pax7 positive SCs. Following isolation, a proportion of myofibres were fixed immediately to be used for T0 quiescent SC analysis, whilst the rest were cultured in suspension in the presence of serum to activate SCs. Myofibres were then fixed at 24, 48 and 72hrs following isolation (**Fig 5.2**). T0 and T24 myofibres were immunostained with antibodies against Myf5 or MyoD. T48 myofibres were immunostained with antibodies against Pax7 and MyoD and T72 fibres were stained with Pax7 and MyoD or MyoD and Mgn antibodies (antibodies used are detailed in **Table 2.7**).

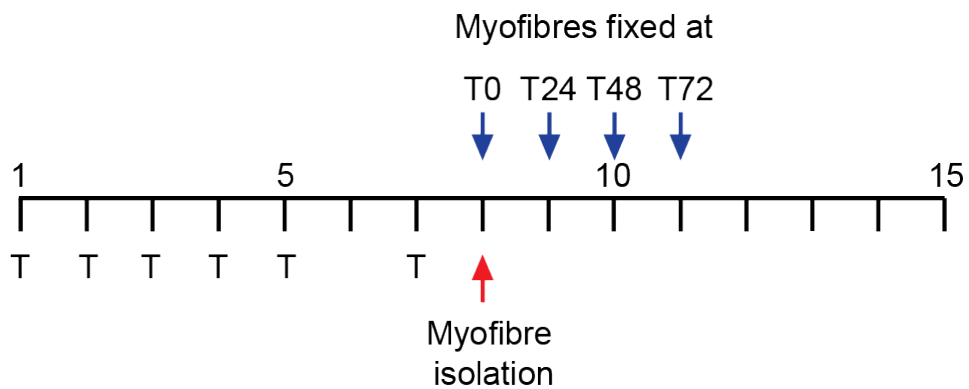


Figure 5.2 Tamoxifen and isolation protocol.

Schematic of tamoxifen protocol and timing of myofibre fixation post isolation.

5.2 Analysis of SC number

Immediately after isolation at T0 the number of SCs on each myofibre was the same in $Ta3^{ff}$ controls and $Pax7-Ta3^{ff}$ mutants, an average of 4.15 ± 0.26 and 4.65 ± 0.88 SCs per myofibre respectively (mean \pm SEM). At T24 and T48 the number of SCs per myofibre was not different in $Pax7-Ta3^{ff}$ mutants compared to $Ta3^{ff}$ controls (T24; $p=0.28$, T48; $p=0.52$) (**Fig. 5.3**). At T72 although not significant there was a trend towards $Pax7-Ta3^{ff}$ mutants having fewer SCs per myofibre compared to controls (T72; $p=0.06$) (**Fig. 5.3**).

The average number of SCs per myofibre increased in $Ta3^{ff}$ controls at each time point, as would be expected due to SC activation and proliferation. In $Ta3^{ff}$ controls at T72 the average number of SCs per myofibre had increased significantly from T0, to 10.06 ± 0.09 SCs ($p<0.0001$, $n=3$). In $Pax7-Ta3^{ff}$ mutants the number of SCs per fibre had not increased ($p=0.27$, $n=3$) (**Fig. 5.3**). This may suggest that $Pax7-Ta3^{ff}$ mutant SCs show delayed proliferation compared to $Ta3^{ff}$ controls.

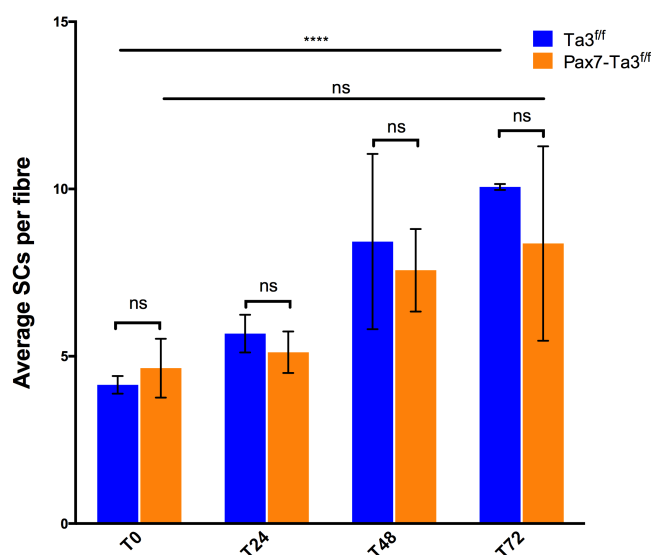


Figure 5.3 The average number of SCs per myofibre increases less over time in mice with SC specific loss of $Ta3$.

Graph to show the average number of SCs per myofibre at T0, 24, 48 and 72 hours after myofibre isolation. **** indicates $p \leq 0.0001$, ns indicates $p > 0.05$ calculated using unpaired, two-tailed t-test. $n=3/4$ Error bars = SEM.

5.3 The expression of Pax7 and Myf5 at SC isolation

The expression of Pax7, through the ZsGreen reporter, Myf5 and MyoD, by immunostaining, was detected in SCs by fluorescence microscopy (**Fig 5.4A, B**). The expression of Pax7 in SCs fixed at T0 was the same in both $Ta3^{ff}$ controls and $Pax7-Ta3^{ff}$ mutants with 100% of SCs being ZsGreen positive (data not shown). A possible trend was observed for Myf5 expression, the proportion of Myf5 positive SCs was smaller in $Pax7-Ta3^{ff}$ mutants (19%) compared to $Ta3^{ff}$ controls (33%) although this difference was not statistically significant ($p=0.09$, $n=4$) (**Fig. 5.4C**). This may in part be due to the high degree of variation between the percentage of Myf5 positive SCs in each $Pax7-Ta3^{ff}$ mutant mouse (3-36%), whereas the proportion was much more consistent in the $Ta3^{ff}$ controls (24-32%). The expression of MyoD was significantly lower in $Pax7-Ta3^{ff}$ mutants (0.6%) compared to controls (7%) ($p=0.04$, $n=4$) (**Fig. 5.4C**).

The majority of SCs in both $Ta3^{ff}$ controls and $Pax7-Ta3^{ff}$ mutants were Pax7 positive only, the proportion in mutants (81%) was not significantly different to controls (64.5%) (**Fig. 5.4D**) however there was a trend towards a higher proportion of Pax7 positive only SCs in $Pax7-Ta3^{ff}$ mutants ($p=0.09$, $n=4$). All SCs were negative for Mgn (data not shown).

The trend in these data suggests that the loss of $Ta3$ in SCs may disrupt the expression of Myf5 and MyoD in quiescent/ early activated SCs.

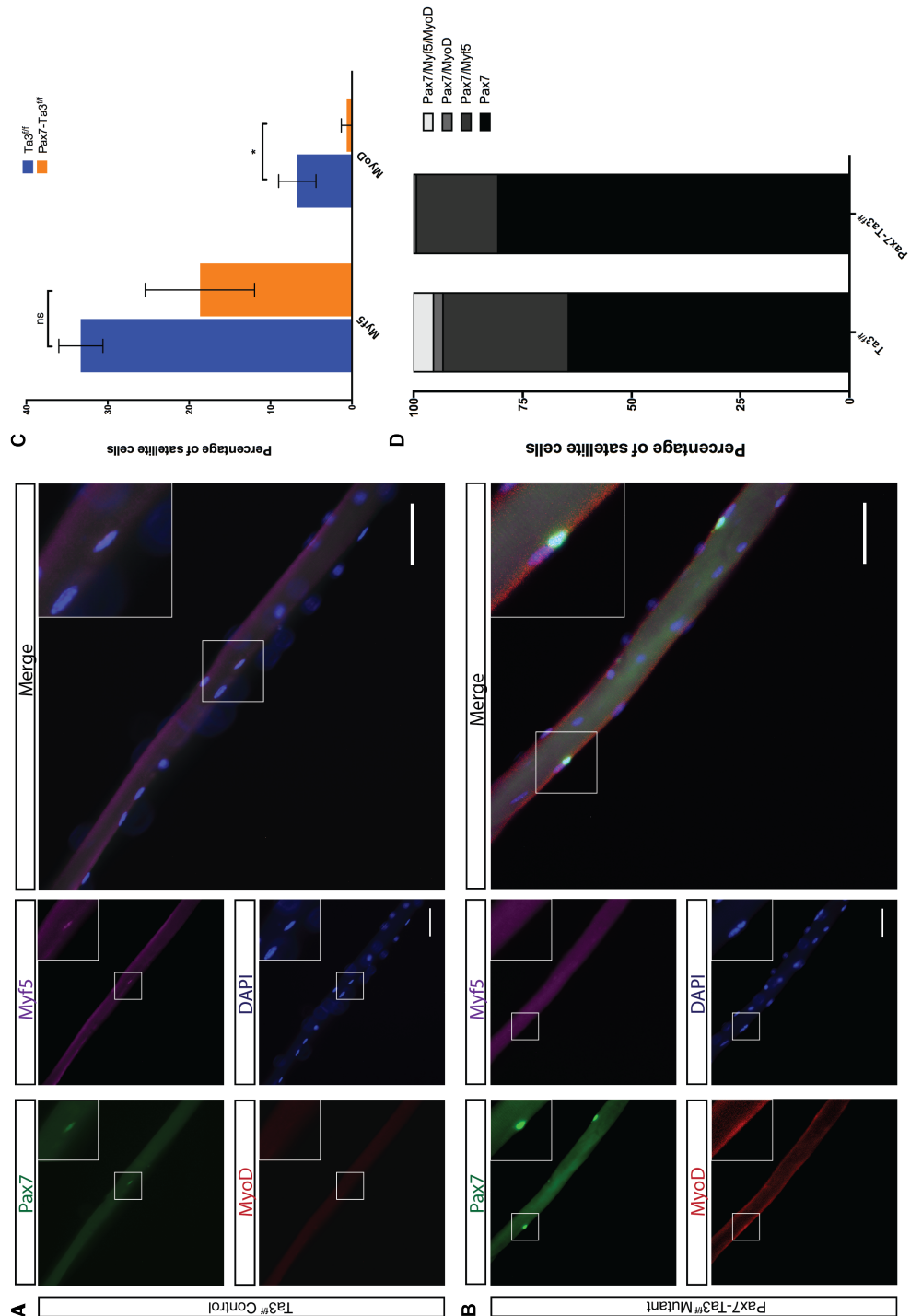


Figure 5.4 The SC specific loss of *Ta3* leads to a reduction in MyoD expression at T0.

(A, B) Example images of *Ta3^{ff}* control and *Pax7-Ta3^{ff}* mutant SCs associated with their myofibre. Pax7 expression detected via ZsGreen fluorescence, Myf5 (magenta) and MyoD (red) detected via immunostaining, nuclei (blue) detected via DAPI staining. Scale bars = 50µm. (A) Pax7 and Myf5 positive, MyoD negative SC. (B) Pax7 positive, Myf5 and MyoD negative SC. (C) Average percentage of SCs expressing Myf5 and MyoD. * indicates $p \leq 0.05$, ns indicates $p > 0.05$ calculated by unpaired, two-tailed t-test. $n = 3/4$. Error bars = SEM. (D) Percentage of SCs expressing each combination of Pax7/Myf5/MyoD.

5.4 The expression of Pax7, Myf5 and MyoD at T24

The expression of Pax7, through the ZsGreen reporter, Myf5 and MyoD, by immunostaining, was detected in SCs by fluorescence microscopy (**Fig 5.5A, B**). The expression of Pax7 in SCs fixed at T24 was the same in both $Ta3^{ff}$ controls and $Pax7-Ta3^{ff}$ mutants with 90% and 91% of SCs being ZsGreen positive, respectively (**Fig. 5.5C**). There was no difference in the proportion of SCs expressing Myf5 and MyoD in $Pax7-Ta3^{ff}$ mutants (76% and 64%, respectively) compared to $Ta3^{ff}$ controls (85.5% and 83%, respectively) (Myf5; $p=0.53$, MyoD; $p=0.30$, $n=3/4$) (**Fig. 5.5C**).

By T24 the majority of SCs in both $Ta3^{ff}$ controls and $Pax7-Ta3^{ff}$ mutants were now Pax7, Myf5 and MyoD triple positive, 69% and 54% respectively (**Fig. 5.5D**), with no difference in proportion between controls and mutants ($p=0.4$, $n=3/4$). The percentage of SCs expressing Pax7 alone or Pax7 and Myf5 was not different between $Pax7-Ta3^{ff}$ mutants compared to $Ta3^{ff}$ controls (Pax7 $p=0.4$, Pax7 and Myf5 $p=0.35$ $n=3/4$) (**Fig. 5.5D**).

Similar to the data at T0, in mutants there was quite a large variability in the proportion of SCs, which were Pax7 positive (4.5-52%), whereas the controls were again much more consistent (0-19%). All SCs were negative for Mgn (data not shown).

At T24 there is no difference in the expression levels of Pax7, Myf5 or MyoD in $Pax7-Ta3^{ff}$ mutants compared to $Ta3^{ff}$ controls.

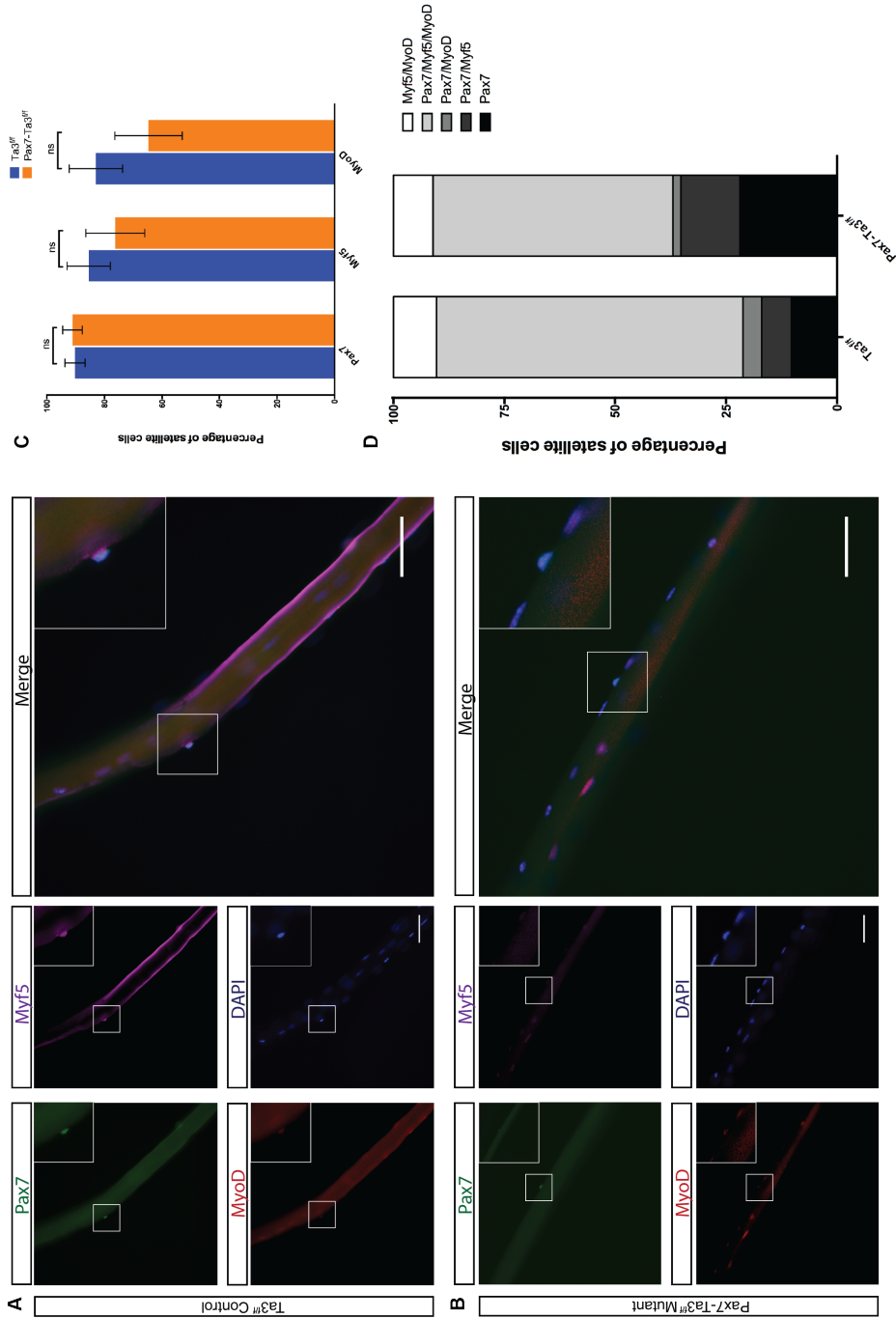


Figure 5.5 A SC specific loss of *Ta3* does not significantly affect the expression of Myf5 or MyoD at T24.

(A, B) Example images of *Ta3^{ff}* control and *Pax7-Ta3^{ff}* mutant SCs associated with their myofibre. Pax7 expression detected via ZsGreen fluorescence, Myf5 (magenta) and MyoD (red) detected via immunostaining, nuclei (blue) detected via DAPI staining. Scale bars = 50µm. (A) Pax7 and Myf5 positive, MyoD negative SC. (B) Pax7 and Myf5 positive, MyoD negative SC. (C) Average percentage of SCs expressing Myf5 and MyoD. ns indicates $p > 0.05$, calculated by unpaired, two-tailed t-test. $n = 3/4$. Error bars = SEM. (D) Percentage of SCs expressing each combination of Pax7/Myf5/MyoD.

5.5 The expression of Pax7 and MyoD at T48

The expression of Pax7 and MyoD, by immunostaining, was detected in SCs by fluorescence microscopy (**Fig 5.6A, B**). At later time points (T48 and T72) antibodies against Pax7 were used rather than ZsGreen. This was to ensure that active Pax7 protein was detected rather than ZsGreen protein that was still present from earlier Pax7 expression.

There was no difference in the proportion of SCs expressing Pax7 at T48 in *Ta3^{ff}* controls (83%) compared to *Pax7-Ta3^{ff}* mutants (69%) ($p=0.50$, $n=3/4$) (**Fig. 5.6C**). There was no difference in the proportion of SCs expressing MyoD in *Pax7-Ta3^{ff}* mutants compared to *Ta3^{ff}* controls (both 93%) (**Fig. 5.6C**).

By T48 the majority of SCs in both *Ta3^{ff}* controls and *Pax7-Ta3^{ff}* mutants were now Pax7, MyoD double positive (75.5% and 62% respectively), there was no difference in the proportion in controls compared to mutants ($p=0.32$, $n=3/4$) (**Fig. 5.6D**). The percentage of SCs expressing Pax7 alone was the same (both 7%), there was also no difference in the proportion of SCs expressing MyoD alone in *Pax7-Ta3^{ff}* mutants (31%) compared to controls (17%) ($p=0.4$, $n=3/4$) (**Fig. 5.6D**). At this time point there was large variability in the proportion of SCs expressing MyoD alone in *Ta3^{ff}* controls (0-37%) and *Pax7-Ta3^{ff}* mutants (12-70%). Due to the low n number it is hard to draw conclusions from these data.

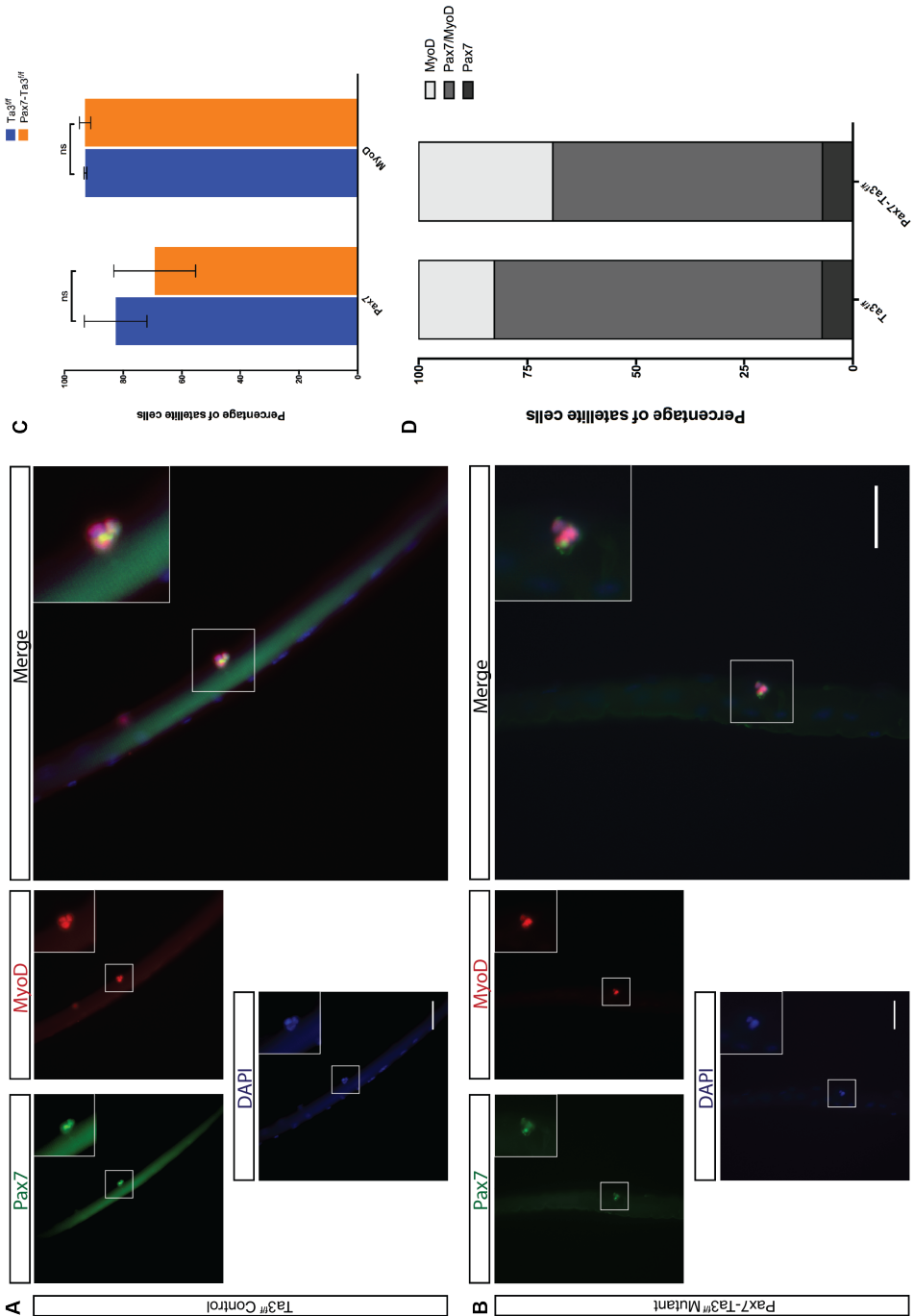


Figure 5.6 A SC specific loss of *Ta3* does not significantly affect the expression of Pax7 or MyoD at T48.

(A, B) Example images of *Ta3^{fl/fl}* control and *Pax7-Ta3^{fl/fl}* mutant SCs associated with their myofibre. Pax7 (green) and MyoD (Red) detected via immunostaining, nuclei (blue) detected via DAPI staining. Scale bars = 50µm. (A) 2 Pax7, MyoD positive SCs and 1 MyoD positive, Pax7 negative SC. (B) 1 Pax7, MyoD positive SC and 1 MyoD positive, Pax7 negative SC. (C) Average percentage of SCs expressing Pax7 and MyoD. ns indicates $p > 0.05$, calculated by unpaired, two-tailed t-test. $n = 3/4$. Error bars = SEM (D) Percentage of SCs expressing each combination of Pax7/MyoD.

5.6 The expression of Pax7, MyoD and Mgn at T72

The expression of Pax7, MyoD and Mgn by immunostaining, was detected in SCs by fluorescence microscopy (**Fig 5.7A, B and 5.7A, B**). To analyse terminal differentiation of SCs, myofibres were immunostained with antibodies against MyoD and Mgn. To analyse SC self-renewal myofibres were immunostained with antibodies against Pax7 and MyoD. Unfortunately, the only antibodies available to us against Pax7 and Mgn were both raised in mouse, we were therefore unable to analyse Pax7 and Mgn together.

5.6.1 Terminal differentiation

There was no difference in the proportion of SCs expressing Mgn at T72 in *Pax7-Ta3^{ff}* mutants (80%) compared to *Ta3^{ff}* controls (69%) ($p=0.21$, $n=3$) (**Fig. 5.7C**). There was also difference in the proportion of SCs expressing MyoD in *Pax7-Ta3^{ff}* mutants compared to *Ta3^{ff}* controls (98% and 99.5%) ($p=0.35$, $n=3$) (**Fig. 5.7C**).

By T72 the majority of SCs in both *Ta3^{ff}* controls and *Pax7-Ta3^{ff}* mutants were now MyoD, Mgn double positive, there was no difference in the proportion in mutants (78%) compared to controls (68%) ($p=0.22$, $n=3$) (**Fig. 5.7D**).

These data suggest that there is no difference in the timing of Myogenin expression in SCs from *Pax7-Ta3^{ff}* compared to *Ta3^{ff}* controls.

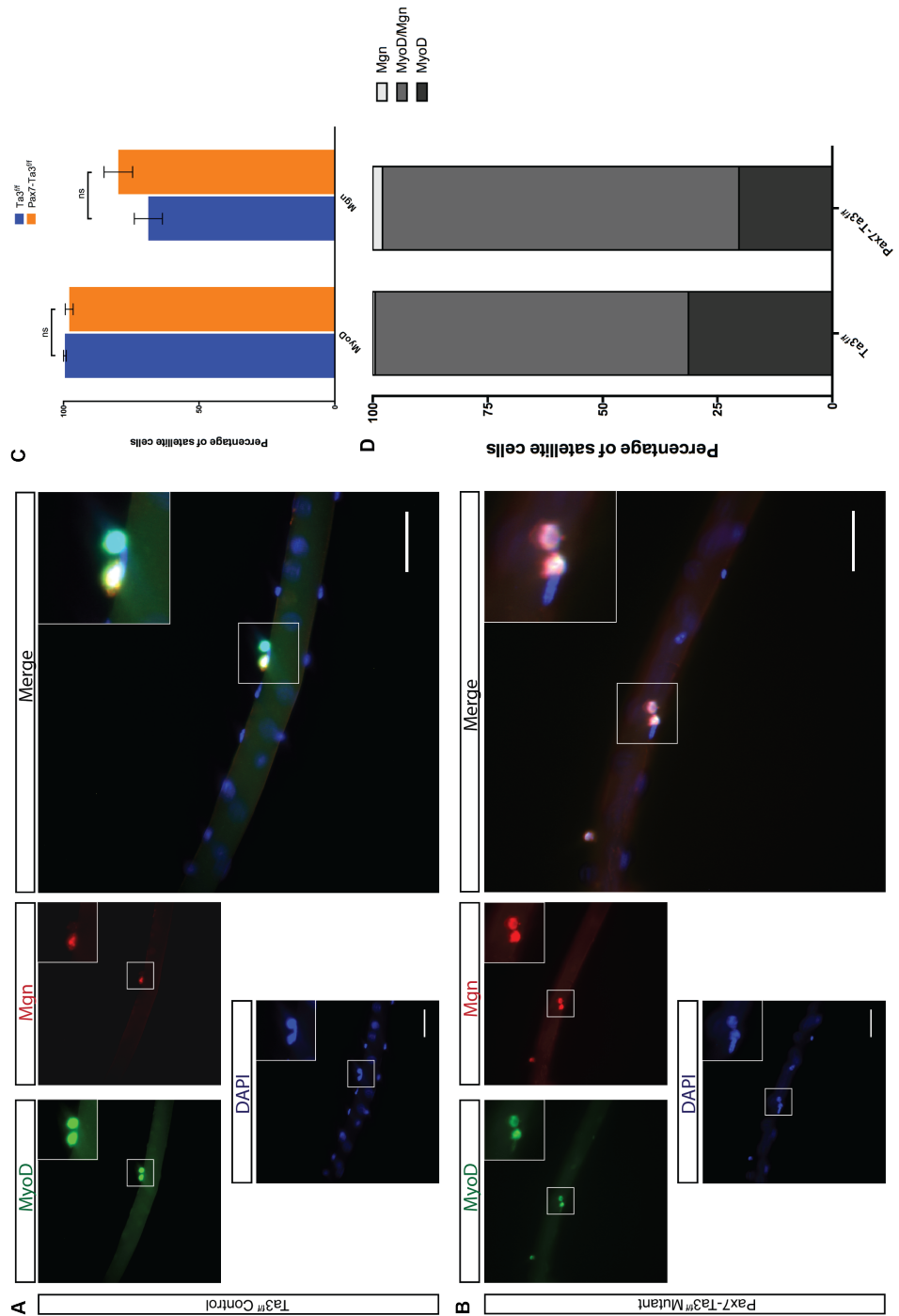


Figure 5.7 A SC specific loss of *Ta3* does not affect the expression of *Mgn* at T72.

(A, B) Example images of *Ta3^{ff}* control and *Pax7-Ta3^{ff}* mutant SCs associated with their myofibre. MyoD (green) and *Mgn* (Red) detected via immunostaining, nuclei (blue) detected via DAPI staining. Scale bars = 50 μ m. (A) 1 MyoD, *Mgn* double positive SC and 1 MyoD positive, *Mgn* negative SC. (B) 2 MyoD, *Mgn* double positive SCs (C) Average percentage of SCs expressing MyoD and *Mgn*. ns indicates $p > 0.05$, calculated by unpaired, two-tailed t-test. $n = 3/4$. Error bars = SEM (D) Percentage of SCs expressing each combination of MyoD/*Mgn*.

5.6.2 Satellite cell self-renewal

The proportion of SCs expressing Pax7 at T72 was higher in $Ta3^{ff}$ controls (21%) compared to $Pax7-Ta3^{ff}$ mutants (9%), unfortunately only fibres from 2 control mice were available so statistical analysis was not performed (**Fig. 5.8C**). There was very little difference in the proportion of SCs expressing MyoD in $Pax7-Ta3^{ff}$ mutants compared to $Ta3^{ff}$ controls (98% and 99.5%) (**Fig. 5.8C**).

By T72 the majority of SCs in this experiment in both $Ta3^{ff}$ controls and $Pax7-Ta3^{ff}$ mutants were MyoD positive alone, the proportion was slightly higher in mutants (91%) compared to controls (79%) however this could not be statistically determined (**Fig. 5.8D**). The percentage of SCs expressing both Pax7 and MyoD was higher in controls (9.5%) compared to mutants (3.5%) but again couldn't be statistically determined (**Fig. 5.8D**).

These data suggest that SCs from $Pax7-Ta3^{ff}$ mutants may not self-renew as efficiently as evidenced by a smaller proportion of cells retaining or reactivating Pax7 expression, however this would need to be repeated to increase the n number so statistical analysis can be performed before firm conclusion can be drawn.

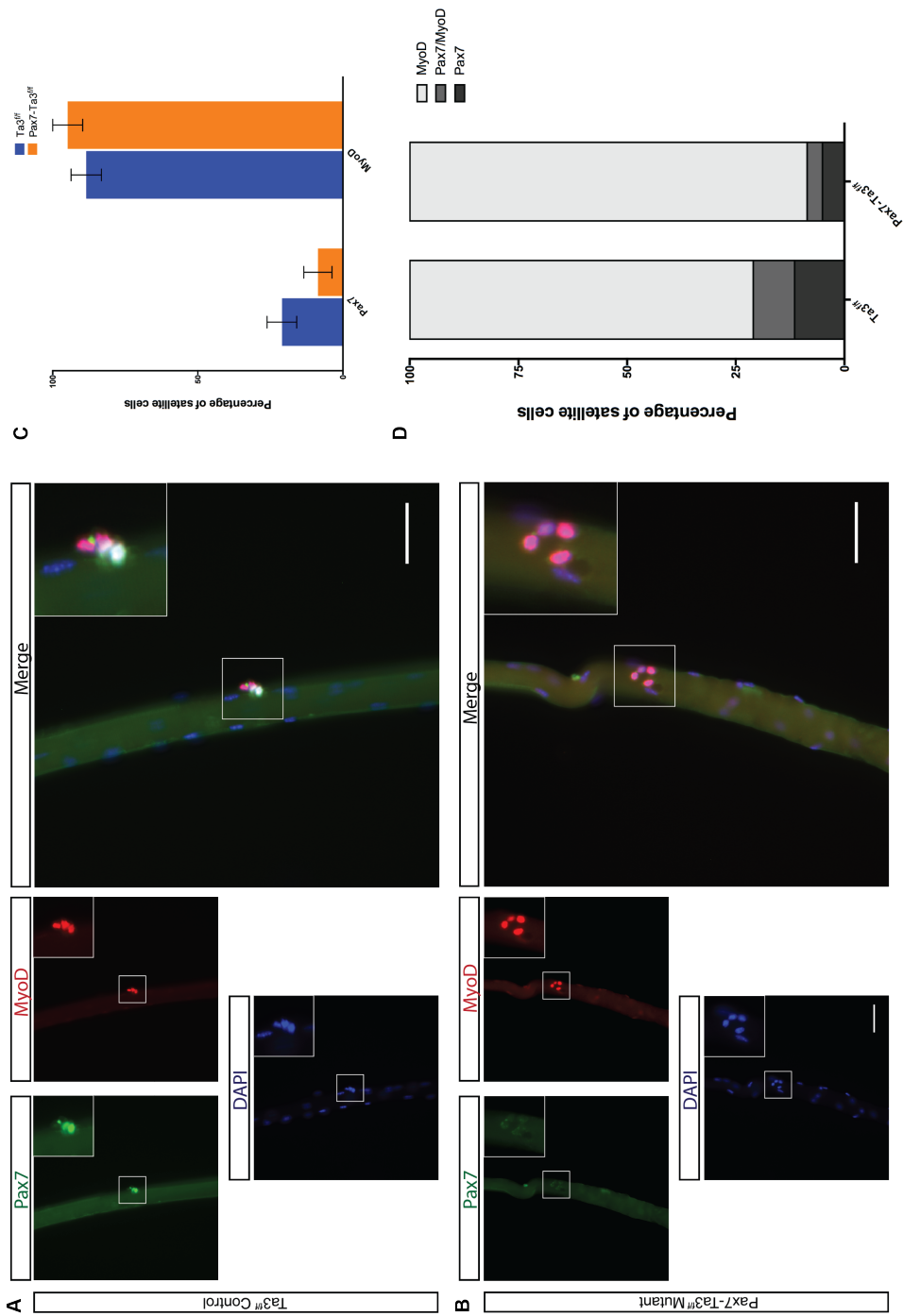


Figure 5.8 The effect of a SC specific loss of *Ta3* on Pax7 expression at T72.

(A, B) Example images of *Ta3^{ff}* control and *Pax7-Ta3^{ff}* mutant SCs associated with their myofibre. Pax7 (green) and MyoD (Red) detected via immunostaining, nuclei (blue) detected via DAPI staining. Scale bars = 50µm. (A) 2 Pax7, MyoD double positive SCs and 1 MyoD positive, Pax7 negative SC. (B) 4 MyoD positive, Pax7 negative SCs (C) Average percentage of SCs expressing Pax7 and MyoD. n=2 (D) Percentage of SCs expressing each combination of Pax7/MyoD. Error bars = SEM.

5.7 Expression of Pax7 and MRFs over time during SC activation and differentiation

The proportion of SCs expressing Pax7 decreased over time following myofibre isolation as would be expected when SCs initiate the myogenic programme this decrease coincided with an increase in the proportion of cells expressing Myf5 and MyoD (Fig. 5.9). This pattern of expression was observed in both $Ta3^{ff}$ control and $Pax7-Ta3^{ff}$ mutant mice. The only difference observed between $Ta3^{ff}$ control and $Pax7-Ta3^{ff}$ mutant mice was a reduction in MyoD expression at T24 in mutant SCs.

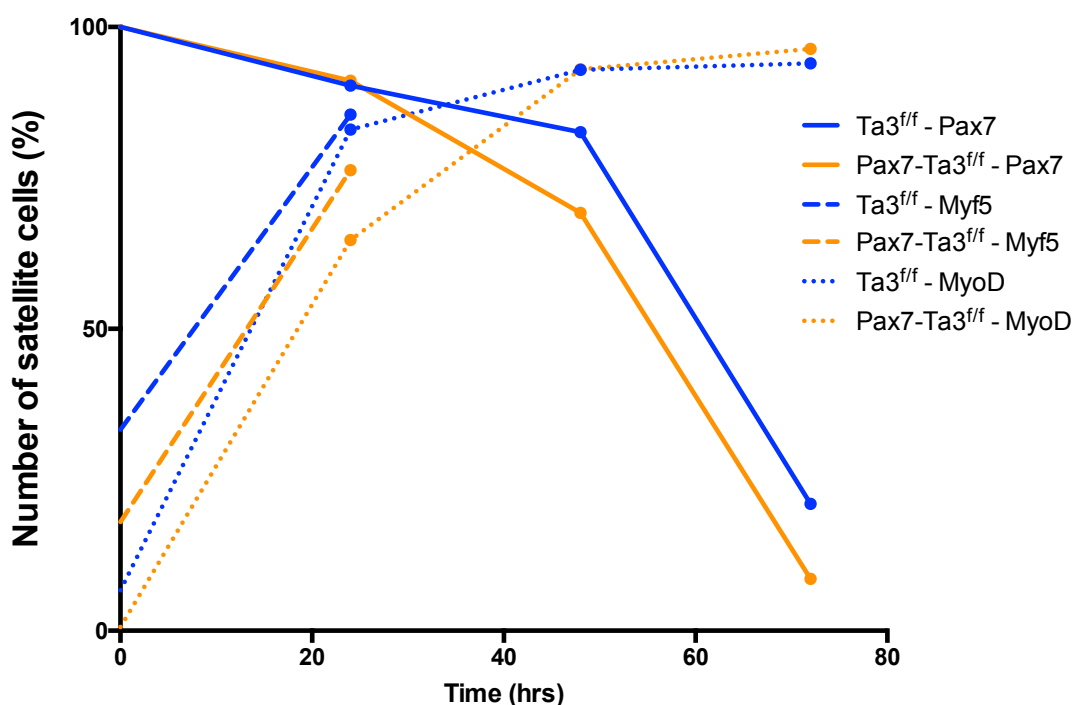


Figure 5.9 Trend in expression of Pax7 and MRFs over 72hrs following SC activation and in vitro culture.

Graph showing the average percentage of SCs expressing Pax7 (full line), Myf5 (dashed line) and MyoD (dotted line) at T0, 24, 48 and 72. n=3/4.

5.8 Discussion

The aim of this chapter was to investigate some of the molecular differences in *Ta3^{ff}* mutant SCs that could be playing a role in the regeneration defect revealed in chapter 3. However, unfortunately due to high variability between biological replicates using an n of 3/4 mice did not allow for enough statistical power to draw definitive statistical conclusion therefore this chapter will act as a pilot study to inform future experiments.

Published data has determined the temporal expression of Pax7 and the MRFs during SC activation, proliferation and differentiation illustrating the importance of correct expression for myogenic progression and SC self-renewal.

SC specific KO of *Ta3* did not affect the number of SCs present on each myofibre immediately after isolation with both *Ta3^{ff}* controls and *Pax7-Ta3^{ff}* mutants having an average of 4 SCs per myofibre (**Fig 5.3**). This is slightly less than previously published data which reported an average of 7-8 SCs per myofibre in EDL muscles (Zammit et al., 2002). The discrepancy between the number of SCs could be due to the number of myofibres analysed. Zammit and colleagues (2002) analysed 178 myofibres, whereas here we analysed 20 myofibres from *Ta3^{ff}* controls and 22 myofibres from *Pax7-Ta3^{ff}* controls. However, the variability in the majority of our data is quite low, therefore counting more fibres may not increase the average to published levels. There is also the possibility of technical issues during cell counting. In particular, the MyoD antibody producing quite a high level of back ground which can make counting positive cells more difficult. It is therefore possible that we were too conservative in our counting to avoid false positives, however, this may have resulted in some positive SCs being missed. It is therefore important that these experiments are repeated and counted by more than one person.

At T72 even though there was not a statistically significant difference between the number of SCs per fibre in *Ta3^{ff}* controls and *Pax7-Ta3^{ff}* mutants (**Fig 5.3**), the number of SCs per fibre had increased significantly in *Ta3^{ff}* controls from T0 to T72 and a significant increase in the number of SCs per fibre in *Pax7-Ta3^{ff}* mutants was not observed. Paired with the results from chapter 4 that showed a lower proportion of *Pax7-Ta3^{ff}* mutant SCs went

through 2 divisions compared to $Ta3^{ff}$ control SCs, it suggests that a SC specific loss of $Ta3$ may lead to decreased proliferation in the mutant population. However, to confirm this more SCs and myofibres will need to be analysed to increase statistical power.

We showed in chapter 4 that SCs with a $Ta3$ mutation do not differentiate as efficiently as control SCs in *in vitro* culture. The importance of the expression of Myf5, MyoD and Mgn for this process has been well documented (reviewed in Section 1.1.4.3). The general trend in Pax7 and MRF expression was the same in both $Ta3^{ff}$ control and $Pax7-Ta3^{ff}$ mutant SCs (**Fig 5.9**) and followed that of previously published data (**Table 5.2**).

Pax7 expression was highest in quiescent satellite cells, gradually decreased over the 48hrs post isolation and eventually decreased dramatically by 72hrs in line with many SCs down regulating Pax7 in order to differentiate, with a small population retaining or re-expressing Pax7 to re-enter the stem cell niche. At T0 and T24 Pax7 expression in control and mutant SCs was similar to published values however at T48 and T72 the number of SCs expressing Pax7 in controls was slightly lower than published, whilst in mutants was quite a lot lower. Together with previous evidence that the loss of primary cilia from SCs impairs their ability to self-renew and leads to a decrease in the number of SCs expressing Pax7 (Jaafar Marican et al., 2016) and our observations of severe defects in muscle regeneration after repeated injuries it is possible that $Pax7-Ta3^{ff}$ SCs may not be retaining Pax7 expression leading to a decreased ability to self-renew. However again immunolabelling for Pax7 expression needs to be repeated.

Table 5.2 Comparison of Pax7 and MRF expression in *Ta3* mutant and control SCs to published data.

Number of SCs are expressed as average percentages. Data from (Beauchamp et al., 2000; Jaafar Marican et al., 2016; Zammit et al., 2004; Zammit et al., 2002; Zammit et al., 2006)

| Time point | Marker | Published data | <i>Ta3^{ff}</i> control | <i>Pax7-Ta3^{ff}</i> mutant |
|------------|--------|----------------|---------------------------------|-------------------------------------|
| T0 | Pax7 | 100 | 100 | 100 |
| | Myf5 | 90 | 33 | 19 |
| | MyoD | 12 | 7 | 0.6 |
| T24 | Pax7 | 98 | 90 | 91 |
| | Myf5 | 98 | 85.5 | 76 |
| | MyoD | 98 | 83 | 64 |
| T48 | Pax7 | 98 | 83 | 69 |
| | MyoD | 99 | 93 | 93 |
| T72 | Pax7 | 40 | 21 | 9 |
| | MyoD | 99 | 99.5 | 98 |
| | Mgn | 60 | 60 | 80 |

The onset of expression of MRFs in SCs following activation happens within a few hours of isolation. Zammit et al. (2002) showed an increase from 11% to 86% of SCs expressing MyoD within 6hrs of isolation. In our investigations, SCs were fixed within 2hrs of isolation (T0) and then again at 24hrs. In doing this we observed a stark increase in the expression of Myf5 and MyoD in both *Ta3^{ff}* control and *Pax7-Ta3^{ff}* mutant SCs. With previous publications showing the expression of MyoD changing so dramatically within a short period of time, and given that primary cilia appear to be active during the first 24hrs of SC activation, it would be interesting to determine the profile of Myf5 and MyoD expression in more detail during the first 24hrs. Straface et al. (2009) have previously reported that blocking Shh signalling can prevent upregulation of Myf5 and MyoD expression that normally occurs following muscle injury. In our experiments, we observe that a smaller proportion of *Pax7-Ta3^{ff}* mutant SCs express MyoD at T0, which could be due to the misregulation of Shh signalling that occurs in *Ta3* mutants.

All of the differences observed in the expression profiles of *Pax7-Ta3^{ff}* mutants and *Ta3^{ff}* controls none of them were statistically significant (except MyoD expression at T0). Although the general timing of expression of the MRFs has been established, this will differ slightly between and within SC populations. This is also evident in the data for this chapter with the proportion of SCs expressing different genes at specific time points varying greatly. By immunostaining it is only possible to capture the expression profile of a SC at the time of fixation. It is therefore necessary to analyse a large number of SCs and myofibres to ensure that effects of variation in timings of expression are reduced. To support more definitive conclusions from this data, it is therefore necessary to repeat this time course again to increase the sample size. However, the data that has been obtained so far, indicate that a loss of *Ta3* from SCs may lead to a slower upregulation of Myf5 and MyoD within the first 24hrs of activation and prevents SCs from re-entering the stem cell niche. Both of these events will contribute to a defect in muscle regeneration.

Chapter 6 Discussion

This project focused on the roles of *Ta3* in skeletal muscle satellite cells by investigating the molecular and phenotypic differences of SCs with a *Ta3* mutation and the implications this has on their ability to repair and regenerate skeletal muscle after injury. *Ta3* null mutants are embryonic lethal (Cole, 1942) therefore to enable the study of adult SCs, mice were generated that had a tamoxifen inducible, SC specific mutation within the *Ta3* gene. Mutant mice showed less efficient muscle regeneration following injury with Ctx. This phenotype became more severe and resulted in a loss of muscle regeneration when the muscle was subject to a repeat injury in 3/4 mice. This defect is potentially due to a reduced ability of *Ta3* mutant SCs to proliferate and sufficiently upregulate the important MRFs, Myf5 and MyoD, leading to a reduced ability to differentiate. It also appears SC specific loss of *Ta3* reduces the number of SCs that re-enter quiescence as a reduced proportion maintain/re-express Pax7 following activation and proliferation, attaining to the more severe regeneration defect observed with repeat injuries.

To date, little has been published on the effects *Ta3* mutations have on skeletal muscle development. It has been briefly reported that epithelial cells within the dermomyotome express MyoD, which is usually restricted to the myotome (Davey et al., 2006). This expansion suggests a gain of Shh function within the developing somite. In terms of adult skeletal muscle regeneration there has been nothing published to date on the role of *Ta3*. Here we provide the first evidence that *Ta3* is essential for normal muscle regeneration after injury. Using an *in vivo* model we provide quantitative analysis that showed muscle fibres in mutant mice were unable to reach the same size as control mice following injury. We also begin to explore how mutations in *Ta3* effect the normal progression of SCs through the myogenic programme through analysis of proliferation, differentiation and the expression of key MRFs.

The impairment we observed in muscle regeneration in *Pax7-Ta3^{ff}* mutant mice could be due to defects in a number of steps of the regeneration pathway: proliferation, differentiation and SC self-renewal, which will be discussed in this chapter.

6.1 Satellite cell proliferation

Following injury SCs are activated and go through a few rounds of proliferation to produce an adequate amount of muscle progenitor cells for regeneration. There is contradictory evidence within the literature as to the role of Shh signalling and primary cilia for this process. *In vitro* studies using mouse SCs (Koleva et al., 2005) and myoblasts isolated from 3 day post hatch chicks (Elia et al., 2007) have shown that proliferation is increased when N-Shh protein is introduced to cultures. This increase in proliferation can be antagonised by adding cyclopamine together with N-Shh, suggesting the observed proliferation increase results from the Shh pathway. From this observation, it is inferred that Shh is therefore required for SC proliferation. Contradictory to this, the loss of primary cilia in C2C12 myoblast cells, which is accompanied by a reduction in the expression of *Ptc1* and *Gli1*, also results in an increase in proliferation (Fu et al., 2014), correlating a reduction in Shh signalling with increased proliferation. The contradictory evidence within these pieces of research are likely due to the methods used to modulate Shh signalling. In the studies by Koleva et al. and Elia et al. proliferation was not assessed when Shh signalling is disrupted without first artificially increasing it via N-Shh, leaving the possibility that the increase in proliferation is an artefact of the artificially high levels of Shh. Whereas, Fu et al. disrupted Shh signalling by disrupting primary cilia formation. This therefore is potentially more biologically relevant, however, this does not exclude the possibility that other pathways may also be affected.

It is of course possible that both findings are relevant and the effects of Shh signalling and the presence of primary cilia act at different levels. The presence of a primary cilium is required for correct transduction of the Shh pathway, as revealed by the plethora of Shh phenotypes seen in cilia mutants (Cortellino et al., 2009; Huangfu et al., 2003; Sasai and Briscoe, 2012), therefore increasing the amount of Shh ligand in the presence of a primary cilium will lead to an increase in Shh signal transduction, which may signal to the SCs to proliferate. However, before an individual cell can divide the primary cilium must be disassembled to allow the centrosome to function as a spindle organiser (Izawa et al., 2015). Therefore, the response to a Shh signal and the proliferation of the cell must be a two step process. By removing the primary

cilium, the cells' ability to respond to Shh is perturbed but its ability to proliferate is not due to the availability of the centrosome.

In our observations, there is a small amount of evidence that proliferation may be reduced in SCs with *Ta3* mutations. This would contradict the evidence provided in C2C12 cells when the primary cilium is disrupted (Fu et al., 2014). However, there are some differences in the methodologies used that could possibly affect the results. Firstly, Fu and colleagues disrupted primary cilia by suppression of Cep290, IFT80 and IFT88 with miRNAs resulting in a reduction in the number of ciliated cells by approximately 50%. The location and function of IFT proteins and *Ta3* within the cilium differ and although disruptions in both seem to affect Shh signalling at the level of Gli proteins (Davey et al., 2006; Wang et al., 2013) it is possible that cilia disruption by these proteins have differing effects on proliferation. Using miRNA to disrupt cilia proteins may also show different effects to genetic disruption as was used in our research, approximately 15-20% of C2C12 cells still presented a cilium when treated with miRNA (Fu et al., 2014), however, *Ta3* genetic mutations have been shown to result in the complete loss of primary cilia in chick and mouse (Bangs et al., 2011; Yin et al., 2009).

Another possibility for a reduction in proliferation in *Ta3* mutant cells could be due to the positioning of the centrosome in *Ta3* mutants. Although it has been robustly shown that *Ta3* mutants fail to form primary cilia this is due to a failure of the centrosome to dock into the plasma membrane (Yin et al., 2009), therefore unlike in other cilia mutants, it is possible that the centrosome in *Ta3* mutants is not available for cell division as it remains located at the cell periphery.

Although the findings by Fu et al. (2014) and (Koleva et al., 2005) appear to contradict each other, the function of the primary cilia in the response to Shh signal may be separate to its function in proliferation. Which of these processes is disrupted in *Pax7-Ta3^{ff}* mutant SCs though remains unclear and more in-depth analysis of proliferation is required by a combination of repeating time lapse imaging experiments and also possibly labelling isolated SCs for markers of proliferation such as EdU.

6.2 Satellite cell differentiation

The activation of SCs after skeletal muscle injury culminates in the differentiation of myoblasts and the formation of multinucleated myofibres. It appears this process is under the control of Shh signalling (Elia et al., 2007; Fu et al., 2014; Koleva et al., 2005), however reports are again somewhat contradictory.

We have observed a striking reduction in MHC positive myotube formation in *Pax7-Ta3^{ff}* mutant SCs grown in culture and a possible delay in the expression of Myf5 and MyoD in SCs following isolation of myofibres. This is similar to observations from C2C12s with disrupted ciliogenesis in which levels of Myf5, MyoD and Mgn are all reduced along with the formation of MHC positive myotubes (Fu et al., 2014). Similar results were also observed in primary chick myoblast cells in which the addition of N-Shh lead to an increase in MHC protein (Elia et al., 2007), contradictory to this addition of N-Shh to mouse SC cultures appeared to block the expression of myogenin and the formation of myotubes. This was rescued by the addition of cyclopamine (Koleva et al., 2005). However, unlike the study by Elia et al. in which they added N-Shh after ensuring primary chick cultures were quiescent, this was not specified by Koleva et al. It is therefore possible that the different response to the addition of N-Shh is due to the timing of exposure, which may lead to different effects in this dynamic system. Again, both of these only assess the consequences of artificial activation of Shh signalling via N-Shh and not what happens when endogenous Shh signalling is perturbed. There is *in vivo* research that provides evidence indicating Shh signalling is necessary for SC differentiation. By blocking endogenous Shh signalling with cyclopamine Straface et al. (2009) showed that the upregulation of Myf5 and MyoD is impaired in injured muscle. This provides a more biologically relevant comparison to our investigations.

Although we have shown a trend suggesting a delay in upregulation of MyoD in cultured *Pax7-Ta3^{ff}* mutant SCs, which could be due to a mis-regulation of the Shh signalling pathway, statistical differences in Myf5 expression were not observed and variability within our data was high. Our data

therefore remains inconclusive and further analysis of MRF expression in mutant SCs is required.

6.3 Satellite cell self-renewal

To ensure skeletal muscle is able to withstand multiple injuries throughout a life time, a proportion of activated SCs re-enter the stem cell niche by self-renewal to maintain the stem cell pool. In our *Pax7-Ta3^{ff}* mutants the almost absence of regeneration in muscles that have undergone consecutive injuries, suggests that *Ta3* is playing a vital role in the ability of SCs to self-renew. This would support research by Jaafar Marican et al. (2016) who reported for the first time the involvement of primary cilia in SC self-renewal, observing the reappearance of primary cilia on a proportion of SCs after 72hrs in culture, these cilia were preferentially distributed to Pax7 expressing cells. When primary cilia were disrupted they observed a reduction in the number of SCs expressing Pax7. These data suggest the need for a primary cilium for self-renewal, however it does not address which signalling pathways may be affected that is leading to the reduction in self-renewal. It is speculated in the paper that Shh would be involved due to its reliance on primary cilia for its transduction. Our observations in *Ta3* mutant SCs provide some evidence that this is likely the case, because of the close link between *Ta3* and the Shh pathway. However, the stability of the primary cilium in the absence of functional TA3 protein still remains to be understood. Therefore, the exact timing that the primary cilium is lost or leads to disruption of the Shh pathway in our model needs to be determined before conclusive links between the phenotypes we observe and disruptions of the Shh pathway can be made.

6.4 *Ta3* mutations and primary cilia

The presence of primary cilia on quiescent SCs was recently confirmed by immunostaining with antibodies against Arl13b, a protein that localises to the primary cilium membrane (Jaafar Marican et al., 2016). A hallmark phenotype of the *Ta3* mutants is their lack of primary cilia in all cell types (Yin et al., 2009), therefore it is assumed that SC specific mutations in *Ta3* will lead to the loss of primary cilia in SCs. Unfortunately, during this project we were unable to

successfully immunolabel primary cilia on SCs and therefore were not able to confirm their loss in *Ta3* mutants. Successful identification of primary cilia was achieved in C2C12 cells by immunostaining using antibodies against acetylated α -tubulin and Arl13b, however when the same antibodies were applied to myofibre preparations we were not able to detect primary cilia on SCs.

It is well documented that primary cilia are highly dynamic, disassembling and re-assembling in cells that are actively progressing through the cell cycle. Jaafar Marican et al. (2016) documented that primary cilia are mainly present on quiescent SCs and 24hrs after isolation of myofibres very few SCs possess a primary cilium. Although we aimed to fix SC whilst they were still quiescent following myofibre isolation it is possible that the cilium had already begun to disassemble.

With the loss of primary cilia being reported in all other cell types analysed in *Ta3* mutants the results presented in this research have been interpreted with the assumptions that unperturbed, quiescent SCs in their niche have a primary cilium and that *Ta3* mutant SCs will lose their primary cilium. However, as previously mentioned it is currently not clear as to when the primary cilium is lost in *Ta3* mutant SCs. Due to the presence of functional TA3 during embryonic and post-natal development QSCs will possess a primary cilium. It is not yet known if TA3 is required for the maintenance of the primary cilium. If it is not required the primary cilium will remain on QSCs even after recombination of the *Ta3* locus by tamoxifen until SCs re-enter the cell cycle, during which time the primary cilium is disassembled. It is critical for the correct interpretation of this data that the presence or absence of primary cilia on SCs are determined in our model.

6.5 *Ta3* mutations and Shh signalling

The effects of mutations in the *Ta3* gene have been well studied in embryonic development in mouse, chick and zebrafish. All *Ta3*^{-/-} models show pleiotropic Shh phenotypes (Bangs et al., 2011; Ben et al., 2011; Ede and Kelly, 1964a, b) caused by a misregulation of the pathway at the level of Gli protein processing (Davey et al., 2006). It has been recently demonstrated that both Gli2 and Gli3 require intact cilia for their correct processing. Gli2 activator

function is disrupted if not localised to the cilium (Liu et al., 2015), whilst Gli3 is dependent on the cilium for processing into the repressor form (Huangfu and Anderson, 2005). A further complexity to the pathway is the differential degradation of Gli3^A and Gli3^R, with the repressor form (^R) being more stable than the activator (^A). The loss or disruption of primary cilia therefore results in a decrease in Gli2^A but also a decrease in Gli3^R and an increase in Gli3^A. Although Gli3^R is more stable the loss of the cilium results in less Gli3^R being produced. This loss of Gli3^R can still allow for a low level of transcription of some Shh response genes. It is this loss of repression that is likely the reason cilia mutants show less severe phenotypes than Shh^{-/-} mutants. There is no comparable data to directly assess the difference between Shh^{-/-} mutants and cilia mutants. However, Shh^{-/-} mutants display complete loss of Myf5 and MyoD expression in the epaxial somite (Borycki et al., 1999) whereas this does not appear to be the case in *Ta3* mutants, they actually display an expansion of MyoD expression in the somite (Davey et al., 2006). This is a possible explanation for the fact that we observe only a delay in muscle regeneration and not a complete loss after a single injury in *Pax7-Ta3^{ff}* mutant mice.

Whether a particular system shows a gain or loss of function of Shh phenotype in *Ta3* mutants is dependent on the endogenous Gli2/3^A:Gli2/3^R ratio required for normal function. At this point it is not known what the normal expression of Gli2 and Gli3 and therefore the Gli^A:Gli^R ratio within SCs at different stages of differentiation is.

Unfortunately, within the timeframe of this project we were not able to explore the effect a SC specific mutation in *Ta3* has on the Shh signalling pathway, which could potentially provide molecular evidence for some of the regeneration phenotypes we observed. For example, the trend in reduced differentiation of *Pax7-Ta3^{ff}* mutant SCs we observed may suggest a loss of function of Shh phenotype. However, without examining changes in the Shh pathway it is not possible to conclude whether *Ta3* mutations lead to a gain or loss of function phenotype in SCs. To begin to answer this question in more detail the ratio of Gli^A:Gli^R in quiescent, activated and differentiating SCs would need to be established and compared to that of SCs with *Ta3* mutations.

6.6 Other signalling pathways

A number of other pathways, aside from Hedgehog signalling, have been shown to depend on primary cilia for their regulation. These include the canonical and non-canonical Wnt pathways (Otto et al., 2008; Wallingford and Mitchell, 2011) and Notch signalling (Ezratty et al., 2011), which have not been studied in this project but are noteworthy due to both also being implicated in the function SCs.

The Wnt/ β -catenin pathway has been shown to promote SC proliferation in the presence of Wnt1, Wnt3a and Wnt5a ligands during muscle regeneration whilst Wnt4 and Wnt6 inhibit proliferation by secluding β -catenin to the cell membrane. This is supported by the presence of Wnt1, Wnt3a and Wnt5a in proliferating myoblasts but the absence of Wnt4 and Wnt6 which are expressed in quiescent SCs (Otto et al., 2008). The Wnt/PCP pathway has been linked to SC self-renewal. Wnt7a has been shown to act through the Frizzled7 receptor to activate the Wnt/PCP pathway (Le Grand et al., 2009). Increasing the expression of Wnt7a stimulates symmetrical cell division and expansion of the stem cell pool, therefore linking the non-canonical Wnt pathway with SC self-renewal.

Notch has been implicated at multiple steps within the muscle regeneration pathway, most notably in the activation and proliferation of SCs. Inhibition of the Notch pathway inhibits SC activation and causes muscle regeneration impairment; however, the inhibition of Notch is required for the onset of myogenic differentiation (Conboy and Rando, 2002). Although the evidence published for the involvement of primary cilia in Notch signalling is limited, it has been reported that *lft74* mutants show decreased activation of Notch reporter activity at an embryonic level (Ezratty et al., 2011).

Evidence linking the Wnt and Notch pathways with primary cilia remains limited and, in the case of Wnt signalling, is conflicting. This is likely due to Wnt and Notch specific phenotypes in cilia mutants being subtle (Wallingford and Mitchell, 2011) and often masked by the obvious Shh phenotypes. This is perhaps why, to date, there has been little investigation into the effect of *Ta3* mutations on Wnt and Notch signalling. However, due to their importance in SC

activity it would be interesting to investigate changes that may be occurring in these pathways in the *Pax7-Ta3^{ff}* mutant.

6.7 Impact of research

Mutations in the human orthologue of *Ta3* have been implicated in the development of some human ciliopathies. Primarily patients with mutations in *TA3* present with Joubert Syndrome, a severe but rare ciliopathy characterised by a mid-hindbrain malformation (Roosing et al., 2015; Stephen et al., 2015), however a couple of patients have been identified that present with both Joubert and Jeune Syndromes (Malicdan et al., 2015). The majority of symptoms of Joubert Syndrome develop due to neurological defects including the presentation of hypotonia and ataxia (Maria et al., 1999). Although these symptoms are neurologically induced it is possible that they are masking an additional skeletal muscle defect arising from poor regenerative ability due to a defect in SCs. Therefore, providing insights into the role of *Ta3* in satellite cells and skeletal muscle regeneration may aid in further understanding these syndromes.

There is growing evidence that modulating the Shh pathway may be a viable treatment for age and disease related defects in muscle regeneration (Piccioni et al., 2014a; Piccioni et al., 2014b). Administration of Shh by injection of plasmid expressing human Shh improved muscle regeneration after injury in aged mice, increasing the number of Myf5 positive cells, the number of regenerating fibres and decreasing the amount of fibrosis. Similar improvements have also been observed with the introduction of human Shh expressing plasmids in *mdx* mice. Our research using the *Pax7-Ta3^{ff}* mutant provides further evidence for the role of Shh signalling and primary cilia in SC mediated muscle regeneration. The generation of a SC specific *Ta3* mutant model and our preliminary results provide a platform for further research, which will aid in a deeper understanding of the function of *Ta3* and the complex process of muscle regeneration.

6.8 Future research

We have demonstrated in this research a clear requirement for *Ta3* in skeletal muscle regeneration, however the exact mechanism and signalling pathways which are disrupted in *Pax7-Ta3^{ff}* mutant SCs remain unclear. Although the Shh signalling pathway is one of the strongest candidates, it is vital to confirm this, potentially through q-PCR analysis of *Ptc1* and *Gli1* to assess the activity of the Shh pathway in *Ta3* mutant SCs. The normal ratio of Gli^A:Gli^R in SCs and how this differs from *Ta3* mutant SCs will be critical to the determination of whether *Ta3* mutations specific to SCs produce a gain or loss of function of Shh signalling phenotype.

The precise phenotypic traits of *Ta3* mutant SCs also requires further investigation. SC migration needs to be re-assessed using time-lapse microscopy. At the same time the rate and dynamics of SC proliferation can be re-analysed. With the evidence that primary cilia are required for SC self-renewal it would be interesting to assess the orientation of SC division whilst associated with their myofibre. Previous studies have shown that apical-basal divisions are more often asymmetric, with the daughter cell that remains in contact with the basal lamina giving rise to a cell that will re-enter quiescence (Kuang et al., 2007). This evidence suggests the niche plays a role in the maintenance of stem cell identity. It would therefore be interesting to analyse if *Ta3* mutant SCs are still able to respond to signals from the niche without a primary cilium. This could be assessed by quantifying the number of apical-basal and planar division during time lapse microscopy. The symmetry of division could be assessed on fixed fibres by immunolabelling pairs of SCs and noting the expression of Pax7 and Myf5 in relation to the plane of division.

More detailed investigations into the proliferative activity of *Ta3* mutant SCs is also important. In this research, we examined proliferation by analysing the number of cell divisions during time lapse imaging. However, it is not always possible to count every division, especially when cell clusters begin to form. It is also possible that some actively cycling cells are missed if they do not divide within the time frame of the imaging, or the cells move out of the field of view. Therefore, measuring the incorporation of EdU in isolated SC cultures will allow

for a more accurate and quantitative representation of the proportion of SCs actively proliferating.

Although we show what appears to be a clear defect in differentiation and myotube formation in *Pax7-Ta3^{ff}* mutant SC cultures there were limitations to these experiments, for example we were not able to accurately count the number of SCs plated and were not able to determine the purity of the culture. These experiments therefore need to be repeated using quantitative seeding of a pure SC population.

Taking advantage of the fact we have generated *Pax7-Ta3^{ff}* mutant mice that also express the Pax7^{ZsGreen} reporter, SCs could be sorted by fluorescence activated cell sorting (FACS) providing a pure and quantifiable culture that can then be used to assess proliferation by EdU incorporation and differentiation by myotube formation and MHC staining. FACS sorted SCs could also be used as a source of mRNA and protein to investigate the expression levels of components of the Shh pathway including *Ptc1* and *Gli1* whilst also assessing the ratio of Gli^A:Gli^R and address the question as to whether *Ta3* mutations produce a loss or gain of function of Shh signalling phenotype in SCs.

Appendix 1

Appendix 1.1 Number of myofibres analysed for quantification for short term injury experiments.

Table detailing the number of myofibres, images and sections analysed for each mouse at each time point.

| Time point | Genotype | Mouse ID | Number of myofibres | Number of images | Number of sections |
|------------|---|----------|---------------------|------------------|--------------------|
| 10 days | <i>Ta3^{ff}</i> Control | 4318 | 2584 | 25 | 5 |
| | | 4319 | 1715 | 20 | 5 |
| | | 4491 | 1912 | 22 | 5 |
| | <i>Pax7- Ta3^{ff}</i> Mutant | 4349 | 2173 | 15 | 4 |
| | | 4344 | 2219 | 14 | 7 |
| | | 4542 | 3659 | 25 | 5 |
| 15 days | <i>Ta3^{ff}</i> Control | 4316 | 953 | 13 | 6 |
| | | 4317 | 1507 | 20 | 4 |
| | | 4547 | 2027 | 25 | 5 |
| | <i>Pax7- Ta3^{ff}</i> Mutant | 4336 | 1892 | 15 | 4 |
| | | 4330 | 740 | 13 | 4 |
| | | 4545 | 3664 | 25 | 5 |
| 25 days | <i>Ta3^{ff}</i> Control | 4649 | 632 | 10 | 8 |
| | | 4650 | 719 | 10 | 7 |
| | | 4651 | 592 | 10 | 7 |
| | | 4685 | 1105 | 10 | 9 |
| | <i>Pax7- Ta3^{ff}</i> Mutant | 4686 | 1327 | 10 | 7 |
| | | 4744 | 1295 | 10 | 7 |
| | | 4745 | 1849 | 10 | 8 |
| | | 4691 | 1456 | 10 | 8 |

Appendix 1.2 Number of myofibres analysed for quantification for long term injury experiments.

Table detailing the number of myofibres, images and sections analysed for each mouse.

| Genotype | Mouse ID | Number of myofibres | Number of images | Number of sections |
|---|-----------------|----------------------------|-------------------------|---------------------------|
| <i>Ta3^{ff}</i> Control | 4320 | 3100 | 29 | 6 |
| | 4558 | 3844 | 39 | 8 |
| | 4576 | 5180 | 37 | 8 |
| | 4587 | 2787 | 40 | 8 |
| <i>Pax7-</i> <i>Ta3^{ff}</i> Mutant | 4350 | 5767 | 30 | 6 |
| | 4351 | 4257 | 25 | 5 |
| | 4620 | 5100 | 36 | 8 |

References

- Abbott, U., Taylor, L., Abplanalp, H., **Year**. A 2nd Talpid-like mutation in the fowl *Poultry Science*, Oxford University Press, OXFORD **38**: 1185-1185
- Ainsworth, C., **2007**. Cilia: tails of the unexpected. *Nature* **448**: 638-641.
- Armand, O., Boutineau, A.M., Mauger, A., Pautou, M.P., Kieny, M., **1983**. Origin of satellite cells in avian skeletal muscles. *Arch Anat Microsc Morphol Exp* **72**: 163-181.
- Armstrong, R.B., **1990**. Initial events in exercise-induced muscular injury. *Med Sci Sports Exerc* **22**: 429-435.
- Asakura, A., Seale, P., Girgis-Gabardo, A., Rudnicki, M.A., **2002**. Myogenic specification of side population cells in skeletal muscle. *J Cell Biol* **159**: 123-134.
- Bai, C.B., Auerbach, W., Lee, J.S., Stephen, D., Joyner, A.L., **2002**. Gli2, but not Gli1, is required for initial Shh signaling and ectopic activation of the Shh pathway. *Development* **129**: 4753-4761.
- Bajard, L., Relaix, F., Lagha, M., Rocancourt, D., Daubas, P., Buckingham, M.E., **2006**. A novel genetic hierarchy functions during hypaxial myogenesis: Pax3 directly activates Myf5 in muscle progenitor cells in the limb. *Genes Dev* **20**: 2450-2464.
- Bangs, F., Antonio, N., Thongnuek, P., Welten, M., Davey, M.G., Briscoe, J., Tickle, C., **2011**. Generation of mice with functional inactivation of talpid3, a gene first identified in chicken. *Development* **138**: 3261-3272.
- Bashford, A., **2015**. An investigation into the roles of Talpid3 and primary cilia in the developing brain. Thesis (Doctor of Philosophy (PhD)). University of Bath
- Beauchamp, J.R., Heslop, L., Yu, D.S., Tajbakhsh, S., Kelly, R.G., Wernig, A., Buckingham, M.E., Partridge, T.A., Zammit, P.S., **2000**. Expression of CD34 and Myf5 defines the majority of quiescent adult skeletal muscle satellite cells. *J Cell Biol* **151**: 1221-1234.
- Beisson, J., Wright, M., **2003**. Basal body/centriole assembly and continuity. *Curr Opin Cell Biol* **15**: 96-104.
- Ben, J., Elworthy, S., Ng, A.S., van Eeden, F., Ingham, P.W., **2011**. Targeted mutation of the talpid3 gene in zebrafish reveals its conserved requirement for ciliogenesis and Hedgehog signalling across the vertebrates. *Development* **138**: 4969-4978.
- Berbari, N.F., O'Connor, A.K., Haycraft, C.J., Yoder, B.K., **2009**. The primary cilium as a complex signaling center. *Curr Biol* **19**: R526-535.
- Bitgood, M.J., McMahon, A.P., **1995**. Hedgehog and Bmp genes are coexpressed at many diverse sites of cell-cell interaction in the mouse embryo. *Dev Biol* **172**: 126-138.
- Bober, E., Franz, T., Arnold, H.H., Gruss, P., Tremblay, P., **1994**. Pax-3 is required for the development of limb muscles: a possible role for the migration of dermomyotomal muscle progenitor cells. *Development* **120**: 603-612.

- Bober, E., Lyons, G.E., Braun, T., Cossu, G., Buckingham, M., Arnold, H.H., **1991**. The muscle regulatory gene, Myf-6, has a biphasic pattern of expression during early mouse development. *J Cell Biol* **113**: 1255-1265.
- Borycki, A.G., Brunk, B., Tajbakhsh, S., Buckingham, M., Chiang, C., Emerson, C.P., Jr., **1999**. Sonic hedgehog controls epaxial muscle determination through Myf5 activation. *Development* **126**: 4053-4063.
- Bosnakovski, D., Xu, Z., Li, W., Thet, S., Cleaver, O., Perlingeiro, R.C., Kyba, M., **2008**. Prospective isolation of skeletal muscle stem cells with a Pax7 reporter. *Stem Cells* **26**: 3194-3204.
- Brack, A.S., Conboy, I.M., Conboy, M.J., Shen, J., Rando, T.A., **2008**. A temporal switch from notch to Wnt signaling in muscle stem cells is necessary for normal adult myogenesis. *Cell Stem Cell* **2**: 50-59.
- Braun, T., Buschhausen-Denker, G., Bober, E., Tannich, E., Arnold, H.H., **1989**. A novel human muscle factor related to but distinct from MyoD1 induces myogenic conversion in 10T1/2 fibroblasts. *EMBO J* **8**: 701-709.
- Braun, T., Rudnicki, M.A., Arnold, H.H., Jaenisch, R., **1992**. Targeted inactivation of the muscle regulatory gene Myf-5 results in abnormal rib development and perinatal death. *Cell* **71**: 369-382.
- Bruusgaard, J.C., Liestol, K., Ekmark, M., Kollstad, K., Gundersen, K., **2003**. Number and spatial distribution of nuclei in the muscle fibres of normal mice studied in vivo. *J Physiol* **551**: 467-478.
- Buckingham, M., **1992**. Making muscle in mammals. *Trends Genet* **8**: 144-148.
- Burke, R., Nellen, D., Bellotto, M., Hafen, E., Senti, K.A., Dickson, B.J., Basler, K., **1999**. Dispatched, a novel sterol-sensing domain protein dedicated to the release of cholesterol-modified hedgehog from signaling cells. *Cell* **99**: 803-815.
- Buxton, P., Davey, M.G., Paton, I.R., Morrice, D.R., Francis-West, P.H., Burt, D.W., Tickle, C., **2004**. Craniofacial development in the talpid3 chicken mutant. *Differentiation* **72**: 348-362.
- Cairns, D.M., Sato, M.E., Lee, P.G., Lassar, A.B., Zeng, L., **2008**. A gradient of Shh establishes mutually repressing somitic cell fates induced by Nkx3.2 and Pax3. *Dev Biol* **323**: 152-165.
- Cantini, M., Giurisato, E., Radu, C., Tiozzo, S., Pampinella, F., Senigaglia, D., Zaniolo, G., Mazzoleni, F., Vitiello, L., **2002**. Macrophage-secreted myogenic factors: a promising tool for greatly enhancing the proliferative capacity of myoblasts in vitro and in vivo. *Neurol Sci* **23**: 189-194.
- Caspary, T., Larkins, C.E., Anderson, K.V., **2007**. The graded response to Sonic Hedgehog depends on cilia architecture. *Dev Cell* **12**: 767-778.
- Chang, C.F., Schock, E.N., O'Hare, E.A., Dodgson, J., Cheng, H.H., Muir, W.M., Edelmann, R.E., Delany, M.E., Brugmann, S.A., **2014**. The cellular and molecular etiology of the craniofacial defects in the avian ciliopathic mutant talpid2. *Development* **141**: 3003-3012.

Chen, Z., Indjeian, V.B., McManus, M., Wang, L., Dynlacht, B.D., **2002**. CP110, a cell cycle-dependent CDK substrate, regulates centrosome duplication in human cells. *Dev Cell* **3**: 339-350.

Ciciliot, S., Schiaffino, S., **2010**. Regeneration of mammalian skeletal muscle basic mechanisms and clinical implications *Curr Pharm Des* **16**: 906 -914.

Clegg, C.H., Linkhart, T.A., Olwin, B.B., Hauschka, S.D., **1987**. Growth factor control of skeletal muscle differentiation: commitment to terminal differentiation occurs in G1 phase and is repressed by fibroblast growth factor. *J Cell Biol* **105**: 949-956.

Cole, R.K., **1942**. The Talpid lethal in the domestic fowl. *J Hered*: 82-86.

Collins-Hooper, H., Woolley, T.E., Dyson, L., Patel, A., Potter, P., Baker, R.E., Gaffney, E.A., Maini, P.K., Dash, P.R., Patel, K., **2012**. Age-related changes in speed and mechanism of adult skeletal muscle stem cell migration. *Stem Cells* **30**: 1182-1195.

Conboy, I.M., Rando, T.A., **2002**. The regulation of Notch signaling controls satellite cell activation and cell fate determination in postnatal myogenesis. *Dev Cell* **3**: 397-409.

Corbit, K.C., Aanstad, P., Singla, V., Norman, A.R., Stainier, D.Y., Reiter, J.F., **2005**. Vertebrate Smoothed functions at the primary cilium. *Nature* **437**: 1018-1021.

Cornelison, D.D., Wold, B.J., **1997**. Single-cell analysis of regulatory gene expression in quiescent and activated mouse skeletal muscle satellite cells. *Dev Biol* **191**: 270-283.

Cortellino, S., Wang, C., Wang, B., Bassi, M.R., Caretti, E., Champeval, D., Calmont, A., Jarnik, M., Burch, J., Zaret, K.S., Larue, L., Bellacosa, A., **2009**. Defective ciliogenesis, embryonic lethality and severe impairment of the Sonic Hedgehog pathway caused by inactivation of the mouse complex A intraflagellar transport gene *Ift122/Wdr10*, partially overlapping with the DNA repair gene *Med1/Mbd4*. *Dev Biol* **325**: 225-237.

Dai, P., Akimaru, H., Tanaka, Y., Maekawa, T., Nakafuku, M., Ishii, S., **1999**. Sonic Hedgehog-induced activation of the Gli1 promoter is mediated by GLI3. *J Biol Chem* **274**: 8143-8152.

Daston, G., Lamar, E., Olivier, M., Goulding, M., **1996**. Pax-3 is necessary for migration but not differentiation of limb muscle precursors in the mouse. *Development* **122**: 1017-1027.

Davey, M.G., James, J., Paton, I.R., Burt, D.W., Tickle, C., **2007**. Analysis of talpid3 and wild-type chicken embryos reveals roles for Hedgehog signalling in development of the limb bud vasculature. *Dev Biol* **301**: 155-165.

Davey, M.G., Paton, I.R., Yin, Y., Schmidt, M., Bangs, F.K., Morrice, D.R., Smith, T.G., Buxton, P., Stamatakis, D., Tanaka, M., Munsterberg, A.E., Briscoe, J., Tickle, C., Burt, D.W., **2006**. The chicken talpid3 gene encodes a novel protein essential for Hedgehog signaling. *Genes Dev* **20**: 1365-1377.

Davis, R.L., Weintraub, H., Lassar, A.B., **1987**. Expression of a single transfected cDNA converts fibroblasts to myoblasts. *Cell* **51**: 987-1000.

De Angelis, L., Berghella, L., Coletta, M., Lattanzi, L., Zanchi, M., Cusella-De Angelis, M.G., Ponzetto, C., Cossu, G., **1999**. Skeletal myogenic progenitors originating from embryonic dorsal aorta coexpress endothelial and myogenic markers and contribute to postnatal muscle growth and regeneration. *J Cell Biol* **147**: 869-878.

Dirksen, E.R., **1991**. Centriole and basal body formation during ciliogenesis revisited. *Biol Cell* **72**: 31-38.

Dummer, A., Poelma, C., DeRuiter, M.C., Goumans, M.J., Hierck, B.P., **2016**. Measuring the primary cilium length: improved method for unbiased high-throughput analysis. *Cilia* **5**: 7.

Ede, D.A., Kelly, W.A., **1964a**. Developmental Abnormalities in the Head Region of the Talpid Mutant of the Fowl. *J Embryol Exp Morphol* **12**: 161-182.

Ede, D.A., Kelly, W.A., **1964b**. Developmental Abnormalities in the Trunk and Limbs of the Talpid3 Mutant of the Fowl. *J Embryol Exp Morphol* **12**: 339-356.

Elia, D., Madhala, D., Ardon, E., Reshef, R., Halevy, O., **2007**. Sonic hedgehog promotes proliferation and differentiation of adult muscle cells: Involvement of MAPK/ERK and PI3K/Akt pathways. *Biochim Biophys Acta* **1773**: 1438-1446.

Epstein, J.A., Shapiro, D.N., Cheng, J., Lam, P.Y., Maas, R.L., **1996**. Pax3 modulates expression of the c-Met receptor during limb muscle development. *Proc Natl Acad Sci U S A* **93**: 4213-4218.

Esner, M., Meilhac, S.M., Relaix, F., Nicolas, J.F., Cossu, G., Buckingham, M.E., **2006**. Smooth muscle of the dorsal aorta shares a common clonal origin with skeletal muscle of the myotome. *Development* **133**: 737-749.

Ezratty, E.J., Stokes, N., Chai, S., Shah, A.S., Williams, S.E., Fuchs, E., **2011**. A role for the primary cilium in Notch signaling and epidermal differentiation during skin development. *Cell* **145**: 1129-1141.

Frontera, W.R., Ochala, J., **2015**. Skeletal muscle: a brief review of structure and function. *Calcif Tissue Int* **96**: 183-195.

Fry, A.M., Leaper, M.J., Bayliss, R., **2014a**. The primary cilium: guardian of organ development and homeostasis. *Organogenesis* **10**: 62-68.

Fry, C.S., Lee, J.D., Jackson, J.R., Kirby, T.J., Stasko, S.A., Liu, H., Dupont-Versteegden, E.E., McCarthy, J.J., Peterson, C.A., **2014b**. Regulation of the muscle fiber microenvironment by activated satellite cells during hypertrophy. *FASEB J* **28**: 1654-1665.

Fu, W., Asp, P., Canter, B., Dynlacht, B.D., **2014**. Primary cilia control hedgehog signaling during muscle differentiation and are deregulated in rhabdomyosarcoma. *Proc Natl Acad Sci U S A* **111**: 9151-9156.

Gayraud-Morel, B., Chretien, F., Flamant, P., Gomes, D., Zammit, P.S., Tajbakhsh, S., **2007**. A role for the myogenic determination gene *Myf5* in adult regenerative myogenesis. *Dev Biol* **312**: 13-28.

Gerdes, J.M., Davis, E.E., Katsanis, N., **2009**. The vertebrate primary cilium in development, homeostasis, and disease. *Cell* **137**: 32-45.

- Goetz, S.C., Anderson, K.V., **2010**. The primary cilium: a signalling centre during vertebrate development. *Nat Rev Genet* **11**: 331-344.
- Goodrich, L.V., Johnson, R.L., Milenkovic, L., McMahon, J.A., Scott, M.P., **1996**. Conservation of the hedgehog/patched signaling pathway from flies to mice: induction of a mouse patched gene by Hedgehog. *Genes Dev* **10**: 301-312.
- Gros, J., Manceau, M., Thome, V., Marcelle, C., **2005**. A common somitic origin for embryonic muscle progenitors and satellite cells. *Nature* **435**: 954-958.
- Gunther, S., Kim, J., Kostin, S., Lepper, C., Fan, C.M., Braun, T., **2013**. Myf5-positive satellite cells contribute to Pax7-dependent long-term maintenance of adult muscle stem cells. *Cell Stem Cell* **13**: 590-601.
- Gussoni, E., Soneoka, Y., Strickland, C.D., Buzney, E.A., Khan, M.K., Flint, A.F., Kunkel, L.M., Mulligan, R.C., **1999**. Dystrophin expression in the mdx mouse restored by stem cell transplantation. *Nature* **401**: 390-394.
- Gustafsson, M.K., Pan, H., Pinney, D.F., Liu, Y., Lewandowski, A., Epstein, D.J., Emerson, C.P., Jr., **2002**. Myf5 is a direct target of long-range Shh signaling and Gli regulation for muscle specification. *Genes Dev* **16**: 114-126.
- Hardy, D., Besnard, A., Latil, M., Jouvion, G., Briand, D., Thepenier, C., Pascal, Q., Guguin, A., Gayraud-Morel, B., Cavaillon, J.M., Tajbakhsh, S., Rocheteau, P., Chretien, F., **2016**. Comparative Study of Injury Models for Studying Muscle Regeneration in Mice. *PLoS One* **11**: e0147198.
- Hasty, P., Bradley, A., Morris, J.H., Edmondson, D.G., Venuti, J.M., Olson, E.N., Klein, W.H., **1993**. Muscle deficiency and neonatal death in mice with a targeted mutation in the myogenin gene. *Nature* **364**: 501-506.
- Hildebrandt, F., Benzing, T., Katsanis, N., **2011**. Ciliopathies. *N Engl J Med* **364**: 1533-1543.
- Huangfu, D., Anderson, K.V., **2005**. Cilia and Hedgehog responsiveness in the mouse. *Proc Natl Acad Sci U S A* **102**: 11325-11330.
- Huangfu, D., Liu, A., Rakeman, A.S., Murcia, N.S., Niswander, L., Anderson, K.V., **2003**. Hedgehog signalling in the mouse requires intraflagellar transport proteins. *Nature* **426**: 83-87.
- Hughes, S.M., Blau, H.M., **1990**. Migration of myoblasts across basal lamina during skeletal muscle development. *Nature* **345**: 350-353.
- Hui, C.C., Angers, S., **2011**. Gli proteins in development and disease. *Annu Rev Cell Dev Biol* **27**: 513-537.
- Hutcheson, D.A., Zhao, J., Merrell, A., Haldar, M., Kardon, G., **2009**. Embryonic and fetal limb myogenic cells are derived from developmentally distinct progenitors and have different requirements for beta-catenin. *Genes Dev* **23**: 997-1013.
- Ingham, P.W., Taylor, A.M., Nakano, Y., **1991**. Role of the Drosophila patched gene in positional signalling. *Nature* **353**: 184-187.

- Ishikawa, H., Marshall, W.F., **2011**. Ciliogenesis: building the cell's antenna. *Nat Rev Mol Cell Biol* **12**: 222-234.
- Izawa, I., Goto, H., Kasahara, K., Inagaki, M., **2015**. Current topics of functional links between primary cilia and cell cycle. *Cilia* **4**: 12.
- Jaafar Marican, N.H., Cruz-Migoni, S.B., Borycki, A.G., **2016**. Asymmetric Distribution of Primary Cilia Allocates Satellite Cells for Self-Renewal. *Stem Cell Reports* **6**: 798-805.
- Jockusch, H., Voigt, S., **2003**. Migration of adult myogenic precursor cells as revealed by GFP/nLacZ labelling of mouse transplantation chimeras. *J Cell Sci* **116**: 1611-1616.
- Joe, A.W., Yi, L., Natarajan, A., Le Grand, F., So, L., Wang, J., Rudnicki, M.A., Rossi, F.M., **2010**. Muscle injury activates resident fibro/adipogenic progenitors that facilitate myogenesis. *Nat Cell Biol* **12**: 153-163.
- Kardon, G., Campbell, J.K., Tabin, C.J., **2002**. Local extrinsic signals determine muscle and endothelial cell fate and patterning in the vertebrate limb. *Dev Cell* **3**: 533-545.
- Kassar-Duchossoy, L., Gayraud-Morel, B., Gomes, D., Rocancourt, D., Buckingham, M., Shinin, V., Tajbakhsh, S., **2004**. Mrf4 determines skeletal muscle identity in Myf5:Myod double-mutant mice. *Nature* **431**: 466-471.
- Katz, B., **1961**. The termination of the afferent nerve fibre in the muscle spindle of the frog. *Phil. Trans. R. Soc. Lond. B* **243**: 221-240.
- Kim, S., Tsiokas, L., **2011**. Cilia and cell cycle re-entry: more than a coincidence. *Cell Cycle* **10**: 2683-2690.
- Kobayashi, T., Dynlacht, B.D., **2011**. Regulating the transition from centriole to basal body. *J Cell Biol* **193**: 435-444.
- Kobayashi, T., Kim, S., Lin, Y.C., Inoue, T., Dynlacht, B.D., **2014**. The CP110-interacting proteins Talpid3 and Cep290 play overlapping and distinct roles in cilia assembly. *J Cell Biol* **204**: 215-229.
- Koleva, M., Kappler, R., Vogler, M., Herwig, A., Fulda, S., Hahn, H., **2005**. Pleiotropic effects of sonic hedgehog on muscle satellite cells. *Cell Mol Life Sci* **62**: 1863-1870.
- Kuang, S., Kuroda, K., Le Grand, F., Rudnicki, M.A., **2007**. Asymmetric self-renewal and commitment of satellite stem cells in muscle. *Cell* **129**: 999-1010.
- Lagha, M., Kormish, J.D., Rocancourt, D., Manceau, M., Epstein, J.A., Zaret, K.S., Relaix, F., Buckingham, M.E., **2008**. Pax3 regulation of FGF signaling affects the progression of embryonic progenitor cells into the myogenic program. *Genes Dev* **22**: 1828-1837.
- Larkins, C.E., Aviles, G.D., East, M.P., Kahn, R.A., Caspary, T., **2011**. Arl13b regulates ciliogenesis and the dynamic localization of Shh signaling proteins. *Mol Biol Cell* **22**: 4694-4703.
- Le Grand, F., Jones, A.E., Seale, V., Scime, A., Rudnicki, M.A., **2009**. Wnt7a activates the planar cell polarity pathway to drive the symmetric expansion of satellite stem cells. *Cell Stem Cell* **4**: 535-547.

- Lepper, C., Conway, S.J., Fan, C.M., **2009**. Adult satellite cells and embryonic muscle progenitors have distinct genetic requirements. *Nature* **460**: 627-631.
- Lepper, C., Partridge, T.A., Fan, C.M., **2011**. An absolute requirement for Pax7-positive satellite cells in acute injury-induced skeletal muscle regeneration. *Development* **138**: 3639-3646.
- Lewis, K.E., Drossopoulou, G., Paton, I.R., Morrice, D.R., Robertson, K.E., Burt, D.W., Ingham, P.W., Tickle, C., **1999**. Expression of ptc and gli genes in talpid3 suggests bifurcation in Shh pathway. *Development* **126**: 2397-2407.
- Li, J., Wang, C., Wu, C., Cao, T., Xu, G., Meng, Q., Wang, B., **2017**. PKA-mediated Gli2 and Gli3 phosphorylation is inhibited by Hedgehog signaling in cilia and reduced in Talpid3 mutant. *Dev Biol* **429**: 147-157.
- Lin Shiau, S.Y., Huang, M.C., Lee, C.Y., **1976**. Mechanism of action of cobra cardiotoxin in the skeletal muscle. *J Pharmacol Exp Ther* **196**: 758-770.
- Liu, J., Zeng, H., Liu, A., **2015**. The loss of Hh responsiveness by a non-ciliary Gli2 variant. *Development* **142**: 1651-1660.
- Lodish, H., Berk, A., Zipursky, S., **2000**. Molecular Cell Biology: Section 18.4, Muscle: A specialised contractile machine, 4th Edition ed. W. H. Freeman, New York.
- Madisen, L., Zwingman, T.A., Sunkin, S.M., Oh, S.W., Zariwala, H.A., Gu, H., Ng, L.L., Palmiter, R.D., Hawrylycz, M.J., Jones, A.R., Lein, E.S., Zeng, H., **2010**. A robust and high-throughput Cre reporting and characterization system for the whole mouse brain. *Nat Neurosci* **13**: 133-140.
- Malicdan, M.C., Vilboux, T., Stephen, J., Maglic, D., Mian, L., Konzman, D., Guo, J., Yildirimli, D., Bryant, J., Fischer, R., Zein, W.M., Snow, J., Vemulapalli, M., Mullikin, J.C., Toro, C., Solomon, B.D., Niederhuber, J.E., Program, N.C.S., Gahl, W.A., Gunay-Aygun, M., **2015**. Mutations in human homologue of chicken talpid3 gene (KIAA0586) cause a hybrid ciliopathy with overlapping features of Jeune and Joubert syndromes. *J Med Genet* **52**: 830-839.
- Manning, J., O'Malley, D., **2015**. What has the mdx mouse model of Duchenne muscular dystrophy contributed to our understanding of this disease? *J Muscle Res Cell Motil* **36**: 155-167.
- Maria, B.L., Boltshauser, E., Palmer, S.C., Tran, T.X., **1999**. Clinical features and revised diagnostic criteria in Joubert syndrome. *J Child Neurol* **14**: 583-590.
- Maroto, M., Reshef, R., Munsterberg, A.E., Koester, S., Goulding, M., Lassar, A.B., **1997**. Ectopic Pax-3 activates MyoD and Myf-5 expression in embryonic mesoderm and neural tissue. *Cell* **89**: 139-148.
- Mauro, A., **1961**. Satellite cell of skeletal muscle fibres. *J Biophys Biochem Cytol* **9**: 493-495.
- McCarthy, J.J., Mula, J., Miyazaki, M., Erfani, R., Garrison, K., Farooqui, A.B., Srikuea, R., Lawson, B.A., Grimes, B., Keller, C., Van Zant, G., Campbell, K.S., Esser, K.A., Dupont-Versteegden, E.E., Peterson, C.A., **2011**. Effective fiber hypertrophy in satellite cell-depleted skeletal muscle. *Development* **138**: 3657-3666.

- McDermott, A., Gustafsson, M., Elsam, T., Hui, C.C., Emerson, C.P., Jr., Borycki, A.G., **2005**. Gli2 and Gli3 have redundant and context-dependent function in skeletal muscle formation. *Development* **132**: 345-357.
- Megeney, L.A., Kablar, B., Garrett, K., Anderson, J.E., Rudnicki, M.A., **1996**. MyoD is required for myogenic stem cell function in adult skeletal muscle. *Genes Dev* **10**: 1173-1183.
- Meijering, E., Dzyubachyk, O., Smal, I., **2012**. Methods for cell and particle tracking. *Methods Enzymol* **504**: 183-200.
- Mesires, N.T., Doumit, M.E., **2002**. Satellite cell proliferation and differentiation during postnatal growth of porcine skeletal muscle. *Am J Physiol Cell Physiol* **282**: C899-906.
- Methot, N., Basler, K., **1999**. Hedgehog controls limb development by regulating the activities of distinct transcriptional activator and repressor forms of *Cubitus interruptus*. *Cell* **96**: 819-831.
- Miller, K.J., Thaloor, D., Matteson, S., Pavlath, G.K., **2000**. Hepatocyte growth factor affects satellite cell activation and differentiation in regenerating skeletal muscle. *Am J Physiol Cell Physiol* **278**: C174-181.
- Miyoshi, K., Kasahara, K., Miyazaki, I., Asanuma, M., **2011**. Factors that influence primary cilium length. *Acta Med Okayama* **65**: 279-285.
- Mohler, J., Vani, K., **1992**. Molecular organization and embryonic expression of the hedgehog gene involved in cell-cell communication in segmental patterning of *Drosophila*. *Development* **115**: 957-971.
- Montarras, D., L'Honore, A., Buckingham, M., **2013**. Lying low but ready for action: the quiescent muscle satellite cell. *FEBS J* **280**: 4036-4050.
- Moss, F.P., Leblond, C.P., **1970**. Nature of dividing nuclei in skeletal muscle of growing rats. *J Cell Biol* **44**: 459-462.
- Munsterberg, A.E., Kitajewski, J., Bumcrot, D.A., McMahon, A.P., Lassar, A.B., **1995**. Combinatorial signaling by Sonic hedgehog and Wnt family members induces myogenic bHLH gene expression in the somite. *Genes Dev* **9**: 2911-2922.
- Munsterberg, A.E., Lassar, A.B., **1995**. Combinatorial signals from the neural tube, floor plate and notochord induce myogenic bHLH gene expression in the somite. *Development* **121**.
- Murphy, M.M., Lawson, J.A., Mathew, S.J., Hutcheson, D.A., Kardon, G., **2011**. Satellite cells, connective tissue fibroblasts and their interactions are crucial for muscle regeneration. *Development* **138**: 3625-3637.
- Murtaugh, L.C., Chyung, J.H., Lassar, A.B., **1999**. Sonic hedgehog promotes somitic chondrogenesis by altering the cellular response to BMP signaling. *Genes Dev* **13**: 225-237.
- Nachury, M.V., Loktev, A.V., Zhang, Q., Westlake, C.J., Peranen, J., Merdes, A., Slusarski, D.C., Scheller, R.H., Bazan, J.F., Sheffield, V.C., Jackson, P.K., **2007**. A core complex of BBS proteins cooperates with the GTPase Rab8 to promote ciliary membrane biogenesis. *Cell* **129**: 1201-1213.

- Nagata, Y., Kobayashi, H., Umeda, M., Ohta, N., Kawashima, S., Zammit, P.S., Matsuda, R., **2006a**. Sphingomyelin levels in the plasma membrane correlate with the activation state of muscle satellite cells. *J Histochem Cytochem* **54**: 375-384.
- Nagata, Y., Partridge, T.A., Matsuda, R., Zammit, P.S., **2006b**. Entry of muscle satellite cells into the cell cycle requires sphingolipid signaling. *J Cell Biol* **174**: 245-253.
- Niewiadomski, P., Kong, J.H., Ahrends, R., Ma, Y., Humke, E.W., Khan, S., Teruel, M.N., Novitch, B.G., Rohatgi, R., **2014**. Gli protein activity is controlled by multisite phosphorylation in vertebrate Hedgehog signaling. *Cell Rep* **6**: 168-181.
- Nigg, E.A., Raff, J.W., **2009**. Centrioles, centrosomes, and cilia in health and disease. *Cell* **139**: 663-678.
- Nusslein-Volhard, C., Wieschaus, E., **1980**. Mutations affecting segment number and polarity in *Drosophila*. *Nature* **287**: 795-801.
- OpenStax, **2016**. Anatomy and physiology. OpenStax CNX. Feb 26, 2016, <http://cnx.org/contents/14fb4ad7-39a1-4eee-ab6e-3ef2482e3e22@8.24>.
- Ordahl, C.P., Le Douarin, N.M., **1992**. Two myogenic lineages within the developing somite. *Development* **114**: 339-353.
- Ott, M., Lyons, G., Arnold, H., Buckingham, M.E., **1991**. Early expression of the myogenic regulatory gene, *myf-5*, in precursor cells of skeletal muscle in the mouse embryo. *Development* **111**.
- Otto, A., Collins-Hooper, H., Patel, A., Dash, P.R., Patel, K., **2011**. Adult skeletal muscle stem cell migration is mediated by a blebbing/amoeboid mechanism. *Rejuvenation Res* **14**: 249-260.
- Otto, A., Schmidt, C., Luke, G., Allen, S., Valasek, P., Muntoni, F., Lawrence-Watt, D., Patel, K., **2008**. Canonical Wnt signalling induces satellite-cell proliferation during adult skeletal muscle regeneration. *J Cell Sci* **121**: 2939-2950.
- Oustanina, S., Hause, G., Braun, T., **2004**. Pax7 directs postnatal renewal and propagation of myogenic satellite cells but not their specification. *EMBO J* **23**: 3430-3439.
- Pan, Y., Bai, C.B., Joyner, A.L., Wang, B., **2006**. Sonic hedgehog signaling regulates Gli2 transcriptional activity by suppressing its processing and degradation. *Mol Cell Biol* **26**: 3365-3377.
- Patapoutian, A., Yoon, J.K., Miner, J.H., Wang, S., Stark, K., Wold, B., **1995**. Disruption of the mouse MRF4 gene identifies multiple waves of myogenesis in the myotome. *Development* **121**: 3347-3358.
- Pathi, S., Pagan-Westphal, S., Baker, D.P., Garber, E.A., Rayhorn, P., Bumcrot, D., Tabin, C.J., Blake Pepinsky, R., Williams, K.P., **2001**. Comparative biological responses to human Sonic, Indian, and Desert hedgehog. *Mech Dev* **106**: 107-117.
- Paul, A.C., Rosenthal, N., **2002**. Different modes of hypertrophy in skeletal muscle fibers. *J Cell Biol* **156**: 751-760.

- Pavlat, G.K., Rich, K., Webster, S.G., Blau, H.M., **1989**. Localization of muscle gene products in nuclear domains. *Nature* **337**: 570-573.
- Pawlikowski, B., Pulliam, C., Betta, N.D., Kardon, G., Olwin, B.B., **2015**. Pervasive satellite cell contribution to uninjured adult muscle fibers. *Skelet Muscle* **5**: 42.
- Piccioni, A., Gaetani, E., Neri, V., Gatto, I., Palladino, M., Silver, M., Smith, R.C., Giarretta, I., Pola, E., Hlatky, L., Pola, R., **2014a**. Sonic hedgehog therapy in a mouse model of age-associated impairment of skeletal muscle regeneration. *J Gerontol A Biol Sci Med Sci* **69**: 245-252.
- Piccioni, A., Gaetani, E., Palladino, M., Gatto, I., Smith, R.C., Neri, V., Marcantoni, M., Giarretta, I., Silver, M., Straino, S., Capogrossi, M., Landolfi, R., Pola, R., **2014b**. Sonic hedgehog gene therapy increases the ability of the dystrophic skeletal muscle to regenerate after injury. *Gene Ther* **21**: 413-421.
- Poleskaya, A., Seale, P., Rudnicki, M.A., **2003**. Wnt signaling induces the myogenic specification of resident CD45+ adult stem cells during muscle regeneration. *Cell* **113**: 841-852.
- Porter, J.A., Ekker, S.C., Park, W.J., von Kessler, D.P., Young, K.E., Chen, C.H., Ma, Y., Woods, A.S., Cotter, R.J., Koonin, E.V., Beachy, P.A., **1996**. Hedgehog patterning activity: role of a lipophilic modification mediated by the carboxy-terminal autoprocessing domain. *Cell* **86**: 21-34.
- Powles-Glover, N., **2014**. Cilia and ciliopathies: classic examples linking phenotype and genotype-an overview. *Reprod Toxicol* **48**: 98-105.
- Praetorius, H.A., Spring, K.R., **2001**. Bending the MDCK cell primary cilium increases intracellular calcium. *J Membr Biol* **184**: 71-79.
- Qin, J., Lin, Y., Norman, R.X., Ko, H.W., Eggenschwiler, J.T., **2011**. Intraflagellar transport protein 122 antagonizes Sonic Hedgehog signaling and controls ciliary localization of pathway components. *Proc Natl Acad Sci U S A* **108**: 1456-1461.
- Rantanen, J., Hurme, T., Lukka, R., Heino, J., Kalimo, H., **1995**. Satellite cell proliferation and the expression of myogenin and desmin in regenerating skeletal muscle: evidence for two different populations of satellite cells. *Lab Invest* **72**: 341-347.
- Relaix, F., Rocancourt, D., Mansouri, A., Buckingham, M., **2004**. Divergent functions of murine Pax3 and Pax7 in limb muscle development. *Genes Dev* **18**: 1088-1105.
- Relaix, F., Rocancourt, D., Mansouri, A., Buckingham, M., **2005**. A Pax3/Pax7-dependent population of skeletal muscle progenitor cells. *Nature* **435**: 948-953.
- Reshef, R., Maroto, M., Lassar, A.B., **1998**. Regulation of dorsal somitic cell fates: BMPs and Noggin control the timing and pattern of myogenic regulator expression. *Genes Dev* **12**: 290-303.
- Reznik, M., **1969**. Thymidine-3H uptake by satellite cells of regenerating skeletal muscle. *J Cell Biol* **40**: 568-571.
- Rhodes, S.J., Konieczny, S.F., **1989**. Identification of MRF4: a new member of the muscle regulatory factor gene family. *Genes Dev* **3**: 2050-2061.

Rodgers, J.T., King, K.Y., Brett, J.O., Cromie, M.J., Charville, G.W., Maguire, K.K., Brunson, C., Mastey, N., Liu, L., Tsai, C.R., Goodell, M.A., Rando, T.A., **2014**. mTORC1 controls the adaptive transition of quiescent stem cells from G0 to G(Alert). *Nature* **510**: 393-396.

Roosing, S., Hofree, M., Kim, S., Scott, E., Copeland, B., Romani, M., Silhavy, J.L., Rosti, R.O., Schroth, J., Mazza, T., Miccinilli, E., Zaki, M.S., Swoboda, K.J., Milisa-Drautz, J., Dobyms, W.B., Mikati, M.A., Incecik, F., Azam, M., Borgatti, R., Romaniello, R., Boustany, R.M., Clericuzio, C.L., D'Arrigo, S., Stromme, P., Boltshauser, E., Stanzial, F., Mirabelli-Badenier, M., Moroni, I., Bertini, E., Emma, F., Steinlin, M., Hildebrandt, F., Johnson, C.A., Freilinger, M., Vaux, K.K., Gabriel, S.B., Aza-Blanc, P., Heynen-Genel, S., Ideker, T., Dynlacht, B.D., Lee, J.E., Valente, E.M., Kim, J., Gleeson, J.G., **2015**. Functional genome-wide siRNA screen identifies KIAA0586 as mutated in Joubert syndrome. *Elife* **4**: e06602.

Rudnicki, M.A., Braun, T., Hinuma, S., Jaenisch, R., **1992**. Inactivation of MyoD in mice leads to up-regulation of the myogenic HLH gene Myf-5 and results in apparently normal muscle development. *Cell* **71**: 383-390.

Rudnicki, M.A., Schnegelsberg, P.N., Stead, R.H., Braun, T., Arnold, H.H., Jaenisch, R., **1993**. MyoD or Myf-5 is required for the formation of skeletal muscle. *Cell* **75**: 1351-1359.

Sasai, N., Briscoe, J., **2012**. Primary cilia and graded Sonic Hedgehog signaling. *Wiley Interdiscip Rev Dev Biol* **1**: 753-772.

Sasaki, H., Nishizaki, Y., Hui, C., Nakafuku, M., Kondoh, H., **1999**. Regulation of Gli2 and Gli3 activities by an amino-terminal repression domain: implication of Gli2 and Gli3 as primary mediators of Shh signaling. *Development* **126**: 3915-3924.

Sassoon, D., Lyons, G., Wright, W.E., Lin, V., Lassar, A., Weintraub, H., Buckingham, M., **1989**. Expression of two myogenic regulatory factors myogenin and MyoD1 during mouse embryogenesis. *Nature* **341**: 303-307.

Scherft, J.P., Daems, W.T., **1967**. Single cilia in chondrocytes. *J Ultrastruct Res* **19**: 546-555.

Schienda, J., Engleka, K.A., Jun, S., Hansen, M.S., Epstein, J.A., Tabin, C.J., Kunkel, L.M., Kardon, G., **2006**. Somitic origin of limb muscle satellite and side population cells. *Proc Natl Acad Sci U S A* **103**: 945-950.

Schultz, E., Jaryszak, D.L., Valliere, C.R., **1985**. Response of satellite cells to focal skeletal muscle injury. *Muscle Nerve* **8**: 217-222.

Seale, P., Rudnicki, M.A., **2000**. A new look at the origin, function, and "stem-cell" status of muscle satellite cells. *Dev Biol* **218**: 115-124.

Seale, P., Sabourin, L.A., Girgis-Gabardo, A., Mansouri, A., Gruss, P., Rudnicki, M.A., **2000**. Pax7 is required for the specification of myogenic satellite cells. *Cell* **102**: 777-786.

Segawa, M., Fukada, S., Yamamoto, Y., Yahagi, H., Kanematsu, M., Sato, M., Ito, T., Uezumi, A., Hayashi, S., Miyagoe-Suzuki, Y., Takeda, S., Tsujikawa, K., Yamamoto, H., **2008**. Suppression of macrophage functions impairs skeletal muscle regeneration with severe fibrosis. *Exp Cell Res* **314**: 3232-3244.

- Shea, K.L., Xiang, W., LaPorta, V.S., Licht, J.D., Keller, C., Basson, M.A., Brack, A.S., **2010**. Sprouty1 regulates reversible quiescence of a self-renewing adult muscle stem cell pool during regeneration. *Cell Stem Cell* **6**: 117-129.
- Siegel, A.L., Atchison, K., Fisher, K.E., Davis, G.E., Cornelison, D.D., **2009**. 3D timelapse analysis of muscle satellite cell motility. *Stem Cells* **27**: 2527-2538.
- Siegel, A.L., Kuhlmann, P.K., Cornelison, D.D., **2011**. Muscle satellite cell proliferation and association: new insights from myofiber time-lapse imaging. *Skelet Muscle* **1**: 7.
- Smith, C.K., 2nd, Janney, M.J., Allen, R.E., **1994**. Temporal expression of myogenic regulatory genes during activation, proliferation, and differentiation of rat skeletal muscle satellite cells. *J Cell Physiol* **159**: 379-385.
- Snow, M.H., **1977**. Myogenic cell formation in regenerating rat skeletal muscle injured by mincing. II. An autoradiographic study. *Anat Rec* **188**: 201-217.
- Spektor, A., Tsang, W.Y., Khoo, D., Dynlacht, B.D., **2007**. Cep97 and CP110 suppress a cilia assembly program. *Cell* **130**: 678-690.
- Stephen, L.A., Davis, G.M., McTeir, K.E., James, J., McTeir, L., Kierans, M., Bain, A., Davey, M.G., **2013**. Failure of centrosome migration causes a loss of motile cilia in talpid(3) mutants. *Dev Dyn* **242**: 923-931.
- Stephen, L.A., Johnson, E.J., Davis, G.M., McTeir, L., Pinkham, J., Jaber, N., Davey, M.G., **2014**. The chicken left right organizer has nonmotile cilia which are lost in a stage-dependent manner in the talpid(3) ciliopathy. *Genesis* **52**: 600-613.
- Stephen, L.A., Tawamie, H., Davis, G.M., Tebbe, L., Nurnberg, P., Nurnberg, G., Thiele, H., Thoenes, M., Boltshauser, E., Uebe, S., Rompel, O., Reis, A., Ekici, A.B., McTeir, L., Fraser, A.M., Hall, E.A., Mill, P., Daudet, N., Cross, C., Wolfrum, U., Jamra, R.A., Davey, M.G., Bolz, H.J., **2015**. TALPID3 controls centrosome and cell polarity and the human ortholog KIAA0586 is mutated in Joubert syndrome (JBTS23). *Elife* **4**.
- Straface, G., Aprahamian, T., Flex, A., Gaetani, E., Biscetti, F., Smith, R.C., Pecorini, G., Pola, E., Angelini, F., Stigliano, E., Castellot, J.J., Jr., Losordo, D.W., Pola, R., **2009**. Sonic hedgehog regulates angiogenesis and myogenesis during post-natal skeletal muscle regeneration. *J Cell Mol Med* **13**: 2424-2435.
- Taipale, J., Cooper, M.K., Maiti, T., Beachy, P.A., **2002**. Patched acts catalytically to suppress the activity of Smoothed. *Nature* **418**: 892-897.
- Tajbakhsh, S., Rocancourt, D., Cossu, G., Buckingham, M., **1997**. Redefining the genetic hierarchies controlling skeletal myogenesis: Pax-3 and Myf-5 act upstream of MyoD. *Cell* **89**: 127-138.
- Tatsumi, R., Anderson, J.E., Nevoret, C.J., Halevy, O., Allen, R.E., **1998**. HGF/SF is present in normal adult skeletal muscle and is capable of activating satellite cells. *Dev Biol* **194**: 114-128.
- Tatsumi, R., Liu, X., Pulido, A., Morales, M., Sakata, T., Dial, S., Hattori, A., Ikeuchi, Y., Allen, R.E., **2006**. Satellite cell activation in stretched skeletal muscle and the role of nitric oxide and hepatocyte growth factor. *Am J Physiol Cell Physiol* **290**: C1487-1494.

- Thomas, G.D., **2013**. Functional muscle ischemia in Duchenne and Becker muscular dystrophy. *Front Physiol* **4**: 381.
- Tidball, J.G., **2005**. Inflammatory processes in muscle injury and repair. *Am J Physiol Regul Integr Comp Physiol* **288**: R345-353.
- Varjosalo, M., Taipale, J., **2008**. Hedgehog: functions and mechanisms. *Genes Dev* **22**: 2454-2472.
- Vivian, J.L., Olson, E.N., Klein, W.H., **2000**. Thoracic skeletal defects in myogenin- and MRF4-deficient mice correlate with early defects in myotome and intercostal musculature. *Dev Biol* **224**: 29-41.
- von Maltzahn, J., Jones, A.E., Parks, R.J., Rudnicki, M.A., **2013**. Pax7 is critical for the normal function of satellite cells in adult skeletal muscle. *Proc Natl Acad Sci U S A* **110**: 16474-16479.
- Wallingford, J.B., Mitchell, B., **2011**. Strange as it may seem: the many links between Wnt signaling, planar cell polarity, and cilia. *Genes Dev* **25**: 201-213.
- Wang, B., Fallon, J.F., Beachy, P.A., **2000**. Hedgehog-regulated processing of Gli3 produces an anterior/posterior repressor gradient in the developing vertebrate limb. *Cell* **100**: 423-434.
- Wang, C., Yuan, X., Yang, S., **2013**. IFT80 is essential for chondrocyte differentiation by regulating Hedgehog and Wnt signaling pathways. *Exp Cell Res* **319**: 623-632.
- Watkins, S.C., Cullen, M.J., **1988**. A quantitative study of myonuclear and satellite cell nuclear size in Duchenne's muscular dystrophy, polymyositis and normal human skeletal muscle. *Anat Rec* **222**: 6-11.
- Willem, M., Miosge, N., Halfter, W., Smyth, N., Jannetti, I., Burghart, E., Timpl, R., Mayer, U., **2002**. Specific ablation of the nidogen-binding site in the laminin gamma1 chain interferes with kidney and lung development. *Development* **129**: 2711-2722.
- Wright, W.E., Sassoon, D.A., Lin, V.K., **1989**. Myogenin, a factor regulating myogenesis, has a domain homologous to MyoD. *Cell* **56**: 607-617.
- Wu, C., Yang, M., Li, J., Wang, C., Cao, T., Tao, K., Wang, B., **2014**. Talpid3-binding centrosomal protein Cep120 is required for centriole duplication and proliferation of cerebellar granule neuron progenitors. *PLoS One* **9**: e107943.
- Yablonka-Reuveni, Z., Rivera, A.J., **1994**. Temporal expression of regulatory and structural muscle proteins during myogenesis of satellite cells on isolated adult rat fibers. *Dev Biol* **164**: 588-603.
- Yin, H., Price, F., Rudnicki, M.A., **2013**. Satellite cells and the muscle stem cell niche. *Physiol Rev* **93**: 23-67.
- Yin, Y., Bangs, F., Paton, I.R., Prescott, A., James, J., Davey, M.G., Whitley, P., Genikhovich, G., Technau, U., Burt, D.W., Tickle, C., **2009**. The Talpid3 gene (KIAA0586) encodes a centrosomal protein that is essential for primary cilia formation. *Development* **136**: 655-664.

Zammit, P.S., Golding, J.P., Nagata, Y., Hudon, V., Partridge, T.A., Beauchamp, J.R., **2004**. Muscle satellite cells adopt divergent fates: a mechanism for self-renewal? *J Cell Biol* **166**: 347-357.

Zammit, P.S., Heslop, L., Hudon, V., Rosenblatt, J.D., Tajbakhsh, S., Buckingham, M.E., Beauchamp, J.R., Partridge, T.A., **2002**. Kinetics of myoblast proliferation show that resident satellite cells are competent to fully regenerate skeletal muscle fibers. *Exp Cell Res* **281**: 39-49.

Zammit, P.S., Relaix, F., Nagata, Y., Ruiz, A.P., Collins, C.A., Partridge, T.A., Beauchamp, J.R., **2006**. Pax7 and myogenic progression in skeletal muscle satellite cells. *J Cell Sci* **119**: 1824-1832.

Zeytinoglu, M., Ritter, J., Wheatley, D.N., Warn, R.M., **1996**. Presence of multiple centrioles and primary cilia during growth and early differentiation in the myoblast CO25 cell line. *Cell Biol Int* **20**: 799-807.

Zhao, Y., Tong, C., Jiang, J., **2007**. Hedgehog regulates smoothed activity by inducing a conformational switch. *Nature* **450**: 252-258.